Sipre Report 33

JULY, 1957

Structure of Ice

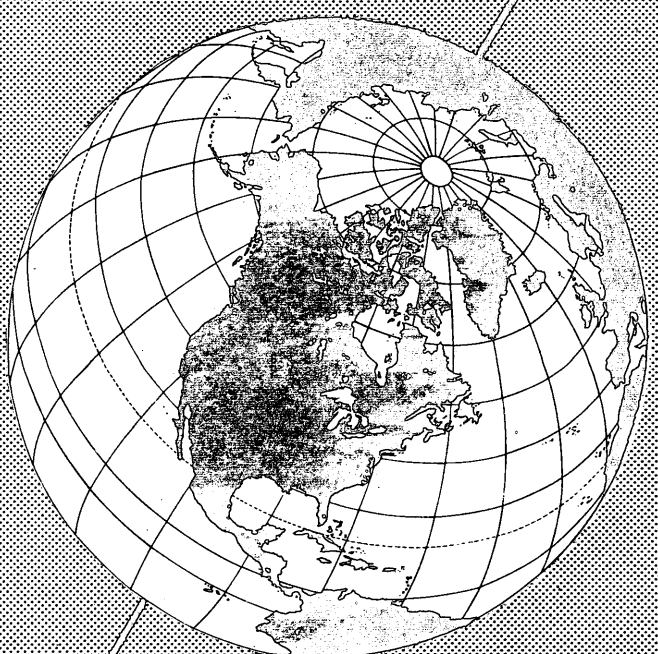

U. S. ARMY
SNOW ICE AND PERMAFROST
RESEARCH ESTABLISHMENT
Corps of Engineers

SIPRE Report 33

STRUCTURE OF ICE

by Rudolph Brill

This report constitutes the final report on contract DA-21-018-ENG-500 (SIPRE Project 22.1-18, *Research for the classification of ice*) with the Department of Physics of the Polytechnic Institute of Brooklyn.

The work described in this report was performed by Dr. Hans Ender, Mr. Norman Kadin, Mrs. Gisela Oster, Mr. Alfred Zajac, and Mr. Sol Zaromb, under the direction of Dr. Brill, project supervisor. The neutron-diffraction experiments on ice crystals were carried out by Drs. L. M. Corliss and J. M. Hastings of the Brookhaven National Laboratory. We wish to thank Drs. Corliss and Hastings and the Director of the Brookhaven National Laboratory for very valuable advice and help.

Work on the general subject is continuing at Polytechnic Institute of Brooklyn under contract DA-11-190-ENG-16 (SIPRE Project 22.1-19, *Investigations on ice.*)

Department of the Army Project 8-66-02-004.

Manuscript received 15 July 1955.

U. S. ARMY SNOW ICE AND PERMAFROST RESEARCH ESTABLISHMENT
Corps of Engineers
Wilmette, Illinois

STRUCTURE OF ICE

by

R. Brill

ABSTRACT

The procedures for growing samples of ice used in the experiments are described. Experiments using the method of bending bars of ice to determine their viscoelastic behavior were made. Tests were conducted on single crystals with various orientations, polycrystalline samples, and mixed crystals of ice-NH_4F. These tests showed that the hexagonal base plane is the gliding plane at plastic deformation and that Becker's equation can be used for the description of the viscoelastic creep of ice.

Studies show that amounts up to 10% of NH_4F may be absorbed in the ice lattice. Dielectric studies indicate that the relaxation time τ_o decreases markedly with increasing concentration of NH_4F, down to a minimum value corresponding to some concentration between 0.1 and 1% NH_4F, and then increases again with further increasing concentration. The dc resistivity of ice-NH_4F increased with the concentration of NH_4F. Investigations were also carried out using x-ray diffraction techniques to determine the thermal amplitudes of H_2O molecules as well as of hydrogen atoms in ice. The molecular vibration can be described by a characteristic temperature of $\theta = 220K$.

CONTENTS

ILLUSTRATIONS

TABLES

LIST OF SYMBOLS

II. MEASUREMENTS ON THE VISCOELASTIC BEHAVIOR OF ICE

E = elastic modulus

P = strain or load applied

t = time (since application of load)

t_1 = time of unloading

$t_r = t - t_1$ = time since removal of load

$t' = t + t_1$

γ = total displacement

γ_1 = elastic displacement

γ_2 = flow displacement

Δ = displacement

η = viscosity

μ = Poisson's ratio

σ = stress

τ = relaxation time; retardation time

III. DIELECTRIC MEASUREMENTS ON ICE-NH_4F MIXED CRYSTALS

C', C'' = real and imaginary components of capacitance

f = frequency (cps)

ϵ = dielectric constant

ϵ_o = dielectric constant at low frequency end of dispersion region; static dielectric constant

ϵ_∞ = dielectric constant at high frequency end of dispersion region

ϵ', ϵ'' = Real and imaginary components of dielectric constant

τ = dielectric relaxation time

IV. INVESTIGATIONS BY X-RAY AND NEUTRON DIFFRACTION

E = energy falling into the camera

F = structure factor

f_n = atomic scattering factors for the n-atoms

I = intensity of reflection

I_o = intensity falling onto the crystal

m = mass of the nth atom

Q = Diffracted x-ray intensity per unit volume

T = absolute temperature

t = thickness of the crystal

x_n, y_n, z_n = atomic coordinates of n-atoms in the elementary cell

δ = phase angle

ϑ_1 = Bragg angle of the ice crystal

ϑ_2 = Bragg angle of the monochromator crystal

θ_n = characteristic temperature of the nth atom

μ = coefficient of absorption

ω = angular velocity of crystal

STRUCTURE OF ICE

by

R. Brill

INTRODUCTION

The report is subdivided into four parts. In the first the methods are described for preparing ice sample; the second part is concerned with measurements of the viscoelastic flow of ice; and the third with the formation of mixed crystals between ice and NH_4F and the influence of NH_4F on the dielectric behavior of ice. NH_4F seems to be the only substance which forms mixed crystals with ice.

The fourth part deals with the measurement of heat movement in ice. These measurements were carried out in connection with neutron-diffraction experiments on ice in collaboration with Drs. Corliss and Hastings of the Brookhaven National Laboratory. These experiments would have brought a decision whether or not ice is polar if crystals had been available which were real single crystals. Unfortunately, we found that the interaction between neutrons and the hydrogen atoms of ice is so strong that the ideal structure of good crystals is destroyed immediately during the diffraction experiment. Therefore these investigations were discontinued. But studies of the heat movement of the oxygen atoms in ice by means of x-rays, started because we needed these data for the evaluation of the experiments on neutron diffraction, were continued and extended to the hydrogen atoms.

I. FORMATION OF ICE UNDER LABORATORY CONDITIONS

Equipment

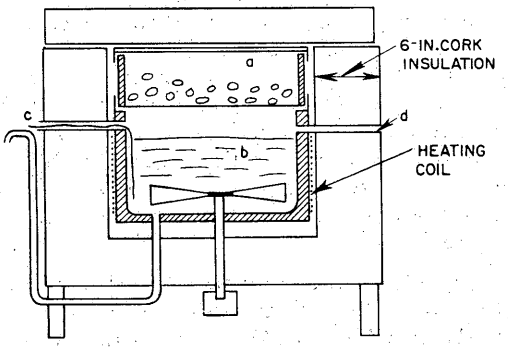

Figure 1. Schematic drawing of device for preparing samples of ice.

For the purpose of preparing samples of ice a special device was constructed (Fig. 1). Two round vessels a and b are placed in a large wooden box with good thermal insulation at all sides, top, and bottom. The inside diameter of a is 16 in and the depth 7 in, the inside diameter of b is 16 in and the depth 10 in. The walls and the top of a and the walls and the bottom of b are insulated against heat transfer. The container a is filled with dry ice and b with water. The dry ice cools the air on top of the water and through the air the water itself. Thus, ice formation starts, as in nature, by cooling the surface of the water exclusively. The openings c and d can be used for blowing cold air through the container or for inserting thermocouples to measure the temperature at different levels in the water. After the surface of the water freezes, the volume of water corresponding to the increase of volume of ice flows out through an opening in the bottom and is caught in a container; its amount indicates the thickness of the ice layer formed at any time. Container b is also provided with a stirrer which can be rotated at variable speed, to study the formation of ice in water under motion. A heating coil around b is used to control the rate of ice formation and, eventually, to prevent crystallization at the rim of the container.

Experiments showed that the thickness, d, of the ice, formed in this equipment, depends upon time, t, according to:

$$d = k \ln \frac{t}{t_o} .$$

Here k is a constant and t_o is the time needed to cool the surface of the water to the freezing point. The ice formed in this way is almost clear, transparent like glass, and contains only a few air bubbles, which often are extended in one direction, exhibiting a needle-like shape. Microscopic investigation showed that the ice has internal stress. The direction of the stress seems to be parallel to the surface and probably is caused by the pressure exerted on the ice by the walls of the vessel. Crystal needles of about 1 mm diam and 10 mm length have been observed in these samples. The needles are oriented parallel in large areas.

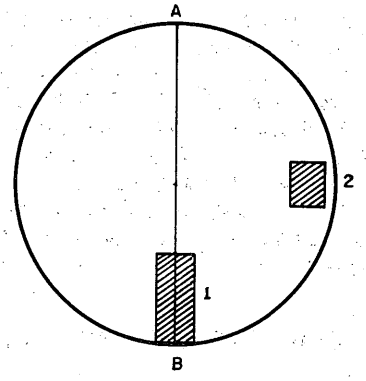

Figure 2. Cuts made in ice crystal (shaded area).

Orientation of crystals

A universal stage was used to determine the orientation of these ice crystals. Two cuts were made as indicated in Figure 2 and the angles which the c-axis forms with the line AB (α) and with the direction perpendicular to the surface of the ice (β) were measured. The results are shown in Figure 3. The numbers in brackets at the points $\alpha = 0°$, $\beta = 90°$, and $\alpha = 90°$, $\beta = 90°$ indicate that the corresponding orientation was found in nine and six crystals respectively.

The graph shows that most of the crystals have an orientation with the c-axis closely parallel to the radius of the specimen and parallel to its surface. If ice crystallizes under similar conditions in nature, the c-axis is almost exclusively perpendicular to the surface. We assumed that this difference is caused by the fact that, in our experiment, the ice starts growing at the wall of the container which, by heat conduction, gets a little cooler than the top of the water. Hence, the container was heated in such a way that no crystallization started at its walls and the ice did not adhere to the walls of the container. Several experiments were carried out, also keeping the temperature of the water near the bottom of the container at +4C. In all these experiments ice specimens were obtained with the c-axis parallel to the surface.

In another effort to imitate natural freezing as closely as possible, cold air was blown into the container until an ice sheet of approximately 0.5 mm was formed. The temperature above the water was approximately -23C to -25C when no air was blown in. The temperature of the air blown in was about -35C. In this case, the appearance of the ice was slightly different. On top, we found an approximately 0.5 mm thick layer with numerous bubbles and very small crystals. Below this bubbly layer, an approximately 3-cm thick layer of relatively large crystals formed long parallel columns perpendicular to the freezing surface. The optic axis in this layer was horizontal in all cases; that is, parallel to the freezing surface. The investigation of the upper layer was rather difficult, but several crystals with their optic axis perpendicular to the freezing surface were found in it. However, when the same experiment was repeated, no crystals could be found with the c-axis perpendicular to the surface.

Influence of impurities

Another experiment was made, adding impurities to water. We chose bentonite because it is one of the most common impurities in natural water, owing to its colloidal character. Ordinarily our ice specimens are made up of needle-shaped crystals of about 2-4 mm diam and a length equal to the thickness of the ice sheet. If the water contains 0.12% bentonite, we obtain crystals of about the same size, but the orientation is slightly changed. There are many crystals present with the c-axis at less than 45° to the surface, but a few crystals have the c-axis almost perpendicular to the surface. If the concentration of bentonite is increased to 0.16%, very large

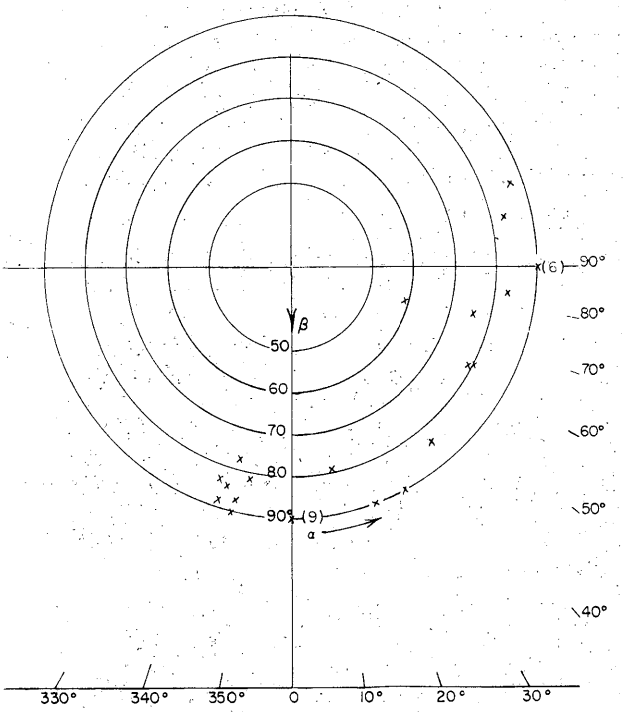

Figure 3. Orientation of ice crystals.

crystals are formed of about 2 to 4 cm length and diameter. All these large crystals, without any exception, are oriented with their c-axis perpendicular to the surface, i.e., in the same way as normally found in nature. Since this experiment was carried out under exactly the same conditions as the other ones, the reason for the change in crystal size and orientation should be the presence of the bentonite. This is very strange, as the presence of impurities usually produces a smaller crystal size rather than a larger one. But the change in orientation of the crystals seems to indicate that orienting forces are exerted in some way by the bentonite or by an impurity of the bentonite. Some experiments carried out later indicate that an impurity of the bentonite might be responsible. It was found that large single crystals form with the c-axis perpendicular to the surface if water is crystallized in waxed containers. For instance, if a layer of beeswax is applied on the rim of container b (Fig. 1), ice crystals form with the c-axis perpendicular to the surface. It might well be that polar molecules of these waxy substances migrate over the surface of the water, forming layers on it with the molecules oriented so that the polar groups are directed towards the water surface. If a monomolecular layer is formed on the surface, the molecules are tightly packed and regularly arranged. The amount of substance needed for the formation of such a layer is very small. The regularly arranged molecules might then act as seeds for crystallization and, if the arrangement over a larger part of the surface is uniform, large crystals will be formed with an orientation determined by the structure of the surface layer. This orientation should be such that the c-axis is perpendicular to the surface. If bentonite is added, surface active substances might be desorbed from this material and accumulated at the surface, providing just the same effect. Since surface active substances are always present on a water surface in nature, the orientation of the ice crystals observed on lakes, ponds, etc. might be caused in this way. This is, of course, a hypothesis and more experiments should be carried out with really clean surfaces and surfaces which contain well defined surface active substances.

Ice formation in flowing water

If the formation of ice took place in flowing water, i.e., if the stirrer (Fig. 1) was in operation, the following phenomena were observed: If the water is flowing fast enough, a layer of soft, slushy ice which looks like frozen snow always forms on the surface. This layer shows a horizontal structure, containing numerous air bubbles of various sizes oriented in horizontal layers. The thickness of this layer depends on the flow rate and varied from about 1 mm to about 1 cm in different experiments. At low flow rates, less than 15 rotations per minute, no soft surface layer appears at all.

Obviously, at high flow rates, many single ice crystals first form on or near the surface and float around in form of slush. As the temperature decreases, they freeze together, forming the surface layer of low rigidity.

Below this surface, we find rather clear, transparent ice with fewer air bubbles. The boundary between the soft, milky surface layer and the clear ice is

rather sharp in all cases. This transparent ice consists of elongated crystals with the optic axis parallel to the direction of growth. Investigation in polarized light shows that almost all the crystals have a certain stress. The size of the crystals varies from about $^1/_{10}$ to 2-3 mm wide and 1 to 20 mm long.

Underneath this clear layer of ice we always find a layer of slush which, surprisingly, is never connected with the solid ice but always floats around without being attached to the solid phase. We assume that in nature, where the flow rate is never as uniform as in our experiments, this kind of slush settles at spots where the flow rate is low and thus causes the thickness of ice to vary greatly.

II. MEASUREMENTS ON THE VISCOELASTIC BEHAVIOR OF ICE

Experimental

To measure the viscoelastic behavior of ice, the method of bending of bars was used, essentially in the same way as described by K'onig (1886). Figure 4 shows the bending apparatus. The bar of ice is supported near its ends on knife edges. At the center of the bar and parallel to the knife edges, a lightweight aluminum rod is placed, which is longer than the width of the bar. At both ends of the rod silk threads are attached carrying a pan for the weights which effect the bending. Provisions were made for placing the aluminum rod precisely at the center of the ice bar. The weight of the aluminum rod and the pan was negligible compared with the actual load applied. In all cases, with one exception, the load applied was 90 g.

The angles of bending were determined in the following manner: Two mirrors, with reflecting faces inward, are attached to the ends of the ice crystal at an angle 14.6° from the normal. The image of an illuminated scale is reflected from one mirror to the other, which in turn reflects the image into a telescope. As the bar is bent, different portions of the scale are reflected into the telescope, and in this manner the change of angle could be observed easily and continually. The use of two mirrors magnifies the deflection of the light beam considerably. A schematic drawing of the arrangement is given in Figure 5: AC = $\underline{D}$ is the horizontal distance of mirror m_1 from the scale ; BC = $\underline{d}$ is the distance between the mirrors at their bases and EG = $\Delta\underline{L}$ is the difference in scale reading for a given angular deflection ϕ. It then follows that, as a first approximation, tan ϕ will be given by:

$$\tan\phi = \frac{\Delta L}{4D+2d} .$$

K"onig's formula assumes that the reflection from mirror m_1 in its undeflected position will be horizontal, which is equivalent to saying that the reflected rays from both mirrors are symmetrical as indicated in the diagram.

To be sure that both mirrors were attached to the ice bar with the same angle, the zero position of the scale at zero deflection was calculated from the known distances and the angle of position of the telescope and compared with the actual position of the scale in the telescope.

Under the conditions of the experiment, $\underline{D}$ = 80.7 cm and $\underline{d}$ = 7.85 cm. Therefore:

$$\tan\phi = 0.00296\Delta L. \qquad (1)$$

Since the above formula, given by K"onig, is only approximate and should deviate appreciably for large deflections, the applicability of the formula under the conditions of our experiments was tested. For this purpose a thin strip of phosphor bronze with mirrors attached at its ends was subjected to various loads at its center. Small increments of weight were added and it was found that the scale reading was directly proportional to the load applied. The deformation of the metal remained

within its elastic range, since the metal was always restored to its original shape after removing the load. It therefore follows that the scale readings are directly proportional to the tangent of the angle of bending.

Since it is assumed that the bar was only loaded in its center, it was necessary to make the mirrors as light as possible. The mirrors were prepared from optically flat microscope cover slips, which were silvered in the usual manner and glued to small brass pieces bent at an angle of 104.6°. This metal base was attached to the upper face of the ice bar.

Preparation of single crystals of ice

Large single crystals of ice were obtained by slow cooling of water. An aluminum container 25 cm in diameter, imbedded in a thick layer of cork insulation, was filled with water and left in a cold room at approximately -5C for 2 to 3 days. The top of the vessel was covered with cloth to prevent any snow crystals falling from the ceiling of the cold room into the water.

Under these conditions the cooling of the water took place from the top as well as from the walls of the container, since no special provision was made to heat the walls of the vessel. The crystals grown in this way showed a random orientation and were generally much larger than those obtained by the rapid freezing method. The crystal boundaries were readily observable, since the ice was very transparent. The crystals were usually elongated in shape, sometimes as long as 10 cm. The cross-sectional areas were up to 10 cm^2 and were irregularly shaped but nevertheless showed 120° angles between the faces occasionally, indicating the hexagonal nature of the crystals.

Preparation of specimen

To locate a single crystal in the blocks of ice, slabs were cut from the blocks in an arbitrary manner and investigated under large sheets of polaroids until a large single crystal was found. Then, the crystal was cut from the slab, a small sample was taken, and its orientation was determined in the universal stage.

After the orientation of the large single crystal was found, a specimen somewhat larger than the sample desired for the bending experiments was cut from the large crystal with an electric saw.

To make the faces of the crystal absolutely flat and parallel to each other, the roughly cut crystal was first put between two L-shaped brass pieces, a few degrees

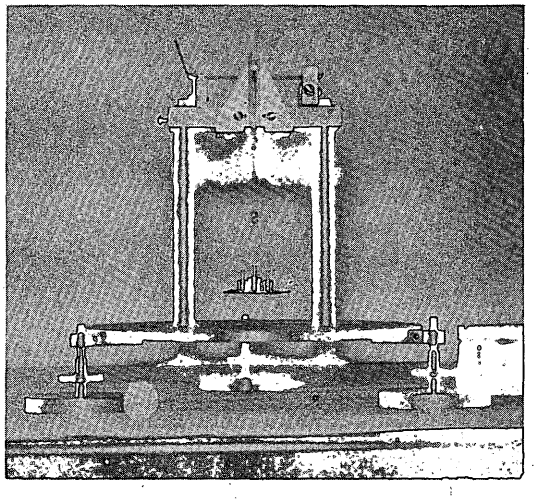

Figure 4. Bending apparatus.

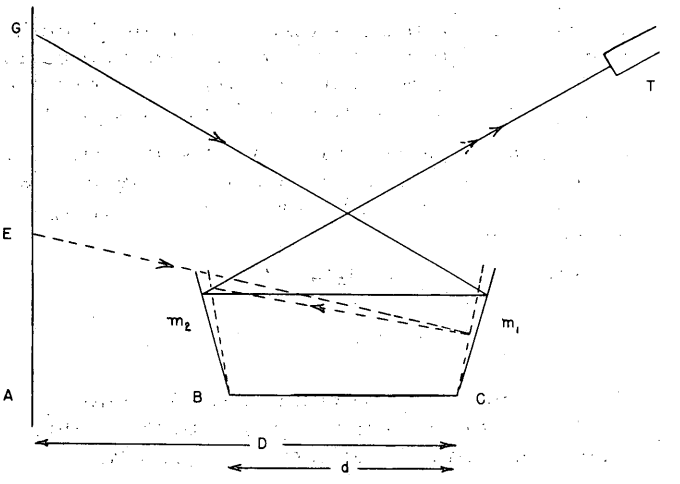

Figure 5. Schematic drawing of arrangement for determining angles of bending.

above 0C, which slowly melted the crystal to the desired shape. It could then be quickly dried between filter paper to prevent freezing of the water on the surface of the crystal. To make the two large faces parallel and obtain the proper thickness of the sample, the crystal was put between two flat brass pieces which were connected by joints in such a manner that they could move only parallel to each other, and then shaped by alternate melting and drying in the same way as before.

The thickness of the crystals was measured with a micrometer. After the bending of the crystals, the samples were re-examined under the polaroids to make sure that the single crystal had remained intact during the experiment.

Procedure of bending experiments

The crystals were kept at approximately -5C and subjected to a load of 90 g at the center of the bar of ice. The instantaneous elastic deformation and the subsequent creep were measured. After a certain time interval the load was removed and the instantaneous elastic recovery and the plastic relaxation were determined.

Theory of viscoelasticity

Combination of Maxwell and Voigt elements. The observed strain-time curves for ice may be represented mathematically by formulas derived from the viscoelastic theory of plastic solids.

For an ideal elastic material, the elastic displacement γ_1 will be proportional to the strain or load P applied, i.e.:

$$\gamma_1 = \frac{P}{E_1}$$

where E_1 is the elastic modulus. The elastic displacement will be instantaneous and, on removal of the load, the material will revert immediately to its original dimensions. This behavior may be represented by a model consisting simply of a spring.

For an ideal Newtonian liquid, the time rate of change of deformation γ_2 (flow displacement) will be proportional to the applied strain, i.e.:

$$\frac{d\gamma_2}{dt} = \frac{P}{\eta_1}$$

where η_1 is called the viscosity of the liquid. Here the flow displacement will be proportional to the duration of load application and, after removal of the stress, the material is permanently deformed. Formally this behavior may be represented by a dashpot, i.e., a piston moving in a viscous fluid.

Maxwell has shown that the deformation with time of certain substances exhibits a linear combination of both phenomena, i.e., a spring and a dashpot in series. Therefore the total displacement $\gamma = \gamma_1 + \gamma_2$ has the time derivative:

$$\frac{d\gamma}{dt} = \frac{1}{\eta_1} P + \frac{1}{E_1} \frac{dP}{dt} .$$

Deformation as a function of time for this model is shown in the diagram to the right, where the load is applied during the time interval $t_1 - t_o$.

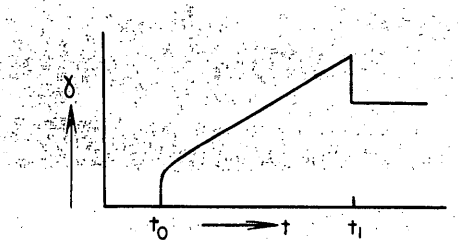

This model does not allow for retarded deformation and relaxation, which is observed with many substances. To explain this phenomenon, Voigt proposed a model in which a spring and a dashpot are coupled in parallel. The differential equation for this model is:

$$\eta_2 \frac{d\gamma}{dt} + E_2\gamma = P \qquad (2)$$

i. e., the strain is distributed between the spring and the dashpot so that the deformation of the spring is always equal to the deformation in the dashpot. The deformation given by this model as a function of time can be represented diagrammatically by:

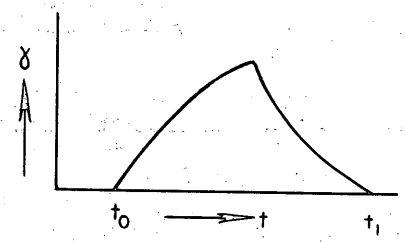

The solution of (2), if the stress is applied during the time $\underline{t} = t_1 - \underline{t_o}$, is:

$$\gamma = P/E_2(1-e^{-t/\tau}) \qquad (3)$$

where $\tau = \eta_2/E_2$ is called the retardation time. After removal of the load, $P = 0$ in Eq. (2) and the solution of (2) is given by:

$$\gamma = \gamma_o e^{-t/\tau} \qquad (4)$$

where τ is called the relaxation time, and in this case equals the retardation time. γ_o is a constant which might be used for the characterization of the sample at the instant the unloading started.

Neither the Maxwell nor the Voigt model alone suffice to represent the viscoelastic properties of ice. The experimental curves show that a model is needed which shows instantaneous elasticity, retarded elasticity, and flow. A model which approximates the behavior of ice at least to a certain extent may be represented by the following arrangement of springs and dashpots:

The deformation as a function of time is then given by the sum of the deformations, i. e.:

$$\gamma = \frac{P}{E_1} + \frac{P}{E_2}(1-e^{-t/\tau}) + \frac{P}{\eta_1}t. \qquad (5)$$

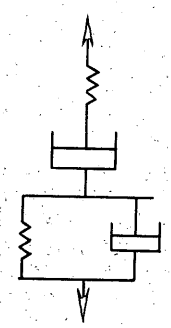

The diagram below shows a curve of the type of Eq. (5), and indicates how the parameters of Eq. (5) may be determined from the experimental curve.

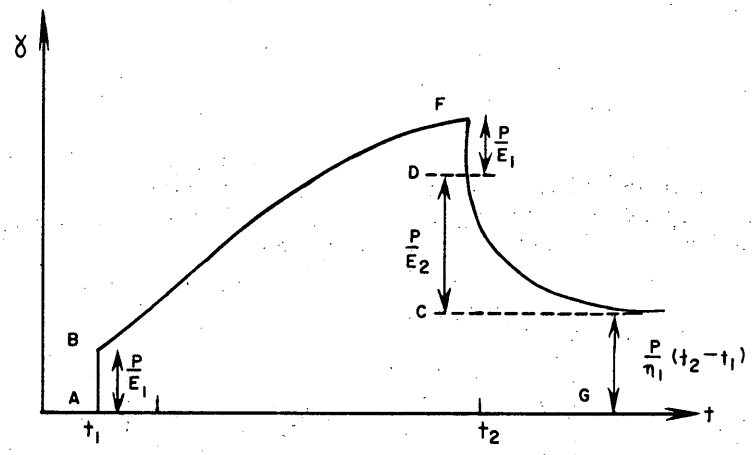

γ is connected with the observed $\tan\phi$ by

$$\gamma = \frac{4bh^3 \tan\phi}{3\ell^2} \tag{6}$$

and for our special arrangement according to (1):

$$\gamma = \frac{4bh^3}{3\ell^2}\,(2.96\times10^{-3})\Delta L \tag{7}$$

In these equations ℓ, b, and h are the length, width, and height of the bar respectively.

The application of (5) to our experimental results showed, however, that this equation describes the experimental results only approximately and only in some cases. An exact representation of the measured values is, certainly, not possible. For instance, Eq. (4) replaces (5) after removing the load and restoration of the purely elastic part of deformation. In this case, the logarithm of γ should be a linear function of t. Figure 6, an example of our measured values, clearly shows that such a linear dependency does not exist. In terms of the spring and dashpot elements, this means that one Voigt element is not sufficient for describing the viscoelastic behavior of ice. More than one relaxation time is needed. Eq. (4) should be replaced by:

$$\gamma = \Sigma_n \gamma_n e^{-t/\tau_n} \tag{8}$$

and correspondingly in (5) the e-function should be replaced by a sum of exponentials.

This is the usual procedure and, of course, a good fit of the curves can be effected. But this is always so if the number of constants is increased. For example it was found that a continuous spectrum of relaxation times is needed for the description of the creep behavior of alloy steel (Lequear and Lubahn, 1952).

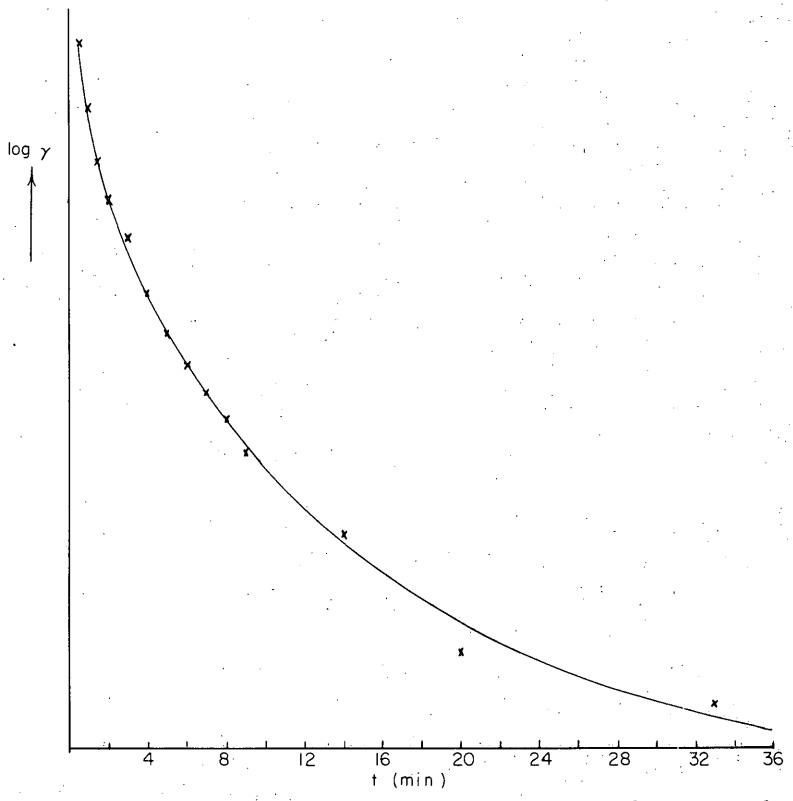

Figure 6. Log γ vs. t, time.

The physical significance of this procedure may be seen from the following consideration: Let us assume that, at deformation in the viscoelastic range, atoms are displaced in such a way that they can return to their original position. Otherwise a viscoelastic recovery would not be possible. One may assume, furthermore, that the force and, thus, also the rate of recovery are proportional to the degree of deformation, i. e., to the displacement of those atoms which have the tendency to move back to their equilibrium position. If γ characterizes the degree of deformation, the rate of relaxation will be given by:

$$-d\gamma/dt = a\gamma \tag{9}$$

where $\underline{a}$ is a constant. Therefore:

$$\ln \gamma = -at + \text{const.}$$

Because $\gamma = \gamma_o$ at $t = 0$, the value of the constant is $\ln \gamma_o$. Thus it follows:

$$\gamma = \gamma_o e^{-at} \tag{10}$$

This formula is identical with (4) if $\underline{a} = 1/\tau$ (τ = time of relaxation). Since the deformation of the lattice is different in different parts of the sample, and since the magnitude of the constant $\underline{a}$ depends upon the presence of faults, dislocations, etc. in the lattice, it can be understood that a certain range of relaxation times will be needed for a representation of the viscoelastic flow at recovery, so that (10) has to be replaced by (8).

To carry this picture further, one may also write in better approximation:

$$-d\gamma/dt = a\gamma - b\gamma^2.$$

The integration of this equation gives:

$$\gamma = \gamma_o/(e^{at}(1-\rho)+\rho); \quad \rho = \frac{b}{a}\gamma_o.$$

This equation describes the relaxation quite correctly as might be seen from the following table:

t(min)	$\gamma_{exp.}$	$\gamma_{calc.}$
0	3.95	3.95
1	3.28	3.36
2	3.00	3.02
3	2.78	2.80
4	2.65	2.65
5	2.55	2.55
6	2.45	2.45
8	2.30	2.33
10	2.27	2.25
15	2.17	2.13
20	2.10	2.06
40	1.95	1.98
65	1.95	1.95

But the agreement between observed and calculated intensities obviously is not significant because the numerical values of the constants which give this agreement are unreasonable ($|b| \gg a$).

Becker's theory. A theory which describes the observed data quite well was given by R. Becker (1925). Since more recent theories (Cottrell, 1953) lead to an expression which is identical with the one given by Becker, Becker's equation was chosen for representing our experimental data.

Instead of operating in the atomic or molecular range, Becker assumes the matter subdivided indomains of different mechanical properties. In the case of metal, for example, the domains could be represented by the randomly oriented crystallites. If a force acts on a material, its effect in different domains might be different. Those in a favorable position for gliding may glide. Others may resume stress. In case of purely elastic deformation the stress σ_o is given by:

$$\sigma_o = fP$$

where P is the load and f a constant. In the case of a viscoelastic deformation, some of the domains or particles will flow and thus the stress σ will be smaller in them. The flow alone effects a deformation of a particle, the quantity of which is given by:

$$\Delta\gamma = \frac{F}{E}\lambda(\sigma_o - \sigma).$$

$\underline{E}$ is the elastic modulus, $\underline{F}$ a factor depending upon the shape of the sample, and $\underline{\lambda}$ a constant. Thus the increase of deformation over that given by the elastic deformation alone is proportional to the diminution of stress in the particles affected by flow. The total deformation, pure elastic plus viscoelastic, is then given by:

$$\gamma(t) = \frac{F}{E}\left[P(t)+\lambda \sum_{1}^{N} (\sigma_o - \sigma)\right]. \tag{11}$$

Determining the value of the summation in this formula, Becker assumes that the diminution of stress with time is proportional to a magnitude $\rho = 1/\tau$, with τ = relaxation time of Maxwell. He further assumes that ρ varies from particle to particle and that this variation is given by a probability function $\underline{F}(\rho) \sim 1/\rho$, with the restriction that for small ρ-values $\underline{F}(\rho) = 0$, because contributions of particles with a small ρ can be neglected. Consequently it is $\underline{F}(\rho) = \underline{c}/\rho$ with the additional condition that

$$\int_{r}^{R} \frac{c}{\rho}\, d\rho = c \ln\frac{R}{r} = N_1$$

where $\underline{N_1}$ is the number of domains for which ρ is sufficiently large, $\underline{c}$ is a constant and $\underline{r}$ and $\underline{R}$ designate an upper and a lower limit of ρ, the lower limit chosen in such a way that for $\rho < \underline{r}$, $\underline{F}(\rho) = 0$ with good approximation.

Since the decrease of stress with time is proportional to ρ as well as to the magnitude of stress:

$$-\frac{d\sigma}{dt} = \rho\sigma. \tag{12}$$

In the following, we derive Becker's formula for constant load, since all our experiments have been performed under this condition. This derivation deviates from that given by Becker but leads to the same result for a constant load.

If the load is applied at $\underline{t} = 0$, a stress σ_o acts immediately on all domains. Under this condition the integration of (12) gives:

$$\sigma(t) = \sigma_o e^{-\rho t}.$$

Therefore:

$$\sigma_o - \sigma(t) = \sigma_o (1 - e^{-\rho t}). \tag{13}$$

With $\underline{F}(\rho)$ defining the number of particles with ρ between ρ and $\rho + d\rho$, from (13):

$$\Sigma(\sigma_o - \sigma) = \sigma_o \int_{o}^{\infty} (1 - e^{-\rho t}) F(\rho)\, d\rho.$$

With $F(\rho) = \underline{c}/\rho$ and inserting the above-defined limits of integration $\underline{r}$ and $\underline{R}$:

$$\Sigma(\sigma_o - \sigma) = c\sigma_o \int_r^R \frac{1-e^{-\rho t}}{\rho}\, d\rho$$

$$= c\sigma_o \left[\ln \frac{R}{r} - Ei(-Rt) + Ei(-rt)\right].$$

Substitution into (11) gives for the loading experiment, i.e., loading at $\underline{t} = 0$ with a constant load $\underline{P}$:

$$\gamma(t) = \frac{F}{E}\left\{P + \lambda c\sigma_o \left[\ln \frac{R}{r} - Ei(-Rt) + Ei(-rt)\right]\right\}.$$

Since $\sigma_o = fP$, with $c\lambda f = \beta$:

$$\gamma(t) = \frac{PF}{E}\left\{1 + \beta\left[\ln \frac{R}{r} - Ei(-Rt) + Ei(-rt)\right]\right\}. \qquad (14)$$

This formula is identical with the one given by Becker if the integration is carried out between limits $\underline{r}$ and $\underline{R}$.

If, on the other hand, plastic flow is involved also, a term $\frac{Pt}{\eta}$ has to be added, so that the complete equation is this case is:

$$\gamma(t) = F\frac{tP}{\eta} + \frac{F}{E} P\left\{1 + \beta\left[\ln \frac{R}{r} - Ei(-Rt) + Ei(-rt)\right]\right\}. \qquad (15)$$

If the load is removed at a time $\underline{t_1}$, it is, according to Boltzmann's theory, for $\underline{t} = 0$ at $\underline{t_1}$:

$$\gamma(t) = \frac{F}{E} P\beta\{-Ei[-R(t+t_1)] + Ei(-Rt) + Ei[-r(t+t_1)] - Ei(-rt)\}. \qquad (16)$$

Determination of the constants in Becker's equation from experimental data. Equations (14), (15), and (16) contain a relatively large number of constants which have to be determined: β, $\underline{R}$, $\underline{r}$, $\underline{E}$, and η. The easiest procedure for the determination of these constants seems to be the following:

First, one may reduce the number of constants by assuming $\underline{r} = 0$. In this case:

$$\lim_{r \to o} \left[\ln \frac{R}{r} + Ei(-rt)\right] = \ln\gamma' + \ln(Rt) = 0.5772 + \ln(Rt)^*$$

---

* $\ln\gamma' = \text{const} = \int_o^1 \frac{1-e^{-t}}{t}\, dt - \int_1^\infty \frac{e^{-t}}{t}\, dt.$

This follows directly if one uses the approximation for small values of x:

$$Ei(-x) \simeq \ln(\gamma' x) = \ln\gamma' + \ln x = 0.5772 + \ln x.$$

Hence, for $\underline{r} = 0$, (15) becomes:

$$\gamma(t) = \frac{PF}{E}\left\{\frac{tE}{\eta} + 1 + \beta[0.5772 + \ln(Rt) - Ei(-Rt)]\right\}. \tag{17}$$

The next step is an approximate determination of η. For this purpose, it is assumed that the relaxation curve represents approximately the deviation of the loading curve from linearity. How good or bad this approximation is can easily be seen by the degree of approximation of the difference curve to a straight line. Indeed, the difference curves are usually straight, at least at large values of $\underline{t}$. Thus η may be calculated from the straight part. Knowing η, the magnitude

$$\xi(t) = \gamma(t) - \frac{PFt}{\eta} = \frac{PF}{E}\{1 + \beta[0.5772 + \ln Rt - Ei(-Rt)]\} \tag{18}$$

can be calculated.

The next step is the determination of $\underline{R}$. For large $\underline{t}$ the product $\underline{Rt}$ is supposed to be large ($\gtrsim 4$), so that $\underline{Ei}(-\underline{Rt}) \sim 0$. It follows then from (18) with $\epsilon = \frac{PF}{E}$, $0.5772 = \alpha$:

$$\xi(t) = \epsilon[1 + \beta(\alpha + \ln R)] + \beta\epsilon \ln t = a + b \ln t \tag{19}$$

$$a = \epsilon[1 + \beta(\alpha + \ln R)]; \quad b = \beta\epsilon. \tag{20}$$

Hence, at large values of $\underline{t}$, the function $\xi(\underline{t})$ should be linear with respect to $\ln \underline{t}$ and $\underline{a}$ and $\underline{b}$ are given by the slope of the linear part of a plot $\xi(\underline{t})$ versus $\ln \underline{t}$ at large $\underline{t}$-values.

It follows from (20): $\ln R = \frac{a - \epsilon}{b} - a.$ (20a)

Substituting this value in (18) for any time $\underline{t}$ for which $\underline{Ei}(-\underline{Rt})$ is not too small, i.e., for a small value of $\underline{t} = \underline{t}'$, gives:

$$\xi(t') = \epsilon + \alpha\beta\epsilon + \beta\epsilon \ln R + \beta\epsilon \ln t' - \beta\epsilon Ei(-Rt')$$

$$= \epsilon + \alpha b + b \ln R + b[\ln t' - Ei(-Rt')] \tag{21}$$

$$= a + b[\ln t' - Ei(-Rt')].$$

Therefore:

$$-Ei(-Rt') = \frac{\xi(t') - a}{b} - \ln t'.$$

Table I. Evaluation of a bending experiment.

Remarks	t(min)	$\gamma(t)\times10^6$	$(P\eta/t)\times10^6$	$\xi(t)\times10^6$	$\xi(t)\times10^6$ calc I	$\xi(t)\times10^6$ calc II	$\gamma(t)\times10^6$ calc
At instant of loading:	0	0	—	—	—	—	—
	0	2.02	2.02	2.02	—	2.35	2.35
	0.5	3.43	2.23	3.20	3.20	3.20	3.43
	1	4.43	2.42	3.96	3.96	3.95	4.42
	1.5	5.24	2.63	4.54	4.59	4.58	5.28
	2	5.92	2.91	4.99	5.14	5.14	6.07
	2.5	6.65	—	5.49	5.62	5.62	6.78
	3	7.25	3.83	5.85	6.05	—	7.45
	3.5	7.94	—	6.31	6.43	—	8.06
	4	8.46	4.44	6.60	6.75	6.77	8.62
	5	9.67	5.27	7.34	7.36	—	9.69
	6	10.48	5.73	7.68	7.85	—	10.65
	7	11.28	6.25	8.02	8.27	—	11.53
	8	12.29	6.98	8.56	8.65	—	12.38
	9	13.10	8.27	8.91	8.97	—	13.16
	10	13.90	—	9.24	9.26	9.11	13.77
	15	17.33	—	10.34	10.36	10.16	17.15
	20	20.55	12.98	11.23	11.17	10.90	20.22
	29	25.79	—	12.28	12.21	11.81	25.32
	33	27.85	19.80	12.47	12.57	12.12	27.50
	44	33.45	24.79	12.95	13.38	12.77	33.27
	54	38.28	28.82	13.12	13.86	13.21	38.37
	61	41.71	$t-t_1$ $\gamma(t-t_1)$ relax	13.28	14.28	13.46	41.89
Unloading t_r (t_1 = 61) 0	61	40.09	0 0	—	—	—	40.04
0.5	61.5	38.89	0.5 1.20	—	—	—	39.19
1	62	38.08	1 2.01	—	—	—	38.46
1.5	62.5	37.48	1.5 2.61	—	—	—	—
2	63	37.08	2 3.01	—	—	—	—
3	64	36.67	3 3.42	—	—	—	—
4	65	36.07	4 4.02	—	—	—	—
5	66	35.67	5 4.42	—	—	—	34.54
6	67	35.34	6 4.75	—	—	—	—
7	68	35.06	7 5.03	—	—	—	—
8	69	34.78	8 5.31	—	—	—	—
9	70	34.46	9 5.63	—	—	—	33.82
14	75	33.65	14 6.44	—	—	—	32.80
20	81	32.52	20 7.57	—	—	—	32.04
33	94	32.04	33 8.05	—	—	—	31.08
44	105	31.43	44 8.66	—	—	—	30.61
54	115	30.63	54 9.46	—	—	—	30.31
63	124	30.23	63 9.86	—	—	—	30.11
73	134	30.02	73 10.07	—	—	—	29.93
97	158	29.62	97 10.47	—	—	—	29.64

From this equation $\underline{R}$ can be determined, since ϵ drops out. Equation (20a) may then be used to calculate ϵ and also $\underline{E}$ by means of the relation $\epsilon = \frac{PF}{E}$, since $\underline{P}$ and $\underline{F}$ are known. β can then be obtained from (20). Thus, all the constants are determined from the experimental data in more or less good approximation and the final adjustment by trial should also result in a value of $\underline{r}$.

The procedure will be illustrated by an example. The sample consisted of single crystals, about 1 cm long and 3 mm in diameter, with the $\underline{c}$-axis perpendicular to the large face of the sample. The dimensions of the sample were 7.20x1.95x0.274 cm^3. The distance between the knife edges was 6.35 cm and the load $\underline{P}$ = 92.15 g. Table I gives the results of the measurements. The values are reduced so that $\underline{F}$ = 1.

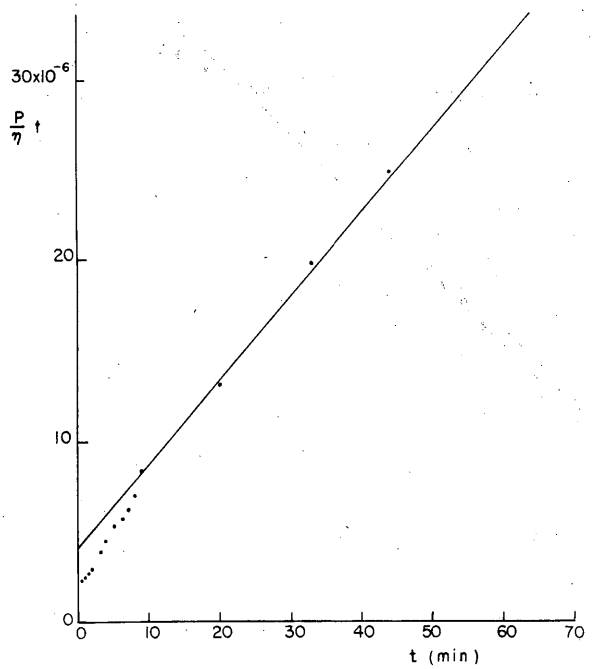

Figure 7. $\frac{Pt}{\eta}$ vs. t, time.

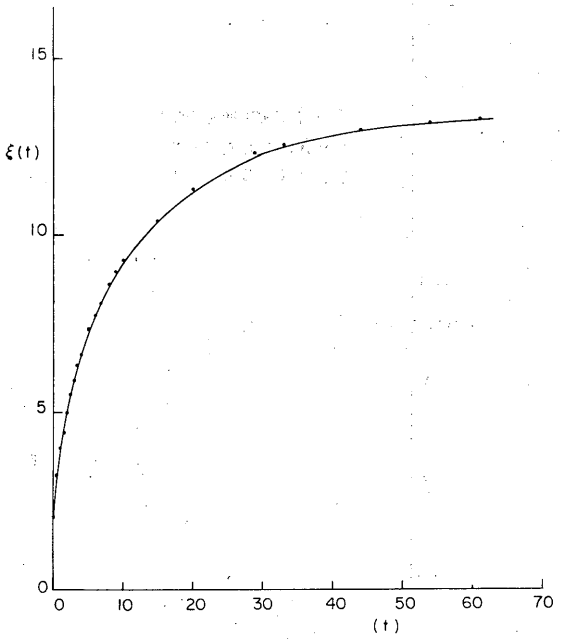

Figure 8. $\xi(t)$ vs. t, time.

The values $\gamma(t)-\gamma(t'-t_1)_{relax} = \frac{P}{\eta} t$, where $t' - t_1 = t$, and t_1 = the time at which the load is removed, are plotted against t in Figure 7. The slope of the straight line is 0.466, so that

$$\xi(t) = \gamma(t) - 0.466\, t \times 10^{-6}.$$

The function $\xi(t)$ vs t is shown in Figure 8, Figure 9 is a plot of $\xi(t)$ against log t. The curve of the experimental points in Figure 9 exhibits an s-shape. A major part at large t-values is linear, whereas at very high t-values the curve bends over towards the abscissa. This probably is caused by the term $Ei(-rt)$. Hence, the large linear part is used for the determination of constants a and b: $a = 2.87 \times 10^{-6}$. For the application of (21) we chose $t' = 1$ and $t' = 0.5$. Comparison of the two R-values obtained gives an idea of the reliability of the method:

$$-Ei(-R/2) = \frac{3.20-2.87}{2.77} - \ln\frac{1}{2} = 0.813$$

and

$$-Ei(-R) = \frac{3.96-2.87}{2.77} - \ln 1 = 0.393.$$

The first equation gives $R/2 = 0.341$ and the second one $R = 0.674$. The agreement is good enough and we put $R = 0.678$.

From (20a): $\epsilon = a - b(0.5772 + \ln R)$. $\epsilon = 2.35 \times 10^{-6}$.

Since $\epsilon = \frac{P}{E}$, we obtain immediately the elastic modulus:

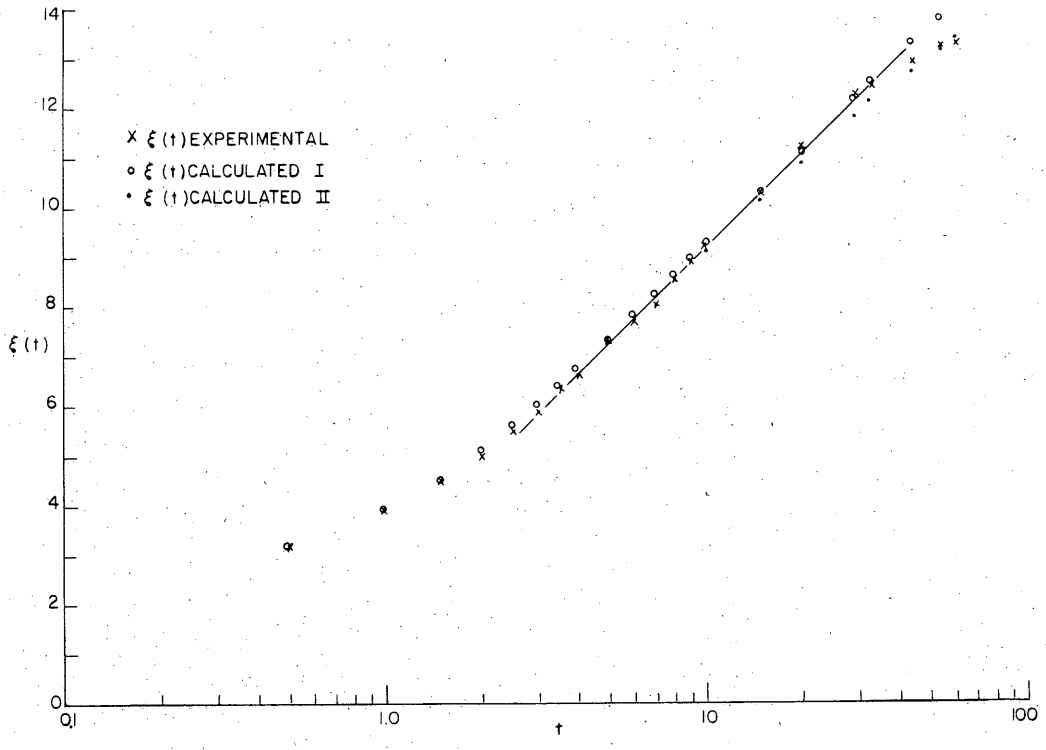

Figure 9. $\xi(t)$ vs. log t, time.

$$E = \frac{P}{\epsilon} = \frac{92.15}{2.35} \times 10^6 \text{ g/cm}^2 = 39.2 \times 10^6 \text{ g/cm}^2 = 392 \text{ kg/mm}^2.$$

This is a relatively small but still reasonable value.

From (20): $\beta = \frac{b}{\epsilon} = 1.18.$

Inserting the constants into (18) gives:

$$\xi(t) = 2.35 \times 10^{-6} \{1 + 1.18[0.577 + \ln(0.678t) - Ei(0.678t)]\}.$$

An inspection of Figure 9 or Table I shows that the values calculated by this equation, $\xi(t)_{\text{calc I}}$, agree rather well with the experimental values. The only discrepancies, at $t > 40$ min, indicate that the limit $r = 0$ is wrong.

For the determination of r this deviation can be used. For this purpose we consider that the ξ values are represented by:

$$\xi(t)_{obs} = \epsilon\left(1 + \beta \int_r^R \frac{1 - e^{\rho t}}{\rho}\, d\rho\right)$$

whereas the values $\xi(t)_{calc}$ were calculated according to:

$$\xi(t)_{calc} = \epsilon\left(1 + \beta \int_0^R \frac{1 - e^{-\rho t}}{\rho}\, d\rho\right).$$

The difference, therefore, is given by:

$$\Delta\xi(t) = \xi(t)_{calc} - \xi(t)_{obs} = \epsilon\beta\{\int_0^R f(\rho)\,d\rho - \int_r^R f(\rho)\,d\rho\}$$

$$\Delta\xi(t) = \epsilon\beta \int_0^r f(\rho)d\rho$$

$$f(\rho) = \frac{1-e^{-\rho t}}{\rho}\,.$$

Therefore: $\Delta\xi(t) = \epsilon\beta(0.5772 + \ln(rt) - Ei(-rt))$

or

$$\ln(rt) - Ei(-rt) = \frac{\Delta\xi(t)}{\epsilon\beta} - 0.5772. \qquad (22)$$

This equation can then be used for calculating r from $\Delta\xi(t)$ at large values of t. This can easily be achieved by plotting the function $f(x) = \ln x - Ei(-x)$. The result is: $r = 0.0052$. The values $\xi(t)_{calc\,II}$ in the table were obtained by using Eq. (14) and are also plotted in Figure 9. One sees that the agreement with the experiment is improved. The deviations are within, or very close to, the limit of experimental error, as can be seen from Figure 10, where the experimental $\gamma(t)$ -values and the values calculated by Eq. (15) are plotted. The calculated numerical values, $\gamma(t)_{calc}$, are also given in the table.

Eq. (16) may now be used to calculate the part of the curve for $t>61$ min, i.e., the relaxation after removing the load. Since plastic deformation was observed, a constant term $\frac{P}{E} \times \frac{61}{\eta} = 28.43\times10^{-6}$ has to be added to the right side of Eq. 16. To obtain a better fit, this constant value was slightly increased to 28.93×10^{-6}. Figure 11 shows the observed and calculated values. The line is drawn through the experimental points so as to get the best agreement with the calculated values. There is no doubt that some of the experimental points (e.g. at $t_r = 33$ and 44) are too high, and this deviation also might give an idea about the limit of error of the experimental values. The deviations between the line and the calculated points are almost as large as the deviation between the line and the experimental points. As also might be seen from Table I the theoretical curve fits the experimental one exactly at the extremes, i.e., at $t = 61$ ($t_r = 0$) and $t = 158$ ($t_r = 97$). But there is a definite deviation from the shape of the experimental curve. This could indicate that perhaps another mathematical function should be used for describing the relaxation function. But plotting $\gamma(t-t_1)_{relax} = \gamma(t_r)$ with respect to $\ln t_r$ (Fig. 12) gives a curve corresponding exactly to that of the $\xi(t)$ function (Fig. 9). For times larger than $t_r = 3$ the plot is linear, i.e., the function seems to be purely logarithmic. But the measured values at $t-t_1>3$ clearly deviate from that straight line, indicating that a function of the type given for $\xi(t)$ describes the experimental results right. Indeed, changing the constants slightly gives a good agreement as might be seen from Figure 12. Here the calculated points are obtained with $R = 0.660$, $r = 0$, $\beta = 2.34$ and $\epsilon = 0.865\times10^{-6}$. The latter value leads to an elastic constant $E = 1065$ kg/mm^2. The values given in the literature vary between about 200 and 1100 kg/mm^2. The lower values are obtained by bending of bars whereas the adiabatic method (propagation of sound) results in values between 900 and 1100 kg/mm^2. Thus both values, one obtained from the loading curve and the other from the relaxation curve, are within a reasonable range. It would be of interest to find out whether such a difference is always found. The two R-values agree practically and the difference between $r = 0$ and $r = 0.0052$ is not very relevant.

From the plot of $\gamma(t)-\gamma(t-t_1)$ versus t (Fig. 7) we obtain:

$P/\eta = 0.466\times10^{-6}$ cm^2/min. This gives $\eta = 1.16\times10^{13}$ poise.

Experimental results

Measurements on single crystals. Measurements on creep were carried out on single crystals as well as on polycrystalline samples (see Fig. 13). The quantitative evaluation of the curves was not carried out by means of Becker's equation at the time covered by this report, but they were evaluated using the simpler equation:

$$\gamma = \frac{P}{E_1} + \frac{P}{\eta_1} + \frac{P}{E_2}(1 - e^{-tE_2/\eta_2}). \qquad (23)$$

This equation does not represent exactly the observed curves but is a rather crude approximation (as mentioned above). The constants of Eq. 23 are given in Table II.

Table II. Calculated viscoelastic constants.

Sample No.	E_1 (dyne cm^{-2} x10^{-10})	E_2 (dyne cm^{-2} x10^{-10})	η_1 (poise x10^{-13})	η_2 (poise x10^{-13})
IIIa	5.96	10.16	22.2	2.41
IIIb	8.50	—	—	—
IVa	5.72	6.62	15.0	2.42
IVb	6.27	8.72	13.2	2.63
Va	7.90	3.01	21.2	4.38
VIa	3.29	0.38	0.202(0.165)	0.328
VIb	4.08	0.43	0.468(0.222)	0.291

One sees from the table that the elastic modulus (E_1) varies rather strongly. Even two specimens cut from the same large crystal (cf. VIa and b, IIIa and b, IVa and b) do not give identical values, differences being of the order of up to 25%. The highest value is that of sample IIIb (8.50×10^{10} dyne/cm^2 = 870 kg/mm^2) which is within 10% of the average values obtained by dynamical methods. The most striking result of these experiments, however, is the fact that E_1 and especially η_1, is relatively low for specimen VIa and b. If we use the relation

$$\eta = \frac{E}{2(1+\mu)} \times \tau$$

with μ = Poissons ratio (0.30) and τ = Maxwell's relaxation time, we may express E and η by only one characteristic constant, namely τ.

The following values are obtained:

Sample	τ_{sec}	τ_{hr}
IIIa	9.30×10^3	2.6
IVa	6.5×10^3	1.8
IVb	5.3×10^3	1.5
Va	6.7×10^3	1.9
VIa	0.15×10^3	0.04
VIb	0.29×10^3	0.08

Whereas the relaxation times for specimens III - V are of the order of 2 hr, the relaxation times for specimen VI are only of the order of a few minutes. This large difference between sample VI and the other ones can be explained in the following way:

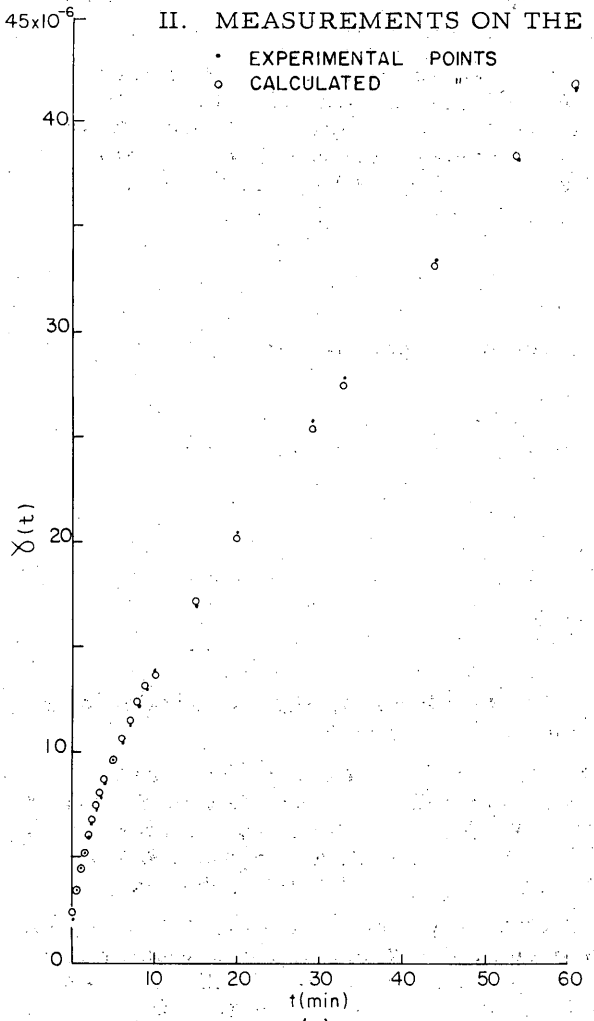

Figure 10. $\gamma(t)$ vs. t, time.

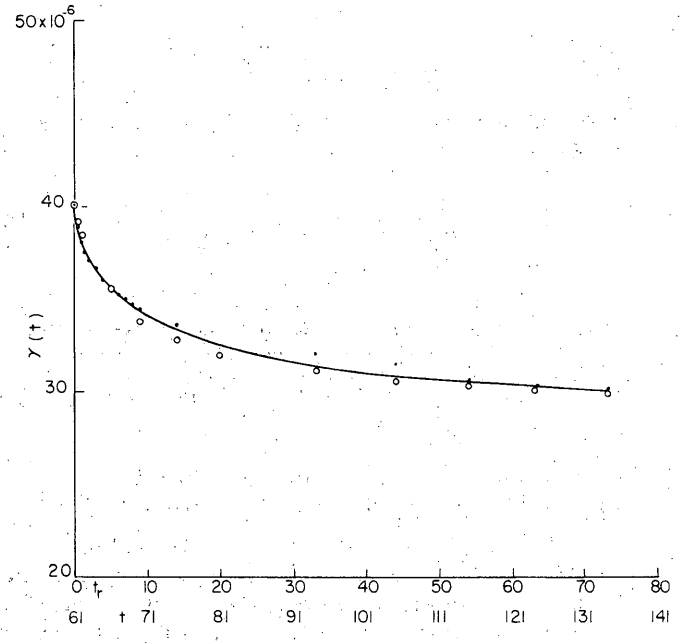

Figure 11. $\gamma(t)$ vs. t_r, time after removing the load.

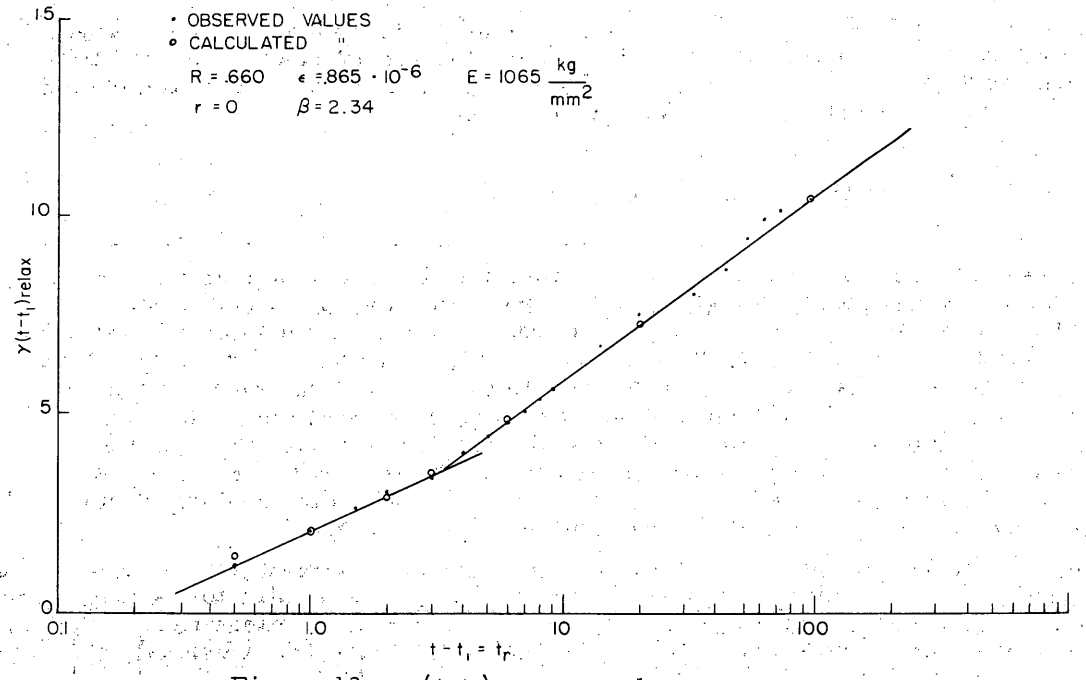

Figure 12. $\gamma\,(t-t_1)_{relax}$ vs. ln t_r.

When the load is applied to a beam of rectangular cross section A, it will deform the beam in such a way that the fibrile elements are elongated parallel to the neutral axis of the beam. These fibrile elements will therefore be subjected to a force which is parallel to the direction of elongation. Consider a plane in the beam whose normal makes an angle θ with the force acting on a fibrile element. This plane will have a cross-sectional area $A/\cos\theta$. The stress S on this plane will be given by:

$$S = \frac{P\cos\theta}{A} = s_x \cos\theta.$$

From the vector diagram (Fig. 14) it is seen immediately that the normal stress s_n is given by:

$$s_n = S\cos\theta = s_x\cos^2\theta = s_x\frac{1+\cos 2\theta}{2}$$

and that the shearing stress s_s is given by:

$$s_s = S\sin\theta = s_x\cos\theta\sin\theta = \frac{1}{2}s_x\sin 2\theta.$$

It therefore follows that the normal stress is zero at $\theta = 90°$ while the shearing stress is maximum and equal to the normal stress for the angle $\theta = 45°$.

The ice samples which seem to be subject to a maximum shearing stress are obviously the samples VIa and VIb, which exhibit greatest flow. According to the above argument, maximum shearing stress would occur on a plane of these ice samples which makes an angle of 45° with the long axis of the specimen. For samples VIa and VIb, such a plane would either cut the optical axis at a right angle or lie along that axis.

It can be shown that the plane which makes a right angle with the optical axis is also characterized by the fact that the density of hydrogen bonds directed perpendicular to it is less than for other planes of the ice lattice with low crystallographic indices. Hence, gliding parallel to it should be easy, and it may be concluded that this plane is responsible for the extraordinary slippage exhibited by samples VIa and VIb.

As a crude hypothesis, it may be assumed that the forces acting on the specimen during gliding cause a rupture of hydrogen bonds. The force exerted on the above-mentioned plane is equal to $(90)\cdot(980)\cdot(\cos 45°)$ g. If this force is acting over a distance one-half that between hydrogen bonds, namely

$$\tfrac{1}{2}\sqrt{3}\,r_o\cos 19.5° \quad (r_o = 2.76\text{Å}),$$

and it is assumed as a very rough approximation that the force is constant over this range, then the work expended is 1.35×10^{-3} ergs. This energy is sufficient to break 4.8×10^{9} hydrogen bonds, if the energy of the hydrogen bond is taken as 4 kcal/mole or 2.8×10^{-13} ergs/bond. Since one hydrogen bond occupies an area of $2.31\ r_o^2$, 4.8×10^{9} hydrogen bonds cover an area of 8×10^{-6} cm^2. But the area of the plane in our specimens was of the order of 1 cm^2. Hence it appears that the gliding of the plane does not involve the simultaneous rupture of all the hydrogen bonds in the plane. This is in accord with the experimental results on metals (Shockley, 1949, Leschen et al., 1948) and shows that, in the case of ice also, slippage starts with the breaking of relatively few intermolecular bonds at places where the lattice is distorted.

These results on single crystals were supplemented by investigations on specimens which contained a large single crystal with the c-axis perpendicular to the large face of the bar and a few smaller crystals with more or less random arrangement. The type of creep-curves obtained with these samples is shown in Figure 15. Obviously the major

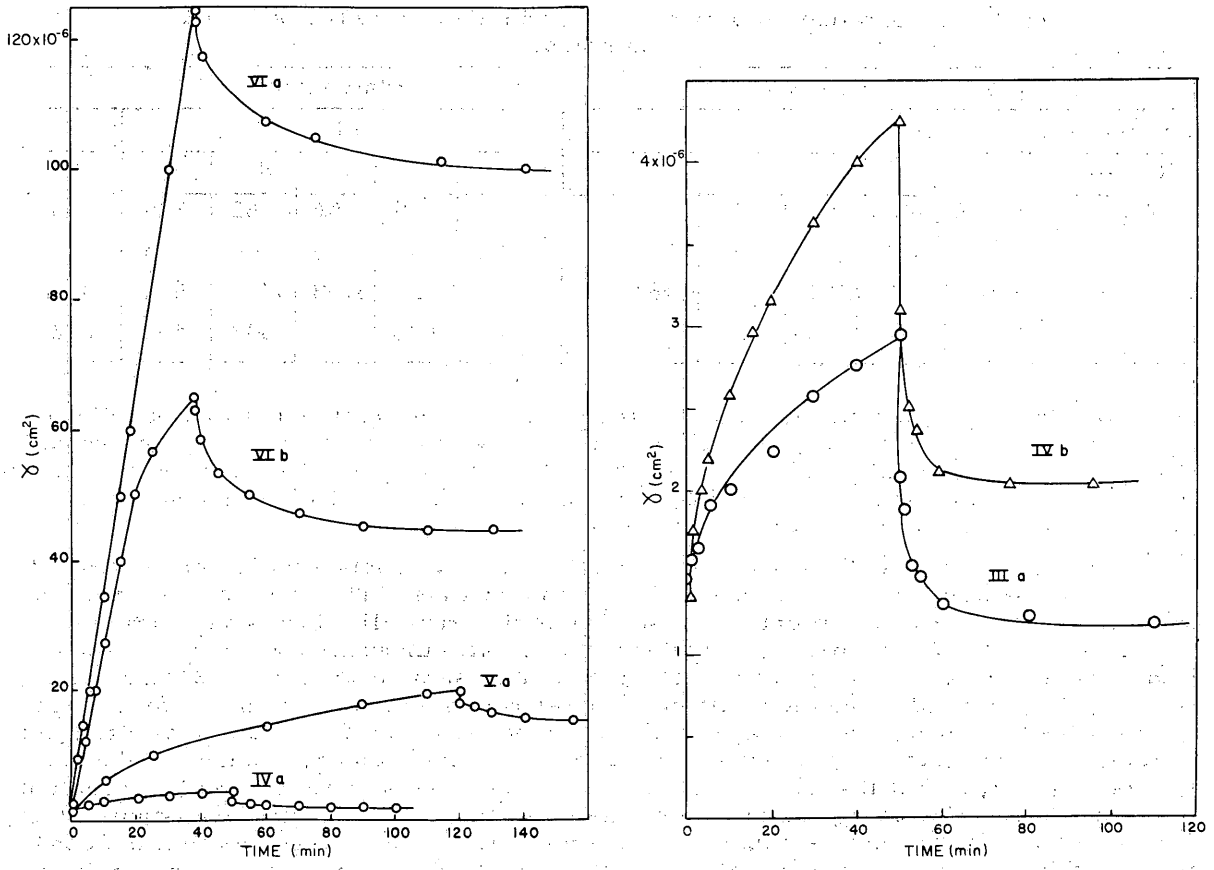

Figure 13. Deformation vs. time, single crystals.

IIIa - c-axis parallel to length of bar. IVa, b - c-axis perpendicular to large face of bar. Va - c-axis inclined 20° to large face of bar and 20° to length of bar. VIa, b - c-axis inclined 45° to large face of bar and 70° to length of bar.

part of the sample, namely the large single crystal, was practically not deformed, in agreement with the experiment on sample IVa. Hence the whole force acted only on the few smaller crystals which were able to creep because of their orientation. Consequently the creep curve shows the characteristics which are observed if a large load is acting. Initially the creep curve bends slightly towards the time axis but then bends toward the strain axis. Griggs and Coles (1954) also found this behavior in ice compressed under large loads.

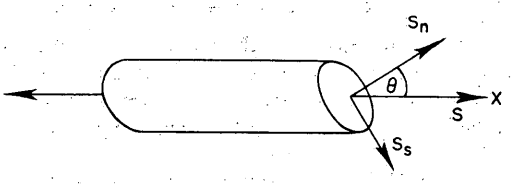

Figure 14. Vector notation of stresses.

Measurements on polycrystals. The strain-time curves of polycrystals are similar in principle to those of single crystals. To check the reproducibility of the experimental results, measurements were made of samples cut from the same batch, and repeated measurements were carried out on the same sample.

Table III. Evaluation of bending experiments on polycrystalline samples.

	Batch 1					Batch 2					
Sample No.	18		19			21					22
Run No.	1	2	1	2	3	1	2	3	4	5	1
E_1	420	420	405	374	374	348	340	306	252	209	293
E_2	241	237	206	192	192	115	106	99	90	63	115
η_1	5981	8674	8741	11870	5762	3166	7065	6803	3796	1530	2387
η_2	1534	1488	1469	1227	1467	865	686	612	533	468	632

In all these polycrystalline samples the c-axis of the crystallites was parallel to the long axis of the specimen. Otherwise the orientation was at random. The results, evaluated by using equation 23, are given in Table III. Samples 18 and 19 were cut from one batch of ice and samples 21 and 22 from another. Figure 16 is a graph of the experimental data obtained with sample 18.

Table III shows that the elastic constant E_1 is fairly constant within one batch but tends to decrease within the sample with successive runs. The same seems to be the case for E_2. This would indicate that the elastic deformability increases with the number of repetitions of loading and unloading. In all our experiments, η_1 shows a remarkable increase at the first repetition (run 2 of sample 18, 19 and 21) and then a decrease. This would mean that, after the first relaxation, a certain reinforcement against plastic flow has taken place, which disappears again if the plastic deformation is repeated. The experiments on sample 21 seem to show that η_2 changes in the same way as E_1 and E_2. But this may be accidental, as η_2 seems to remain rather constant for sample 19. Also the η_2 values are not as well defined as the other constants. Comparing the first runs of samples of the same batch, one recognizes that the constants agree within a limit of error of about 5 to 25% for E_1, E_2 and η_2 whereas the limit of error is larger for η_1. We think that this error is due not to a failure of our experimental device but to differences in the structure of different samples of the same batch. The differences between samples of two different batches are much larger (Table IV).

The viscoelastic flow was also measured on ice samples which were heated and cooled repeatedly, to find out whether this treatment influences the constants of Eq. 23. Three samples from one batch of ice were investigated. No. 1 was tested in the original state. No. 2 was treated five times by cooling it to -78C overnight and warming it up to about -5C during the day. For No. 3, the operation was repeated ten times. The constants obtained are given in Table V.

The increase of the elastic constant E_1 in No. 3 is remarkable and seems to be beyond our limit of error. It is also interesting to note that η_1-values of different samples of the same batch vary much more than the E_1-values. Hence the effect of alternating cooling and warming seems to be an increase of the elastic modulus.

Table IV. Comparison of elastic and viscoelastic constants for specimens from different batches. (Mean values of Run 1.)

	Batch 1 (Samples 18, 19)	Batch 2 (Samples 21, 22)
E_1	413	321
E_2	225	115
η_1	7361	2777
η_2	1502	749

Table V. Influence of repeated heating and cooling on the elastic and viscoelastic constants.

	Sample		
	No. 1	No. 2	No. 3
E_1	327	361	578
E_2	131	275	132
η_1	4030	9630	3360
η_2	1231	1407	863

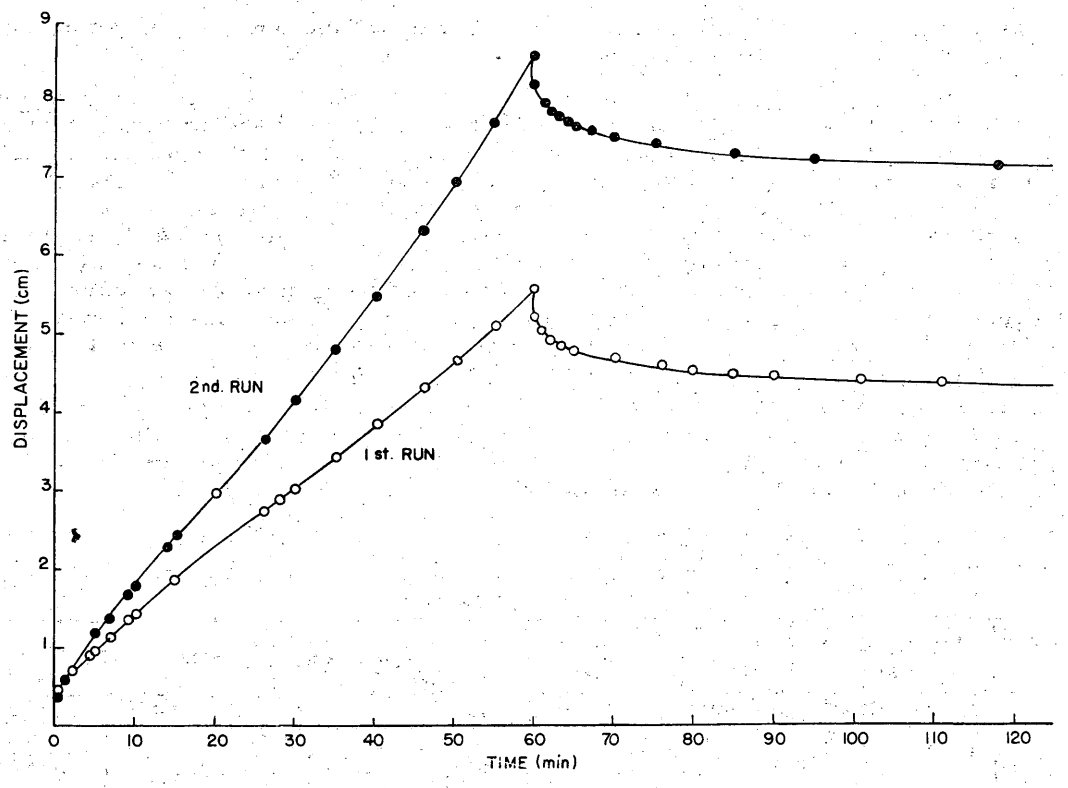

Figure 15. Displacement vs. time, specimen containing a large single crystal with the c-axis perpendicular to the large face of the bar and a few smaller crystals with more or less random arrangement.

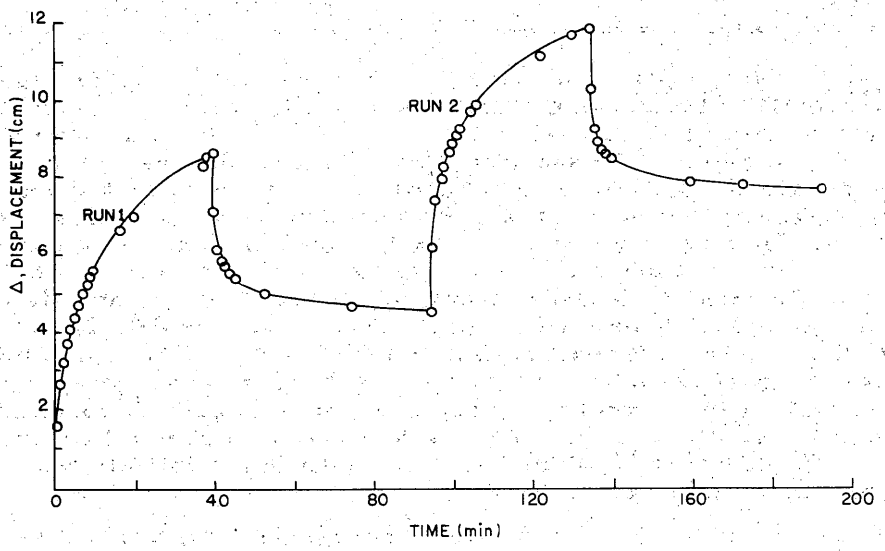

Figure 16. Displacement vs. time, polycrystalline sample 18 (Table III); c-axis parallel to long axis of specimen.

The results of bending experiments on polycrystalline ice samples which were evaluated by Becker's formula are given in Table VI.

In most cases $\underline{r}$ is assumed to be zero. For sample 2 only, the value of $\underline{r}$ was determined and the evaluation was carried out for both $\underline{r} = 0$ and for the actual value of $\underline{r} = 0.005$/min. It can be seen that the other constants do not change much if $\underline{r} \neq 0$. Hence the approximation $\underline{r} = 0$ is good enough for our purposes. The elastic modulus is given in dyne/cm^2. To obtain its value in kg/mm^2, the figures given in the table must be multiplied by 1.02×10^{-8}. The observed values vary between 240 and 420 kg/mm^2. Dorsey (1940) gives values between about 600 - 1000 kg/mm^2 for sheet ice (load applied in the direction of the c-axis) and between 220 and 620 kg/mm^2 for granular ice. Our values seem to correspond to the latter data. The dependency of $\underline{E}$ upon the orientation of the c-axis in the polycrystalline samples seems to be small, if any. For sample 3 no $\underline{\eta}$-value could be determined. No straight line at large $\underline{t}$ values was obtained by subtracting the relaxation curve from the loading curve. Thus, strain hardening might have taken place in this case. The $\underline{R}$-values lie in the range of 0.2 to 0.7, corresponding to relaxation times of 5 to 1.5 min. Only for sample 3 a relatively low relaxation time of 0.1 min is observed.

Table VI. Evaluation of bending experiments on polycrystals, by Becker's equation.

Sample No.	Orientation of c-axis	$E\left(\frac{dyn}{cm^2}\right)$	R/min	r/min	β	η(poises)	$\bar{\rho}(sec^{-1})$	$\frac{\beta R}{\bar{\rho}}$
1	⊥ to width	2.88×10^{10}	.29	—	.416	4.05×10^{13}	2.8×10^{-4}	4.3×10^{2}
2	⊥ to large face	3.61×10^{10}	.58	—	1.15	1.16×10^{13}	12.5×10^{-4}	5.3×10^{2}
2	"	3.84×10^{10}	.67	.005	1.18	1.16×10^{13}	13.2×10^{-4}	6.0×10^{2}
3	∥ to width	4.11×10^{10}	9.0	—	.294	—	—	—
4	∥ to large face	4.11×10^{10}	.15	—	.584	6.82×10^{13}	2.4×10^{-4}	3.7×10^{2}
5	random	2.35×10^{10}	.62	—	.54	1.21×10^{13}	7.7×10^{-4}	4.4×10^{2}

Discussion of the results. Comparing the values of the viscosity η for polycrystalline samples with those of the single crystals, we find differences which are beyond the limit of our experimental error. The reason for this is obvious. The single crystals were oriented in such a way that the shear strength on the gliding plane was either very small or very large. Thus the η-values give the two extremes for the single crystals. Consequently, in polycrystals we find values between these extremes. Hess (1902) determined the viscosity of ice by the method of bending bars, but his values deviate from other values of η found in the literature by several orders of magnitude. This is due to the fact that Hess did not distinguish between plastic flow and viscoelastic creep, but used the rate of flow generated by both processes for the calculation of η. Consequently his values are much too small and also depend upon the time of bending. Other values for polycrystalline ice (Dorsey 1940) agree well with our results. The figures reported for the viscosity of glacier ice, for example, lie between 0.6 and 8.5x 10^{13} poises at temperatures comparable to the ones at which our measurements were carried out. Hence our measurements, carried out in a relatively short time of observations, seem to be quite correct.

As might be seen from Eq. 14, $\beta = \lambda f c$, where λ and $\underline{f}$ are constants. Also $\underline{c}$ is a constant, but it depends upon the mean plasticity $\bar{\rho}$ of the sample. As shown by Becker it is:

$$c = N\bar{\rho}/(R-r)$$

and, if r is small with respect to R, can be approximated by $c = N\bar{\rho}/R$. Here N means the number of domains within the sample. Hence:

$$\beta = \lambda f N\bar{\rho}/R \qquad \text{or} \qquad \frac{\beta R}{\bar{\rho}} = \lambda f N.$$

According to Becker, the constants λ, f, and N are not independent of each other, so that for a cylindrical sample under homogeneous stress $\lambda fN = 1$. Now, $\bar{\rho}$ can be calculated from E and η. Assuming that Poisson's ratio is about 0.3, $\bar{\rho} = E/2.5\eta$. Hence:

$$2.5\,\frac{\beta \times R\eta}{E} = \text{const.}$$

The last column of Table VI shows that the equation is indeed fulfilled with good approximation. The value of the constant is about 450. The β values vary in the ratio 1:4, the E values are rather constant (ratio of variation less than 1:2) and the η values vary in the ratio 1:6, whereas the variation of the $\beta R/\bar{\rho}$ value is less than 1:2. Hence, the constancy of $\beta R/\bar{\rho}$ seems to be significant.

Hooke's law. Young's modulus can be determined in two different ways, either using the instantaneous deformation at the moment when the load is applied or using Becker's equation. The first method has the disadvantage that creep also starts immediately after applying the load and that a certain amount of time always elapses before the experimenter can make the first reading. But, since the extrapolation of the creep curves to t = 0 agrees in most cases with the observed values, the influence of creep at the time of reading the instantaneous value of deformation is negligible. This is also shown by the fact that the E-values determined in both ways agree rather well with each other.

It, therefore, was also possible to check whether or not Hooke's law is fulfilled. Figure 17 shows results obtained on single crystals. Obviously, these crystals follow Hooke's law and Young's modulus does not, or only to a very small extent, depend upon the orientation of the crystal.

Viscoelastic flow of mixed crystals ice-NH_4F. Experiments on the viscoelastic flow were also carried out on crystals of ice mixed with ammonium fluoride (see section III). These bars of ice were grown by placing two rigidly connected plates of aluminum in a bath of water. The plates were plane and parallel and $^1/_8$ in. apart. The water was cooled to about 3C and then a circular cylinder of 1 cm diam, filled with powdered dry ice, was placed on the center of the upper plate. In this way, polycrystalline samples can be prepared quickly. Because the crystallization occurs rather rapidly, the concentration of NH_4F in the sample should correspond to the concentration of the solution. By storing the samples for a couple of days a uniform distribution of the NH_4F in the samples can be achieved. Distilled water was used to prepare the

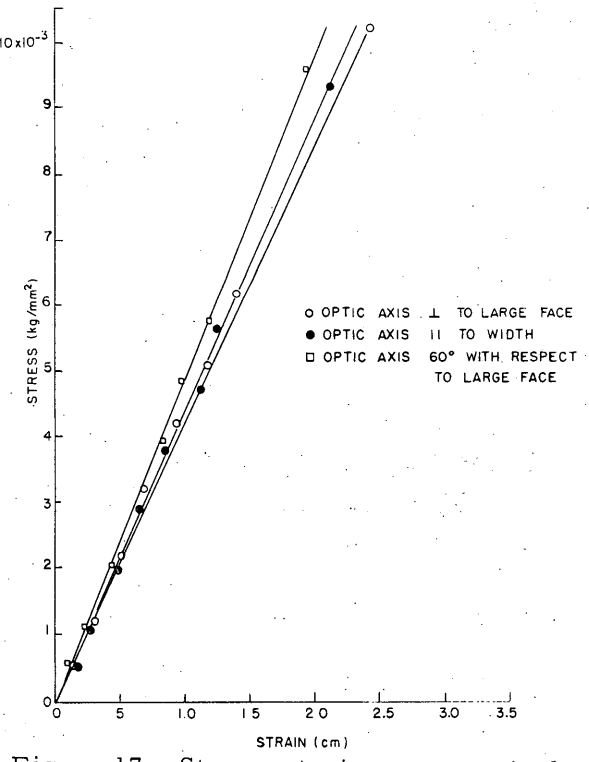

Figure 17. Stress-strain curves, single crystals of ice.

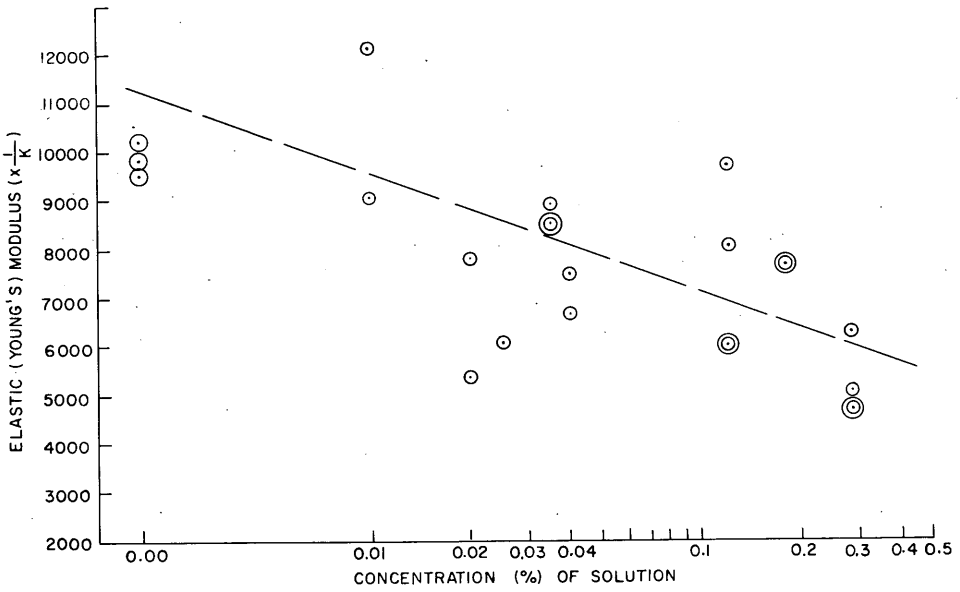

Figure 18. Young's modulus vs. concentration of NH_4F. Temp. = -2.5C±2C.

solutions, and the plates and the container were washed carefully and boiled in distilled water for at least 15 min before use.

The creep curves obtained for samples of varying composition show the same characteristics as those for pure ice. The characteristic constants vary within a certain range in a manner similar to that found for pure ice. A plot of the elastic modulus versus the concentration of NH_4F (Fig. 18) seems to indicate that the Young's modulus decreases with increasing concentration of NH_4F.

Summary. The study of viscoelastic creep of ice has shown that the hexagonal base plane is the gliding plane at plastic deformation; that Becker's equation can be used for the description of the viscoelastic creep of ice; and that mean values of the constants given in Table VI can be used for calculating the viscoelastic flow of ice.

The continuation of these investigations should provide more insight into the mechanism of elastic creep in ice. For this purpose more recent theories might have to be taken into consideration also. The fact that some of these theories lead to equations identical with Becker's (only with another significance of the constants) emphasizes the value of the present evaluation.

III. DIELECTRIC MEASUREMENTS ON ICE-NH_4F MIXED CRYSTALS

Formation of ice-NH_4F mixed crystals

Introduction. Intersolubility of different non-reacting chemical compounds depends mainly on the interactions and - in the solid state - volume relations between these compounds. In the gaseous phase, where the interactions between molecules of the same or of different kinds are slight, it is possible to form a macroscopically homogeneous mixture of any composition. In the liquid phase, association occurs between molecules of the same kind, and solubility is possible only if association of comparable strength can also occur between molecules of different kinds. In the solid phase, not only bonding between molecules or ions, but also the shape and dimensions of the different particles must be considered. The more complex the shape of the particles, the smaller is the probability that they would intermingle in the solid state with particles of a different kind. However, even spherical particles of two kinds cannot form solid solutions if their interatomic bonds are not of similar character or if

their effective radii differ too much. The character of bonding is an important factor in the formation of solid solutions. Ionic bonding is isotropic, and hence the shape and amount of charge of the particular ions are not as important as their volume. On the other hand, association between covalent compounds requires certain preferred configurations of the molecules for maximum stability; hence solubility must depend largely on the shapes of the different molecules. If polar groups are present in a covalent compound they have a predominant influence on the arrangement in solid state. Consequently formation of solid solutions will require a solute having both a similar shape and polar groups.

The water molecule can be considered as consisting practically of only two polar O-H-groups having the oxygen atom in common. A small positive charge is associated with each H-atom and a negative with each oxygen, so that, although the H_2O molecule as a whole is electrically neutral, the charge distribution within the molecule is not symmetrical, and the molecule represents an electrical dipole. It is known from spectroscopic data that the H-O-H bond angle is circa $104\frac{1}{2}°$, and the O-H distance is circa 1.0A. It was believed that, in ice, the H-O-H angle widens to 109° so as to form a perfectly tetrahedral configuration. At least from a simplified viewpoint, an H_2O molecule in ice can be considered as a regular tetrahedron with positive charges in two corners and negative charges in the other two, each charge being equal to 0.175e. Each molecule in ice has four nearest neighbors placed tetrahedrally at a distance of 2.76 Å, with one H-atom located between each two oxygens; the crystal structure is open, tridymite-like.

The position of the oxygen atoms has been determined accurately by x-rays. The location of hydrogens has been investigated by neutron diffraction (Wollan et al., 1949). The results of the neutron diffraction experiments can best be explained by the assumption that each oxygen atom has two close hydrogen neighbors, so that H_2O molecules are present in ice. But, in spite of this, the hydrogen atoms are arranged somewhat at random, the randomness being restricted by the conditions that only one hydrogen is located between two oxygens, that this hydrogen atom is bound to one of the oxygens, and that only two hydrogens can be bonded to one oxygen. These restrictions do not follow directly from the neutron diffraction experiments but they are in agreement with the residual entropy of ice (Pauling, 1948; Bjerrum, 1951) and with other observations on hydrogen bonds where a similar randomness of H-atoms was found (Bacon and Pease, 1953). There is no doubt that between H_2O molecules in ice there are hydrogen bonds which essentially are caused by electrostatic forces (Pauling, 1948; Briegleb, 1949), but in which covalent bonding is also involved to a certain extent (Nukasawa et al., 1953). This makes ice a rather peculiar solid. Since the hydrogen bonds are rather strong and control the extraordinary properties of ice and water (high melting and boiling points, anomalous density maximum at 4C, etc.), a single crystal of ice can be considered as one three-dimensional macromolecule. Therefore, very special requirements have to be fulfilled by a substance forming mixed crystals with it. Former attempts to form solid solutions of ice failed. Reports that hydrogen peroxide is soluble in ice (Giguere and Maass, 1940; Kubachewski and Weber, 1950) were shown to be erroneous (Mironov and Bergman, 1951).

Regarding this question, it might be advantageous to consider ice as analogous to SiO_2. In SiO_2 each silicon is surrounded by four oxygens. But the oxygens are located midway between two silicons and thus connect two silicons much more strongly than do the hydrogens in water. In spite of this, two silicons in SiO_2 can be replaced by one aluminum and one phosphorous, thus forming mixed crystals between SiO_2 and $AlPO_4$. The possibility of mixed crystal formation in this case might be connected with the fact that Al and P together have eight outer electrons just as two silicons do, and that the affinity of Al and P towards oxygen is rather large. Furthermore, the crystal structures of $AlPO_4$ and SiO_2 are related. Applying the same considerations to H_2O, one sees that N+F has the same number of outer electrons as two oxygens, and that both these elements have a strong affinity towards hydrogen. Therefore, NH_4F might form mixed crystals with ice just as $AlPO_4$ does with SiO_2. Furthermore NH_4F has the Wurtzite structure, i.e., there is a tetrahedral surrounding of the N atoms by F ions with hydrogen bridges between them. This resembles ice. NH_4F also gives very

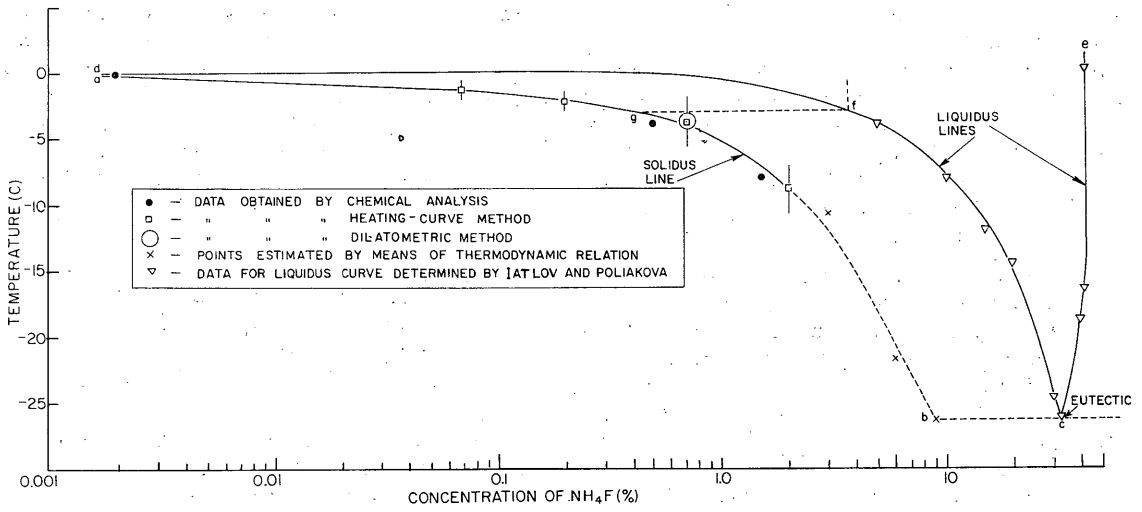

Figure 19. Phase diagram for the system H_2O-NH_4F.

similar diffuse star-shaped streaks on Laue x-ray patterns, which were attributed to thermal vibrations of hydrogen nuclei (Lonsdale, 1948). The distance N-F is 2.66 Å as compared with 2.76 Å in ice.

For the system H_2O-NH_4F, the liquidus lines and the eutectic point have been determined by Iatlov and Poliakova (1945). Table VII and the liquidus curve in Figure 19 are taken from their report. Although the solid phases in their table are listed as ice, ice+$NH_4F \cdot H_2O$, $NH_4F \cdot H_2O$+NH_4F, and NH_4F, the composition of the ice was obviously not determined by these investigators.

Table VII. Liquidus line for the system H_2O - NH_4F.

Temperature (C)	%NH_4F in Liquid	Solid Phase
- 4.1	5.0	Ice
- 8.2	10.0	Ice
-12.1	15.0	Ice
-14.7	20.0	Ice
-24.9	30.0	Ice
-26.5	32.3	Ice+$NH_4F \cdot H_2O$

We used data for the liquidus curve to estimate corresponding points on the solidus line, using the equation (Seltz, 1934; Eucken, 1950):

$$\ln \frac{N_\ell}{N_s} = \frac{H}{R} \left(\frac{1}{T_o} - \frac{1}{T} \right) \qquad (24)$$

where H is the heat of melting of ice, T_o its melting point, and T the melting point of the mixed crystals. N_ℓ and N_s are the concentrations of H_2O in liquid and solid phase respectively.

Preparation of mixed crystals between ice and NH_4F. Preliminary quantitative determinations of the amount of NH_4F absorbed in the ice lattice from solutions of NH_4F

in water gave the following approximate results:

% NH_4F	in liquid:	0.1	5	10
	in ice:	0.002	0.5	1.5

The procedure consisted of filling one 1500-cc beaker with a solution of NH_4F and another beaker with a solution of NH_3 of the same nitrogen content, placing the beakers into 4-qt open-mouth Dewar flasks, and leaving the flasks, covered with cork, overnight in a dry ice storage box. Fairly large crystals were thus obtained from dilute solutions. The nitrogen content of these crystals was determined colorimetrically using Nessler's reagent and a set of 12 Nessler tubes (Kolthoff and Sandell, 1949). However, solutions of several percent NH_4F yielded extremely thin platelets of ice which could not be separated from each other. It was then assumed that the amount of nitrogen trapped in the grain boundaries was approximately the same with NH_4F as with NH_3, and that the NH_3 was present only in the boundaries. For example, the ice obtained from a solution of about 5% NH_4F contained 0.66% NH_4F, while that from a solution of 2.5% NH_3 contained 0.06% NH_3 or the equivalent of 0.12% NH_4F. The actual amount of NH_4F absorbed by the ice crystals was therefore estimated at 0.66 - 0.12 or 0.5%. The error due to the presence of solution in the grain boundaries was thus of the order of 20%.

Solidus line of the system H_2O-NH_4F. Besides being inaccurate, the above procedure did not give conclusive proof that mixed ice-NH_4F crystals were actually formed. Although microcrystalline inclusions of NH_4F were not seen in a single crystal examined through a microscope at magnifications of 100 and 300 times, positive proof could best be obtained by means of time-temperature (cooling and heating) curves.

In the absence of a solid solution (mixed crystals), all time-temperature curves should show a break at the eutectic temperature, regardless of the composition of the sample; whereas, for a solid solution, the breaks should occur at temperatures higher than the eutectic temperature and different for different compositions. Theoretically, the breaks in the cooling curves should correspond to points on the liquidus and solidus lines of the equilibrium diagram. Actually, however, the solidus line so determined usually shows lower melting temperatures than the true ones, because equilibrium in the solid phase is attained very slowly. The rate of attainment of equilibrium can be greatly accelerated by reducing the size of the crystals. Hence, instead of cooling liquid samples, as is frequently done, we started out with finely powdered ice at about -40C and heated it up to above 0C. In order to ensure uniformity of composition, the powdered sample was allowed to recrystallize at a temperature just below its estimated melting point and then reground before testing.

The heating curves were obtained with equipment consisting of two parallel stirrers for the purpose of mixing powdered ice or mixtures of powdered ice and water, placed in a silvered Dewar flask externally warmed by running water (Fig. 20). The running water was maintained at a constant temperature $\underline{T}$, while readings were taken of the temperature $\underline{t}$ of the ice, at various times, θ. It can be shown that log $(\underline{T}-\underline{t})$ should be almost linear with θ when only one phase is present (Mair et al., 1941).

The data thus obtained proved the existence of solid solutions of NH_4F in ice. Figure 21 shows some of the curves of log $(\underline{T}-\underline{t})$ versus θ for ice-samples of various compositions. The points of the solidus line thus determined are:

% NH_4F	Temperature (C)	Maximum Error (C)
0.07	-1.5	±0.5
0.2	-2.5	±0.5
0.7	-4	±1
2	-9	±2

With increasing concentration of NH_4F, the breaks in the heating curves became less sharply defined; hence, the limit of error increased, as shown above.

Another method used to determine the solidus curve consisted of measuring the effective coefficient of expansion of a solid solution at different temperatures.

The apparatus (Fig. 22) consisted of a 50-ml U-tube closed by a stopcock at one end and terminating with the outer part of a ground glass joint at the other end. A 0.2-ml pipette graduated in 0.001-ml divisions was connected to the inner part of the ground glass joint. The U-tube was filled with powdered solid solution of ice-NH_4F and the space between the grains of solid was filled with n-hexane. Then the inner ground joint was connected, the U-tube placed in a thermostat bath, and the level of the hexane in the graduated capillary was raised to the lowest mark by opening the stopcock. Readings of the capillary were taken as the bath temperatures were slowly increased. Incipient melting was indicated by a short reversal in the sign of the effective coefficient of expansion. A plot of the readings of the capillary at different temperatures for two samples of a solid solution of 0.7% NH_4F (Fig. 23) shows that thawing starts between -3.5 and -4C, which is in agreement with the results obtained by heating curves.

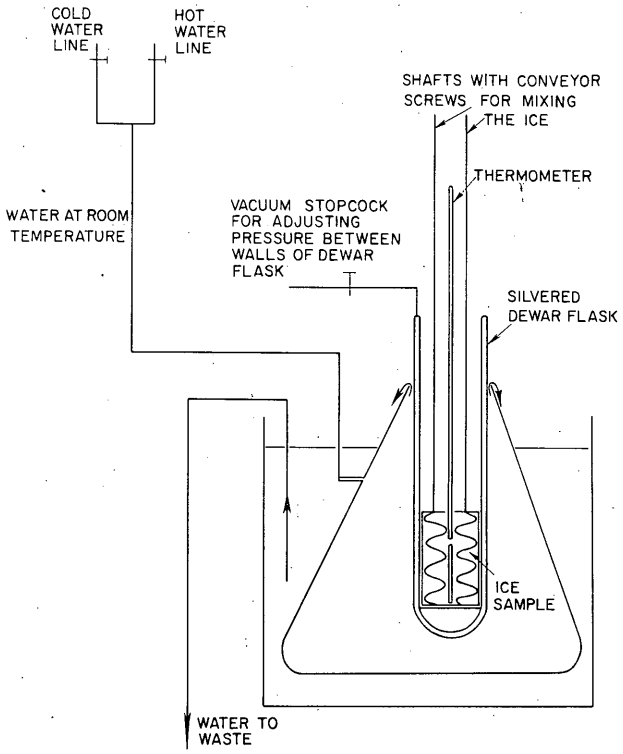

Figure 20. Schematic diagram of apparatus for heating-curve measurements.

Figure 19 shows the solidus line, as determined above, as well as part of the liquidus line. The dashed part of the curve was estimated from the data for the liquidus line using Equation (24). From Table VIII and Figure 24, which are based on the experimental points, it is found that K = 1460 cal/mole, which agrees well with the value of 1435 cal/mole, for the heat of fusion of ice. Equation (24) thus becomes $\log N_\ell/N_s = -320/T+1.17$. If we assume that this relation remains valid for the higher concentrations of NH_4F, then the limit of solubility of NH_4F in ice is roughly 10%. It might be possible, however, to determine the solubility limit with greater accuracy by measuring the lattice constants of different concentrations of ice-NH_4F at the eutectic temperature (-26.5C).

Table VIII. Correlation between the solidus and liquid curves for the system H_2O-NH_4F.

T(K)	% NH_4F	Ice N_s	Log N_s	% NH_4F	Liquid N_ℓ	Log N_ℓ	- log N_ℓ/N_s	1/T
273	0	100	2.00000	0	100	2.00000	0	0.00366
271.5	0.07	99.93	1.99970	1.5	98.5	1.99344	0.0063	0.00368
270.5	0.2	99.8	1.99913	3.0	97.0	1.98677	0.0124	0.00370
269	0.7	99.3	1.99695	5.0	95.0	1.97772	0.0192	0.00372
264	2	98	1.99123	11.0	89.0	1.94939	0.9418	0.00379

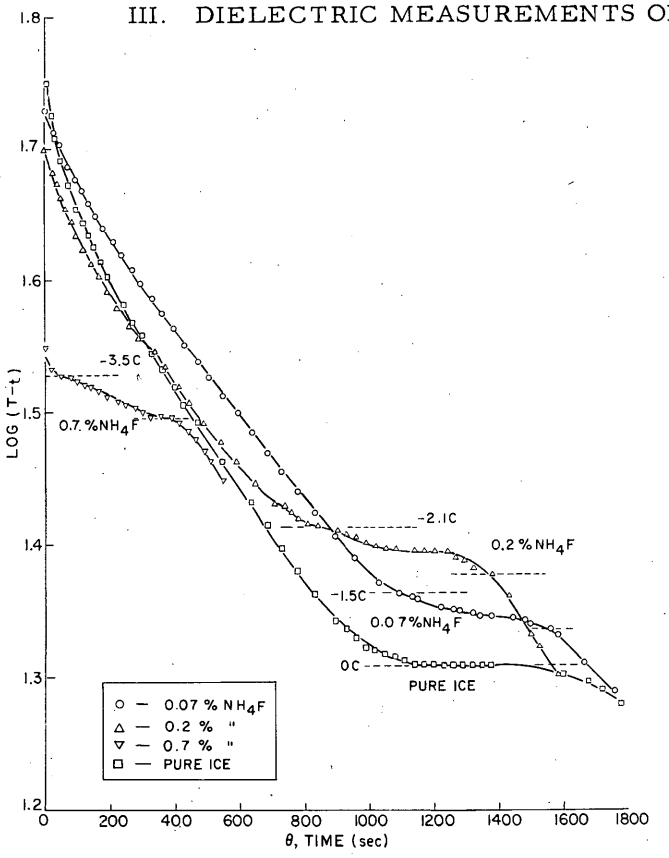

Figure 21. Typical heating curves for ice-NH_4F solutions.

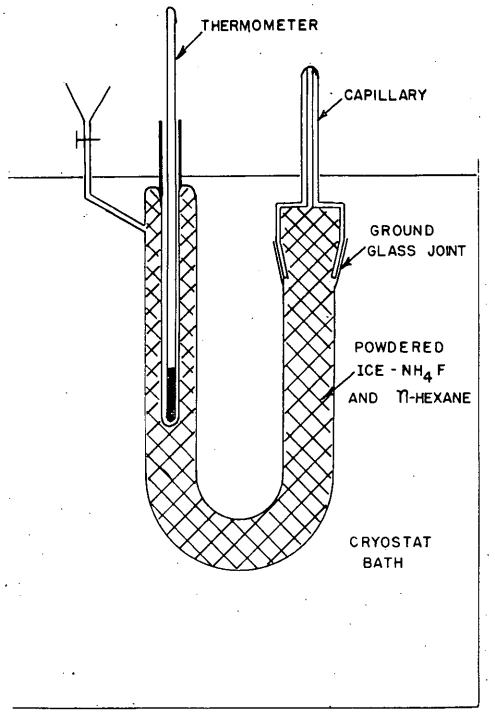

Figure 22. Schematic diagram of apparatus for dilatometric measurements.

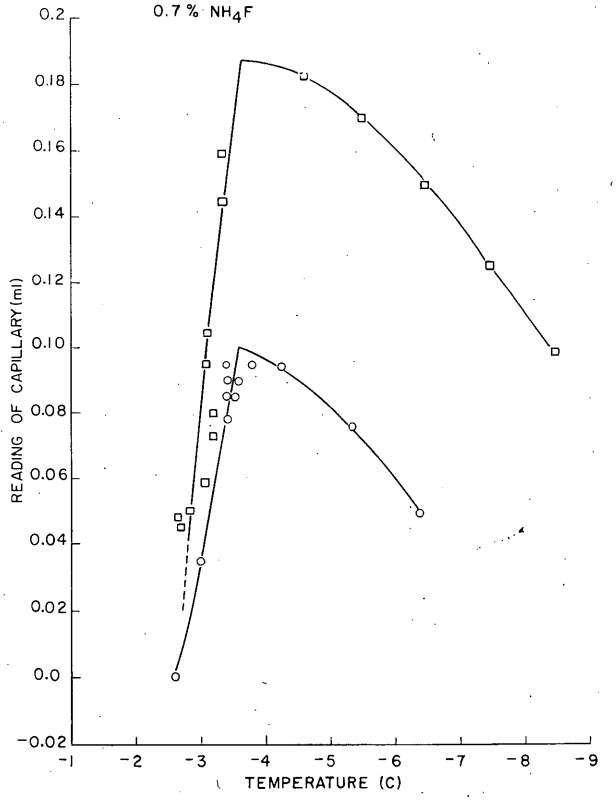

Figure 23. Typical changes in the volume of ice-NH_4F near the melting point.

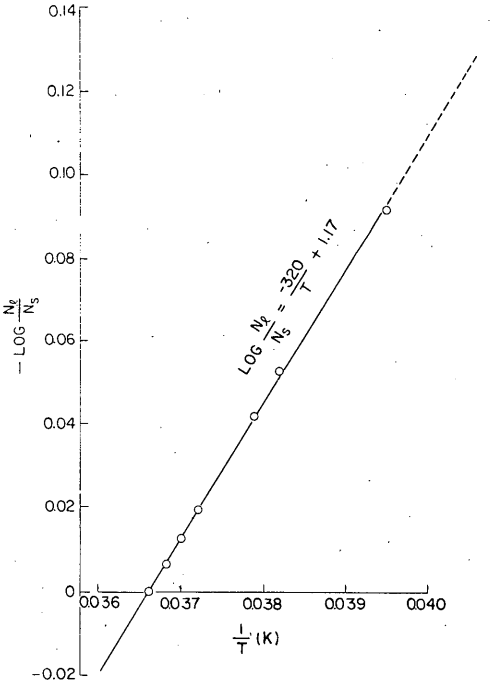

Figure 24. Relation between liquids and solidus curves for the system H_2O-NH_4F.

It appears reasonable that the solubility of NH_4F into the ice lattice is bound to produce distortions. The configurations of H-atoms in ice will also be affected by the presence of NH_4F. According to Pauling's model (1948) all configurations of H-atoms are equally stable in ice; hence, any rearrangement required by the presence of NH_4F would be of little significance. However, if the numerous objections to Pauling's model (Bjerrum 1951; Rundle, 1953, 1954) are justified, then the H-atoms would tend to arrange themselves in a rather regular manner. The presence of NH_4F would necessarily upset this regularity, as shown schematically to the right, which might tend to decrease the stability of the lattice. If the H-atoms in ice are regularly arranged, substitution of two H_2O molecules by NH_4^+ and F^- ions would require some disordered regions such as the one surrounded by dotted lines in the schematic arrangement to the right.

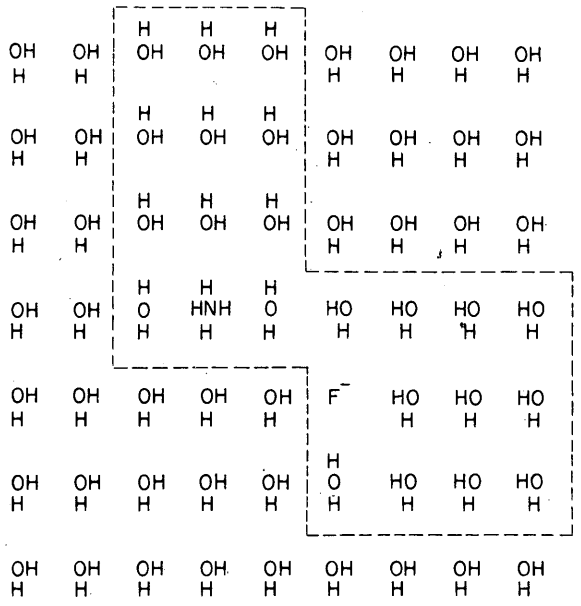

Electrical properties of ice-NH_4F solutions

Introduction. The response of pure ice to alternating currents of various frequencies has been studied by several investigators (Lamb and Turney, 1949; Murphy, 1934; Smyth and Hitchcock, 1932). The most recent and most reliable experimental data are those of Auty and Cole (1952) and of Humbel, Jona, and Scherrer (1953). The results of both groups are in good agreement. Their measurements were taken for ice temperatures of -0.1 to -65C with frequencies of 20 to 50,000 cps.

Debye (1929) has shown that the dipole moment per unit volume, $\vec{P}$, induced by an electric field is due partly to deformation of atoms, ions, and molecules (distortion polarization) and partly to orientation of permanent dipoles (orientation polarization) under the influence of the field. Distortion polarization occurs very rapidly; is the sole contributor to $\vec{P}$ under rapidly changing fields (and also under steady fields of substances which are not composed of polar particles); and is independent of temperature. Orientation polarization, on the other hand, occurs only under steady or slowly changing fields in substances containing permanent dipoles, and is proportional to $1/T$ (T = absolute temperature). This temperature dependence is due to the interference of thermal movements with the orienting effects of the field.

If a given substance is polarized by a constant field $\vec{E}$, and the field is then suddenly removed, the time required for the orientation polarization to be reduced to 1/e-th of its value is called the dielectric relaxation time, τ, of the substance. If an alternating field is applied having a period $1/f$ (f = frequency in cps) of the same order as τ, then the orientation polarization must fluctuate partly in phase with the field. The field must then act on the dipoles in the direction of their displacement, and therefore work must be accomplished and electrical energy dissipated. Such dissipation of energy introduces an imaginary component into the dielectric constant, ϵ.

The frequency f_m, corresponding to maximum dissipation of power, is exactly equal to $1/\tau$. However, power dissipation occurs over a range of frequencies which are higher and lower than f_m. This range of frequencies is called the "region of anomalous dispersion". If ϵ_o and ϵ_∞ denote the values of the dielectric constant at the low-frequency and high-frequency ends, respectively, of the dispersion region, then for any intermediate frequency, f, the dielectric constant, ϵ, can be shown to be:

$$\epsilon = \epsilon_\infty + (\epsilon_o - \epsilon_\infty)/[1 + i(2\pi f\tau)] = \epsilon' - i\epsilon''. \tag{28}$$

The dielectric constant under steady fields, ϵ_o, often referred to as the "static dielectric constant", has been calculated for ice on the basis of its structure by Schellmann and Kauzmann (Schellmann, 1950) and Haggis, Hasted and Buchanan (1952) using Kirkwood's theory, and by J. G. Powles (1952), applying a more general relation proposed by Fröhlich. In all three cases, the calculated values agree roughly with the observed ones, thus bearing out the current theories.

Since both ϵ_o and ϵ_∞ are real numbers, it follows from relation (28) that:

$$\epsilon' = \epsilon_\infty + (\epsilon_o - \epsilon_\infty)/[1 + (2\pi f\tau)^2] \tag{29}$$

and

$$\epsilon'' = (\epsilon_o - \epsilon_\infty)\frac{2\pi f\tau}{1 + (2\pi f\tau)^2} \tag{30}$$

Elimination of $(2\pi f\tau)$ from equations (29) and (30) yields:

$$\left(\epsilon' - \frac{\epsilon_o + \epsilon_\infty}{2}\right)^2 + \epsilon''^2 = \left(\frac{\epsilon_o - \epsilon_\infty}{2}\right)^2 \tag{31}$$

It follows from equation (31) that when ϵ'' is plotted against ϵ', a semicircle is obtained with radius $(\epsilon_o - \epsilon_\infty)/2$ and center on the abscissa at $(\epsilon_o + \epsilon_\infty)/2$ from the origin. Such plots are called "Cole plots" after their authors (Cole and Cole, 1941). Since circles can be drawn as easily as straight lines*, the Cole plots offer a very useful method of estimating and compensating for random errors in a series of measurements.

The Cole plots are most useful, however, in the study of substances having more than one relaxation time, such as anisotropic solids, which exhibit a different behavior along different crystal axes, and also mixtures or solutions. Even though solutions are microscopically homogeneous, microscopic regions which are different from the bulk of the substance must occur in the vicinity of the solute particles. Yet, in most of these cases it is found that the plots of ϵ'' against ϵ' are still circular arcs, though of less than 180°. According to Böttcher (1952) this means that equation (28) must be modified to:

$$\epsilon = \epsilon_\infty + (\epsilon_o - \epsilon_\infty)/[1 + (i2\pi f\tau_o)^{1-h}] \tag{32}$$

where $(1-\underline{h})$ is the circular arc subtended by the ϵ'-axis, and τ_o is some average value around which the relaxation times are spread. Furthermore, it can be shown that, as a corollary of equation (32), the values of τ_o can be obtained from any point P_1 in the Cole plot corresponding to a frequency $\underline{f}_1$ by means of the relation (Böttcher, 1952):

$$v_1/u_1 = (2\pi f_1\tau_o)^{1-h} \tag{33}$$

* To draw the best circle readily through a set of plotted points, semi-transparent polar coordinate graph paper (manufactured by the Keuffel and Esser Co., New York City) can be used.

where u_1 and v_1 are the respective distances from P_1 to the intersection points ϵ_∞ and ϵ_o of the curve with the abscissa.

This offers the simplest and most accurate method of determining τ_o that has been devised so far.

Besides its value in defining the frequency dependence of the dielectric constant, as given by equations (28) or (32), the dielectric relaxation time is important in the study of the behavior of the dipoles composing a given substance. By regarding dielectric relaxation as a chemical rate process, it can be shown (Böttcher, 1952; Eyring, 1936; Frank, 1936) that dipoles jump from one position of maximum stability to another with an average frequency, $1/\tau^*$, where:

$$\tau^* = \tau(\epsilon_\infty+2)/(\epsilon_o+2); \tag{34}$$

τ^* is called the intrinsic relaxation time. Like any other chemical reaction rate, $1/\tau^*$ can be described by the Arrhenius relation:

$$1/\tau^* = Ae^{-E/RT} \tag{35}$$

where A is a frequency factor, E an activation energy, R the gas constant and T the absolute temperature. Furthermore, if relaxation is considered as a unimolecular reaction, then, according to Eyring's absolute rate theory, the frequency factor represents:

$$A = \frac{kT}{h} e^{\Delta S^*/R} \tag{36}$$

where k is Boltzmann's constant, h is Planck's constant, and ΔS^* is the activation entropy. The latter is a measure of the number of ways in which an activated dipole can change its orientation. An alternative treatment of unimolecular reactions leads to (Böttcher, 1952):

$$A = \nu \frac{(E/RT)^{s-1}}{(s-1)!} \tag{37}$$

where s is the number of vibrational degrees of freedom in a dipole and ν the frequency of its oscillation about an equilibrium position.

The present work is concerned with the variation of τ with temperature and concentration in solid solutions of ice-NH_4F, as deduced from measurements of real and imaginary dielectric constants over frequencies of 20 cps to 600 kc.

Experimental.

Preliminary measurements of dielectric constants: Preliminary measurements of the dielectric constants of pure ice and of ice-NH_4F solutions were taken at the temperature of -78.5C, which was easily maintained in a Dewar flask filled with dry ice. Pure water or aqueous solutions of NH_4F were frozen in a condenser consisting of two parallel rhodium-plated brass rectangles of 2x7.5 cm, each of which fitted exactly into a recess of a U-shaped slab of polystyrene to form a flat, upright container open from the top. The freezing was performed very rapidly by first embedding the empty condenser in dry ice and then introducing the liquid through the top with a polyethylene pipette. The aqueous solutions of NH_4F were never allowed to come in

contact with glass, because of the reactivity of HF with silicates. The solutions were prepared from distilled water with a specific conductivity of 10^{-6} $(ohm\text{-}cm)^{-1}$ supplied by the Great Bear Spring Company, and NH_4F supplied by the Fisher Scientific Company. The analyses of the distilled water and of the NH_4F as quoted by the suppliers are as follows:

Sample Test of Great Bear Spring Distilled Water

Chemical Analysis	Parts Per Million
Total Solids	0.280 (1,000 ml sample)
Reaction	6.600 pH (electric test)
Chlorides	none
Sulphates	none
Ammonia	none
Calcium	none
Carbon Dioxide	none
Heavy Metals	none
Oxidizable Substances	none
Nitrogen, as Nitrites	0.050
Nitrogen, as Nitrates	none
Silica	0.025
Iron	none
Copper	0.001
Magnesium	none

Analysis of NH_4F

Nonvolatile Matter	0.09%	Chloride (Cl)	0.000%
Insoluble Matter			0.000%
Sulfate (SO_4)			0.005%
Heavy Metals (as Pb)			0.0005%

The solid NH_4F was broken up with a clean rhodium-plated spatula, weighed, and then poured into polyethylene bottles containing distilled water. Bottles, condenser, and pipette were all cleaned and rinsed several times before use. Nevertheless, slight impurities were introduced into the first samples investigated.

The capacity and power dissipated of the ice and ice-NH_4F condensers were measured first at 60 and 1000 cps with a Type 650-A General Radio impedance bridge*. The initial measurements showed that addition of 0.2-7% NH_4F caused a tenfold increase in ϵ' at 1 kc and a two- to threefold increase at 60 cps. This indicated that addition of NH_4F must cause a marked and readily observable shift of the region of anomalous dispersion towards higher frequencies.

These results were sufficiently encouraging to warrant extension of the measurements to a wide range of frequencies. A Hewlett-Packard Model 200-AB audio oscillator was used as a variable source of voltage for frequencies of 20 cps to 40 kc. Because the shielded transformer Type 578-A is designed for frequencies above 50 cps, it was replaced by Type 578-B for measurements at 20 to 40 cps.

---

* We thank the Microwave Research Institute of the Brooklyn Polytechnic Institute for kindly lending this bridge to us.

The complete results of measurements at -78.5C are summarized in Table IX and Figure 25. The values of τ_o were roughly determined from the observed data using Cole plots and equation (33):

$$v_1/u_1 = (2\pi f_1 \tau_o)^{1-h}.$$

The best average value of τ_o was obtained by drawing the best straight line through a plot of log v_1/u_1 versus log f_1, and determining the value of f_1 corresponding to $v_1/u_1 = 1$. If this value of f_1 is called f_m, then:

$$\tau_o = \frac{1}{2}\pi f_m. \tag{38}$$

Figure 25 and Table IX show that τ_o decreases markedly with increasing concentration of NH_4F, up to a minimum value corresponding to some concentration between 0.1 and 1% NH_4F, and then increases again with further increasing concentration.

Preliminary experiments showed that the following source of error had to be considered especially:

Inhomogeneities in composition of the samples can be introduced by freezing them too quickly. If a sample starts freezing when its temperature is brought down to point f (Fig. 19), the concentration of the first crystals formed is given by point g. This is much lower than the concentration of the original liquid. As freezing proceeds the liquid becomes more concentrated at an accelerating rate; e.g., when half, three-quarters, and nine-tenths of the material are frozen, the concentration of the liquid will usually be almost twice, four, and ten times the original value, respectively.

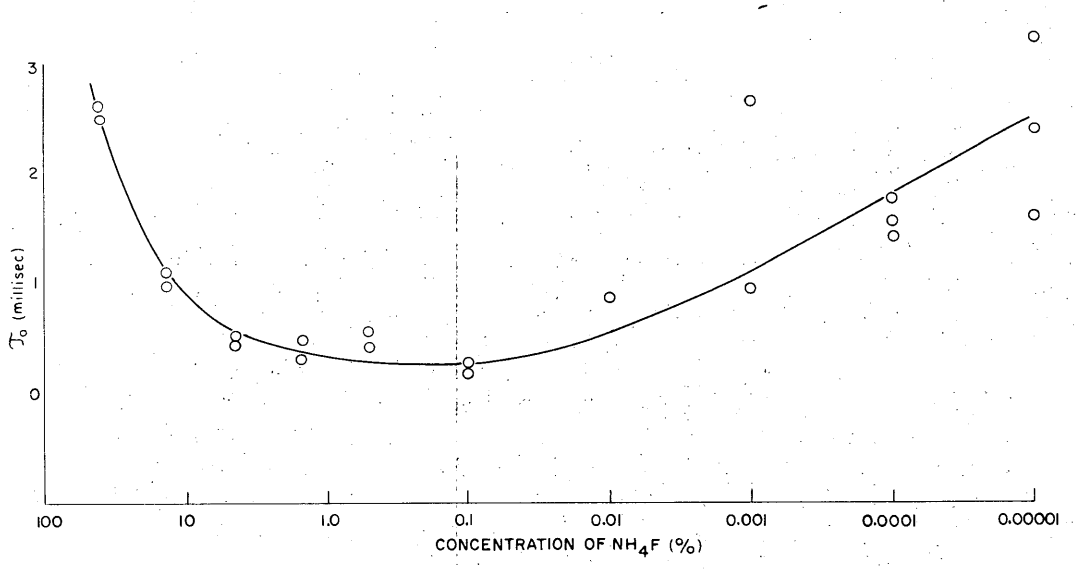

Figure 25. Effect of NH_4F on τ_o at -78.5C (preliminary experiments).

As diffusion in the solid phase proceeds rather slowly, especially at low temperatures, the material frozen first will have a much lower concentration than that frozen last. If the rate of diffusion is so slow as to be insignificant, the bulk of the material will have a relatively low concentration, and most of the solute will be contained in the last fraction frozen. In that case, the over-all behavior of a given sample will be close to that of a more homogeneous solid solution having a much lower average concentration of NH_4F. This last concentration will henceforth be called the "effective concentration" of a given sample, as distinguished from the actual average concentration.

Table IX. Dielectric relaxation times of ice-NH_4F solutions at -78.5C.

Sample	%NH_4F	Relaxation Time (millisec)	Sample	%NH_4F	Relaxation Time (millisec)
1	0	3.0	15	0.1	0.18
2		6.6	16		0.26
3		9.1	17	0.5	0.39
4	10^{-5}	3.2	18		0.52
5		2.4	19		0.54
6		1.6	20		0.54
7	10^{-4}	1.75	21	1.5	0.48
8		1.52	22		0.29
9		1.4	23	4.4	0.50
10	10^{-3}	0.91	24		0.44
11		0.91	25	13	0.47
12		2.65	26		0.59
13	10^{-2}	0.84	27	40	3.1
14		0.84	28		3.0

Measurement of the resistivity: The direct-current resistivity of ice - NH_4F increased with the concentration of NH_4F, whereas the reverse was true of frozen aqueous solutions of NH_4Cl, which showed a resistivity of only 7 megohm-cm at -78.5C for the concentration of 0.05 mole/l NH_4Cl as compared with 200,000 megohm-cm observed for pure ice. The observed resistivities are listed in Table X.

Table X. Resistivity of ice-NH_4F solutions at -78.5C.

%NH_4F	d-c Resistivity (10^6 megohm/cm)	%NH_4F	d-c Resistivity (10^6 megohm/cm)
0	0.2 (0.06-0.6)	0.5	0.1-0.15
10^{-5}	0.06-0.07 (0.03-0.13)	0.7	0.2-0.7
10^{-4}	0.06-0.07 (0.04-0.5)	1.5	0.4-1.5
0.001	0.04-0.08	2	0.6-2.0
0.01	0.3	4.4	0.4
0.07	0.2-0.3	7	0.4-1.5
0.2	0.25-0.5	20	0.8-1.0

Note: Values in parentheses indicate the range of readings obtained for a given concentration. Values outside parentheses are probably the best readings.

Since the resistivity of ice containing 10^{-5} % NH_4F is lower than that of pure ice, it is concluded that there must be a range of concentrations lower than 10^{-5} % for which the resistivity decreases with concentration. The resistivities were measured with a crudely improvised Wheatstone bridge, designed for measuring resistances up to 10^6 megohms. Because of extremely rapid polarization of the ice, the measured values are valid only to the first figure, and even the first figure could have been in error due to cracks and air gaps in the samples. Nevertheless, the general trend in resistivity appears to agree with observations of Workman and Reynolds (1951) who reported an increase in the resistivity of ice by two orders of magnitude upon increasing the concentration of NH_4F in a freezing solution from 10^{-5} to 10^{-3} mol/l.

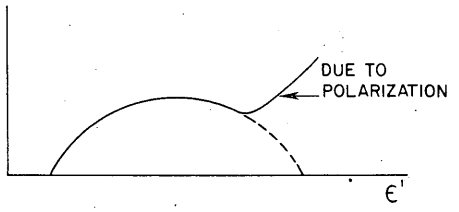

Figure 26. Polarization as revealed by Cole plots.

A thorough study of the resistivity of ice-NH_4F solutions in relation to concentration and temperature could be a major project in itself. At present, therefore, direct current conductivity is considered only as far as it could affect the measurement of ϵ' and ϵ''. It has been shown by Auty and Cole (1952) that polarization due to d-c conductivity causes transitions from the circular form in the Cole plots to a linear form (Fig. 26). The frequency at which such a transition occurs decreases with increasing resistivity and with increasing thickness of the specimens. Only points on the circular part of the plot can be interpreted in terms of equations (28) or (32). Hence, for the experimental data to be most useful, the linear part of the plot must be shifted as far to the right as possible, i.e., polarization should not occur except at the very low frequencies. In order for the experimental data to be of any use whatsoever, the circular part of the plot must bend over beyond the maximum value of ϵ'' so as to be clearly distinguishable from the straight line. This can occur only if the major part of anomalous dispersion occurs at higher frequencies than those for which polarization is significant.

On the basis of the above considerations and of the results and experience gained from the preliminary experiments, the following procedure was worked out for studying the anomalous dispersion of ice-NH_4F solutions at different temperatures.

Preparation of aqueous solutions: The Great Bear distilled water was redistilled under vacuum in a Pyrex glass apparatus, to eliminate absorbed gases. The conductivity of the water dropped to about 5×10^{-7} $(\text{ohm-cm})^{-1}$, half its original value. The redistilled water was kept in air-tight polyethylene containers, and was not allowed to come in contact with air except for brief periods. A weighed quantity of NH_4F (specifications listed above) was dissolved in one of the containers so as to make up a 10% solution. Of this solution 20 cm^3 was added from a polystyrene burette to 180 cm^3 of water in another polyethylene bottle. In this manner, 11 solutions were prepared having concentrations ranging from 5×10^{-5} % up to 10%NH_4F. All containers used in preparing these solutions had been previously soaked in distilled water for 24 hr and then rinsed until the water from the last rinsing had a conductivity of not more than 10^{-6} $(\text{ohm-cm})^{-1}$.

The absence of bubbles in samples frozen from these solutions indicated that absorbed gases had been effectively eliminated by the redistillation. It is also believed that the above procedure ensured a satisfactory purity in the samples studied.

Freezing of the solutions: The liquid was introduced into the annular space between two concentric cylindrical rhodium-plated brass tubes which fitted tightly into a Teflon base. A loose Teflon plug formed the cover of the condenser and also ensured concentricity of the tubes. The outside diameter of the inner tube was 0.566 in. and the inner diameter of the outer tube was 0.870 in.; the effective length between the Teflon plugs was 2.75 in.

The condenser was placed in a cylindrical brass container, 1.5 in. in diameter and 9 in. deep, and the assembly was immersed in a 4-qt Dewar flask containing acetone at -70 to -80C. The brass container was connected electrically to the ground, thereby shielding the condenser not only from the acetone but also from stray electric fields.

This procedure had the following advantages:

(1) All samples were frozen at approximately the same rate.

(2) The space between the condenser tubes was reasonably thick (0.30 in.), which tended to reduce polarization. At the same time, the capacity of the condenser was not too small for accurate measurements, and the over-all size of the condenser was not inconveniently large.

(3) The edge effect in the cylindrical condensers was entirely negligible.

However, the following disadvantages must be cited:

(1) Inhomogeneities in sample composition could not be eliminated, and the magnitude of the resulting error could not be estimated.

(2) For concentrations below 0.006% NH_4F, polarization was still so large as to render the experimental data worthless.

A second procedure was therefore used for preparing a condenser of ice containing 0.002% NH_4F. A 1-in. x3-in. rectangular aluminum plate, cooled at the center by a tube filled with dry ice, was suspended over 1 liter of a solution of 0.012% NH_4F so as to just wet its surface. The initial temperature of the solution was circa 3C. Within a half hour, a slab of ice-NH_4F about $\frac{1}{4}$ in. thick adhered to the aluminum plate. This slab was partly melted between parallel brass plates until it formed a rectangular plate with smooth, parallel surfaces. The ice-NH_4F plate was then inserted between one fixed and one movable rhodium-plated brass electrode; a spring pressed the movable electrode against the fixed one, thereby eliminating air gaps between the electrodes and the sample. The parallel plate condenser thus formed was tested in the same way as the cylindrical condenser.

The advantages of this second procedure were:

(1) The composition of the sample was homogeneous, because only a small fraction of the liquid was frozen.

(2) The thickness of the sample could be adjusted to eliminate polarization.

(3) Stresses due to contraction and expansion with changing temperature were eliminated by the spring action.

However, ice frozen from aqueous solutions of more than 0.2% NH_4F was very brittle and fell apart before a satisfactory plate could be obtained. The second procedure was therefore applicable only to dilute solutions.

Electrical measurements: As the temperature of the acetone bath in the Dewar container rose slowly from -70 to -10C over a period of 4-5 hr, the parallel capacitance, C_p, and resistance R_p, of the condenser were measured for frequencies of 20 cps to 600 kc. To test the reproducibility of these measurements, two identical condensers were immersed in the bath in each experiment, and each was measured alternately over the entire frequency range. It was usually possible to cover the frequency range about 5 or 6 times in a single experiment.

For frequencies up to 40kc the same bridge and accessories were used as in the preliminary experiments.

For frequencies above 40 kc, radio-frequency bridge Type B-601, manufactured by the Wayne Kerr Laboratories, Great Britain, was used with a radio-frequency oscillator Type WR-67A, manufactured by the Radio Corporation of America, and the following detectors:

GPO 804860—7

(a) Amplifier Model 102-B, manufactured by the Kalbfell Labs , Inc., San Diego, California, used with a cathode ray oscilloscope (Du Mont Labs Inc., Passaic, New Jersey) for frequencies up to 300 kc, and

(b) A Hallicrafter Radio receiver which detected an audiomodulated voltage at 600 kc.

Bridge Type B-601 should, according to the manufacturer's specifications, be accurate to within 1%. However, a subsequent calibration showed deviations much larger than 1% from the correct values. All measurements were corrected for these deviations.

Electrical connections were made with shielded cable and were kept mostly unchanged throughout the entire series of measurements, including the calibration, for which a standard variable condenser in parallel with different carbon resistors was used.

It was found convenient to measure the temperature of the acetone bath with a Pt-resistance thermometer. The difference between the temperature of the ice-NH_4F samples and that of the acetone bath was determined by copper-constantan thermocouples in conjunction with a Weston Model 440 microammeter. Temperature gradients in the acetone bath itself were reduced by an efficient air-driven glass stirrer.

Temperatures were read at intervals of 10 to 20 min, the time of the readings was noted, and a plot was drawn of sample temperature against time. The time at which balance was obtained in each bridge measurement was also recorded. The temperature corresponding to each bridge reading was then obtained from the time-temperature plots. Direct-current resistance measurements were made at intervals of $\frac{1}{2}$-1 hr with an ohmmeter, for resistance up to 100 megohms. For higher d-c resistances no correction was necessary for the observed values of the imaginary dielectric constant.

Evaluation of the data. Bridge readings were corrected with the aid of the calibration curves and also for d-c conductivity, and the corrected values of the real and imaginary components of capacitance, $\underline{C}'$ and $\underline{C}''$, were plotted against temperature (Figs. 27-34) for different frequencies. To draw the best curves through the plotted points, it was necessary to consider the general trend in variation of the slope of the curves with temperature and frequency. For example, if curves for 0.1, 0.6 and 1 kc were all concave upward, then the curve for 0.3 kc was also drawn concave upward, even though the experimental points for this particular frequency tended to slope concavely downward. In such cases it was believed that one or two readings were probably in error, whereas it appeared most unlikely that some peculiar anomaly would occur at just one temperature or frequency.

From the temperature-capacitance curves, values of $\underline{C}'$ and $\underline{C}''$ at a fixed temperature were read off for different frequencies and plotted on Cole plots (Figs. 39-46). These were then used to determine τ_o (see Eq. 33).

Discussion of results.

Errors and reliability of the measurements: The various errors can be due to three sources: (a) the measuring circuit; (b) the graphical evaluation; and (c) the samples.

Some idea of the magnitude of the overall error resulting from the first two sources was obtained from preliminary measurements on pure ice (Figs. 35-38). It appears from Figure 38 that our ϵ_o (Zaromb's data) may be in error by circa 10%. An error of such magnitude is reasonable because our measurements covered a range of circa 50C in each single experiment, whereas the accuracy obtained by other experimenters who worked at constant temperatures is of the order of 5% (cf. Jona). However, approximate values of ϵ_o estimated from Figures 39-46 indicate that any variations in ϵ_o with concentration could not be much more than 10%. Hence, the accuracy of the measurements does not permit any conclusions as to the effect of NH_4F on ϵ_o in ice.

GPO 826455-6

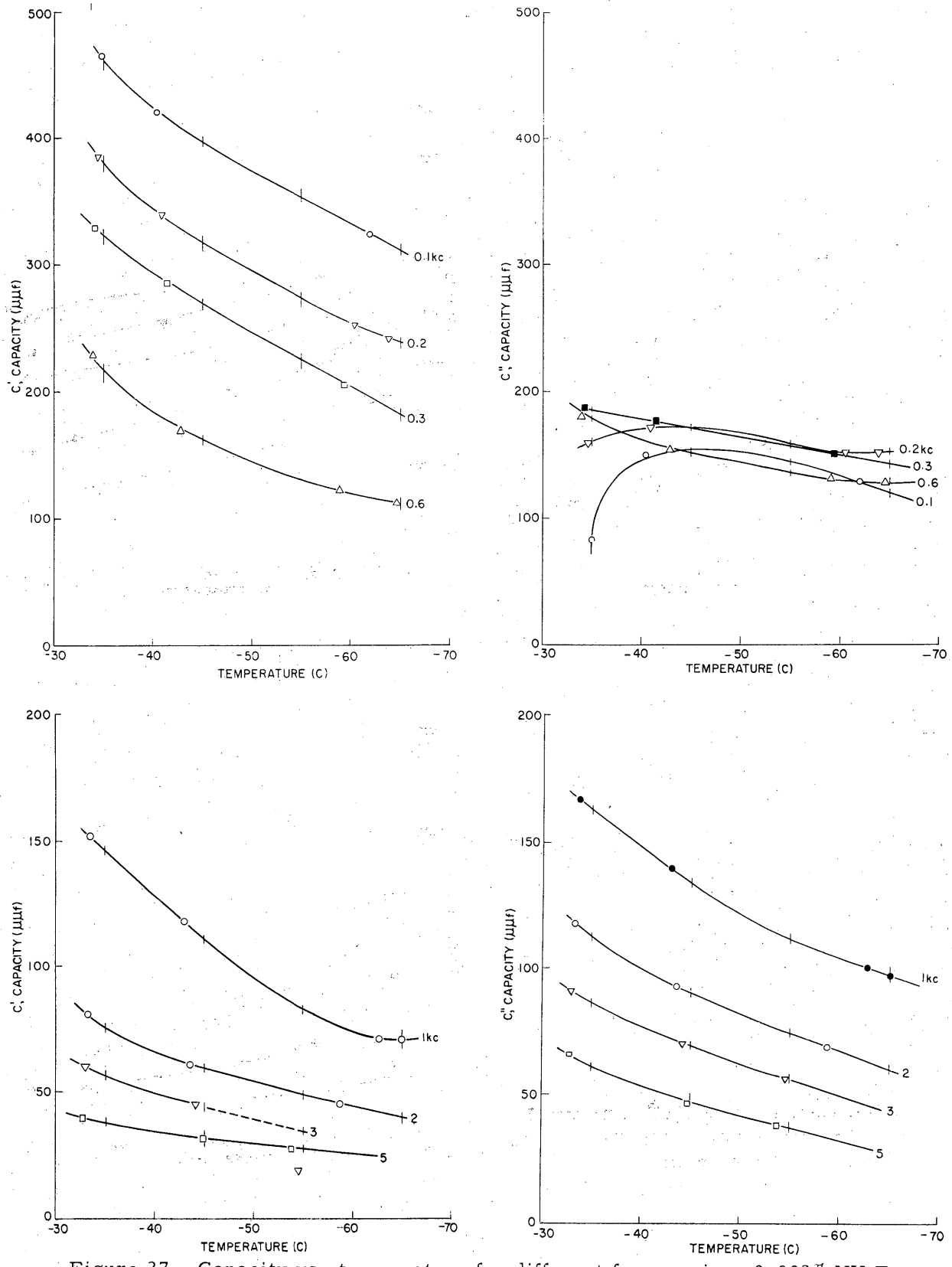

Figure 27. Capacity vs. temperature for different frequencies. 0.002% NH_4F.

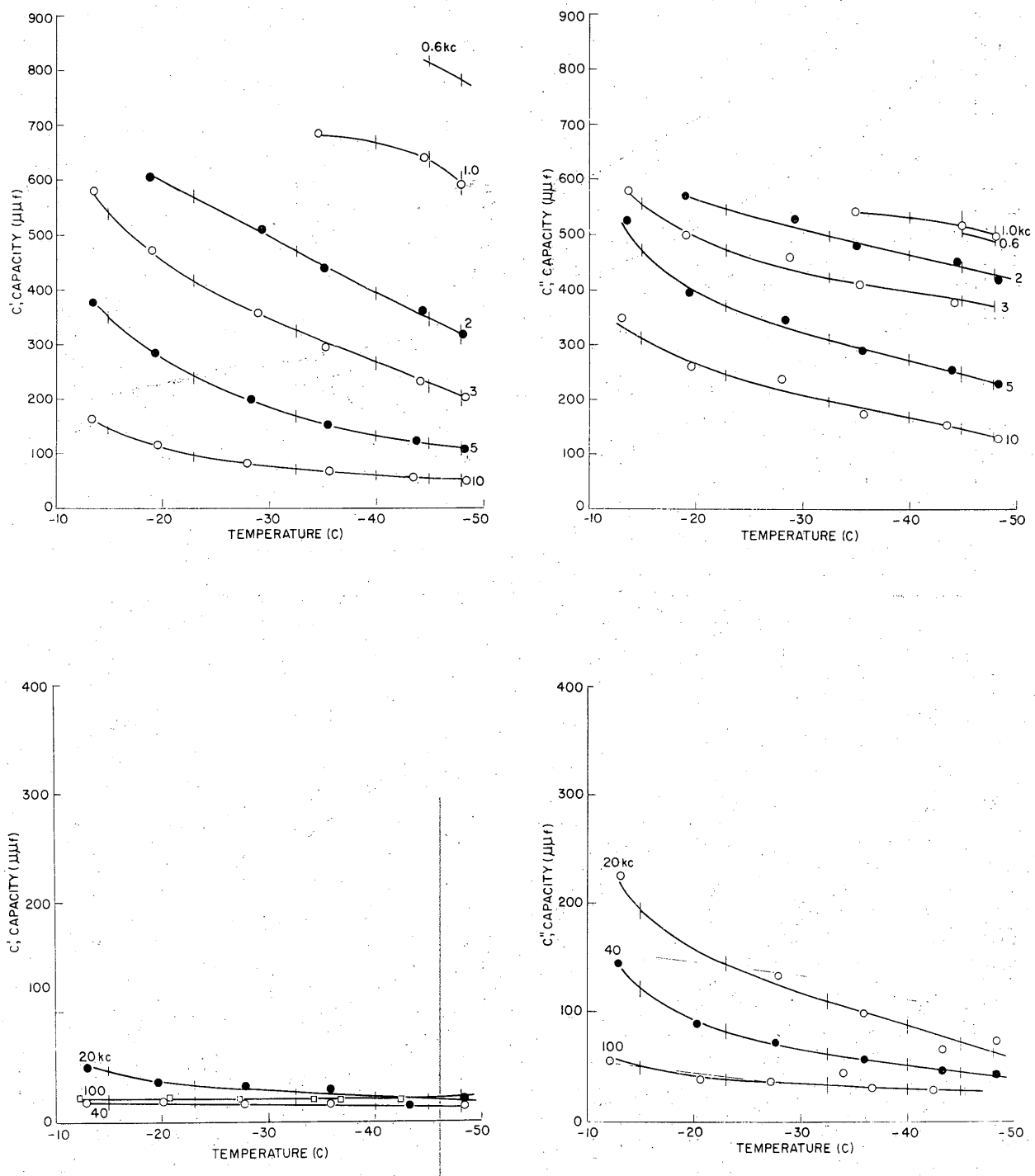

Figure 28. Capacity vs. temperature for different frequencies. 0.006% NH_4F.

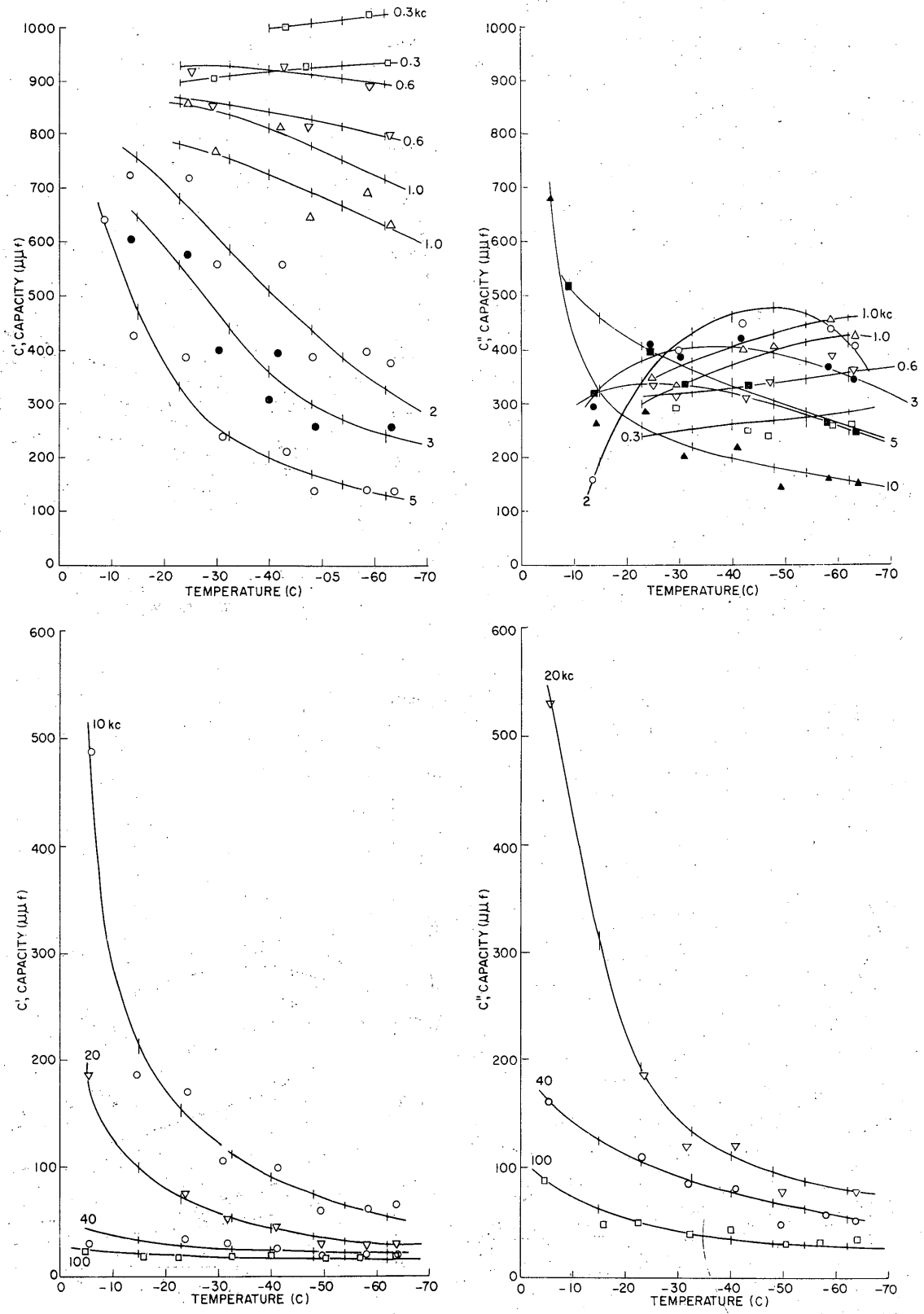

Figure 29. Capacity vs. temperature for different frequencies. 0.015% NH_4F.

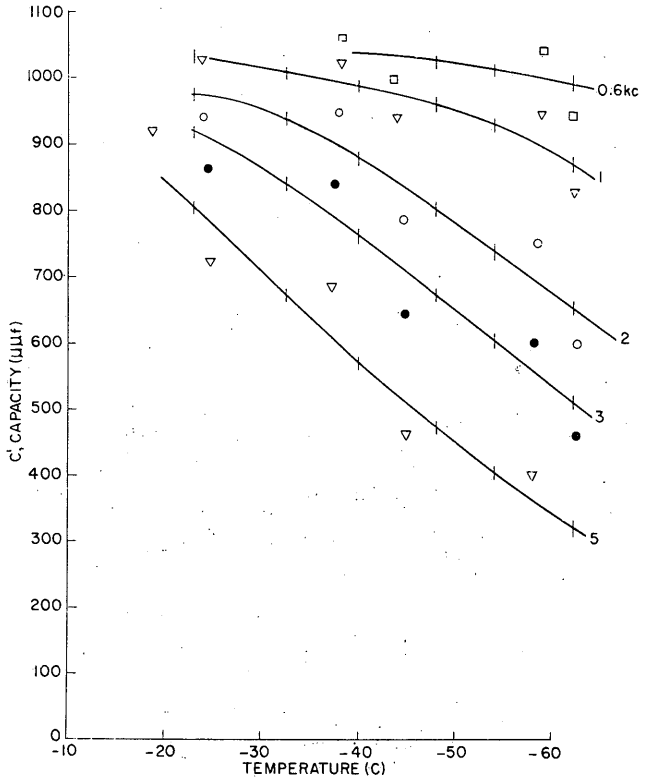

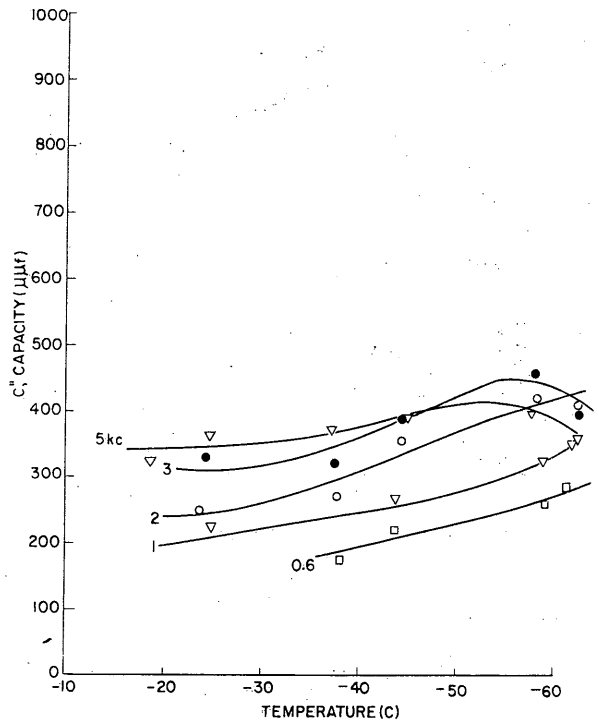

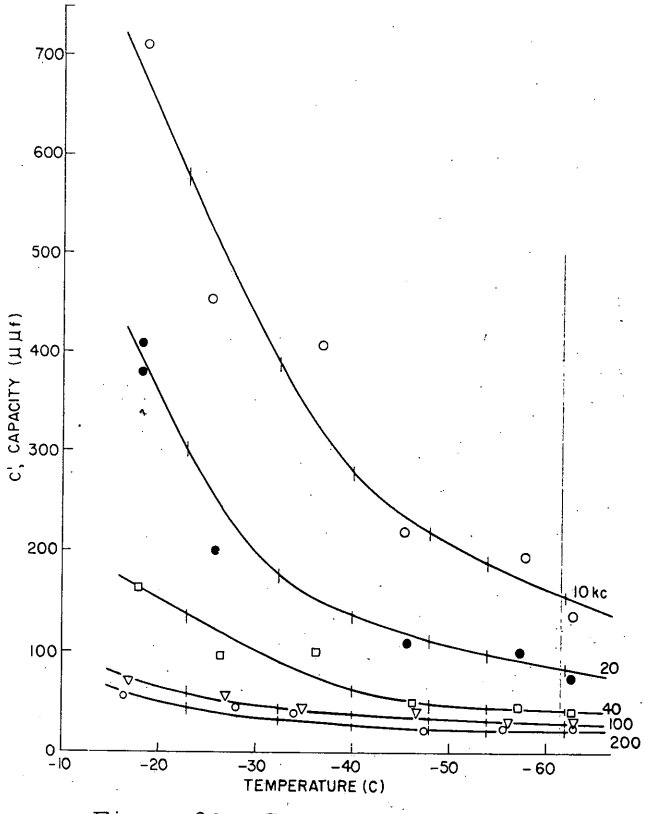

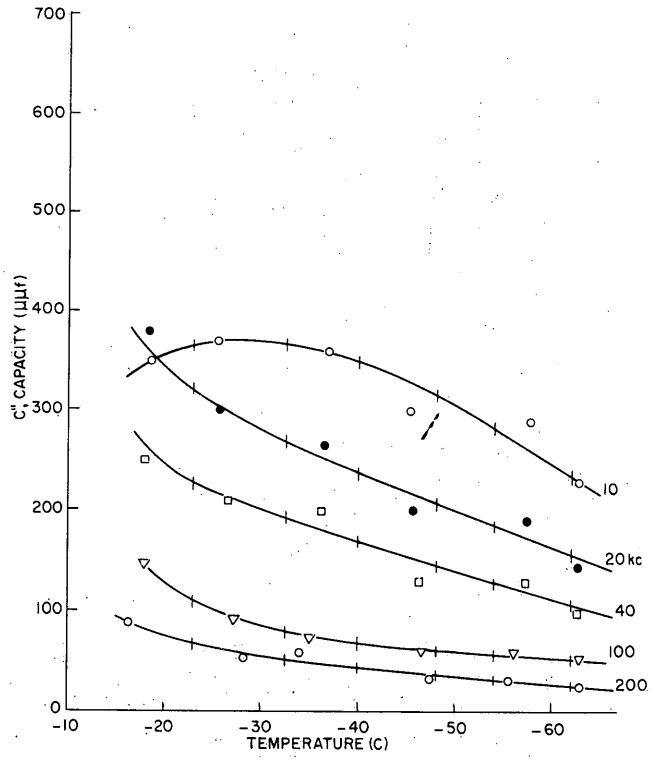

Figure 30. Capacity vs. temperature for different frequencies. 0.05% NH_4F.

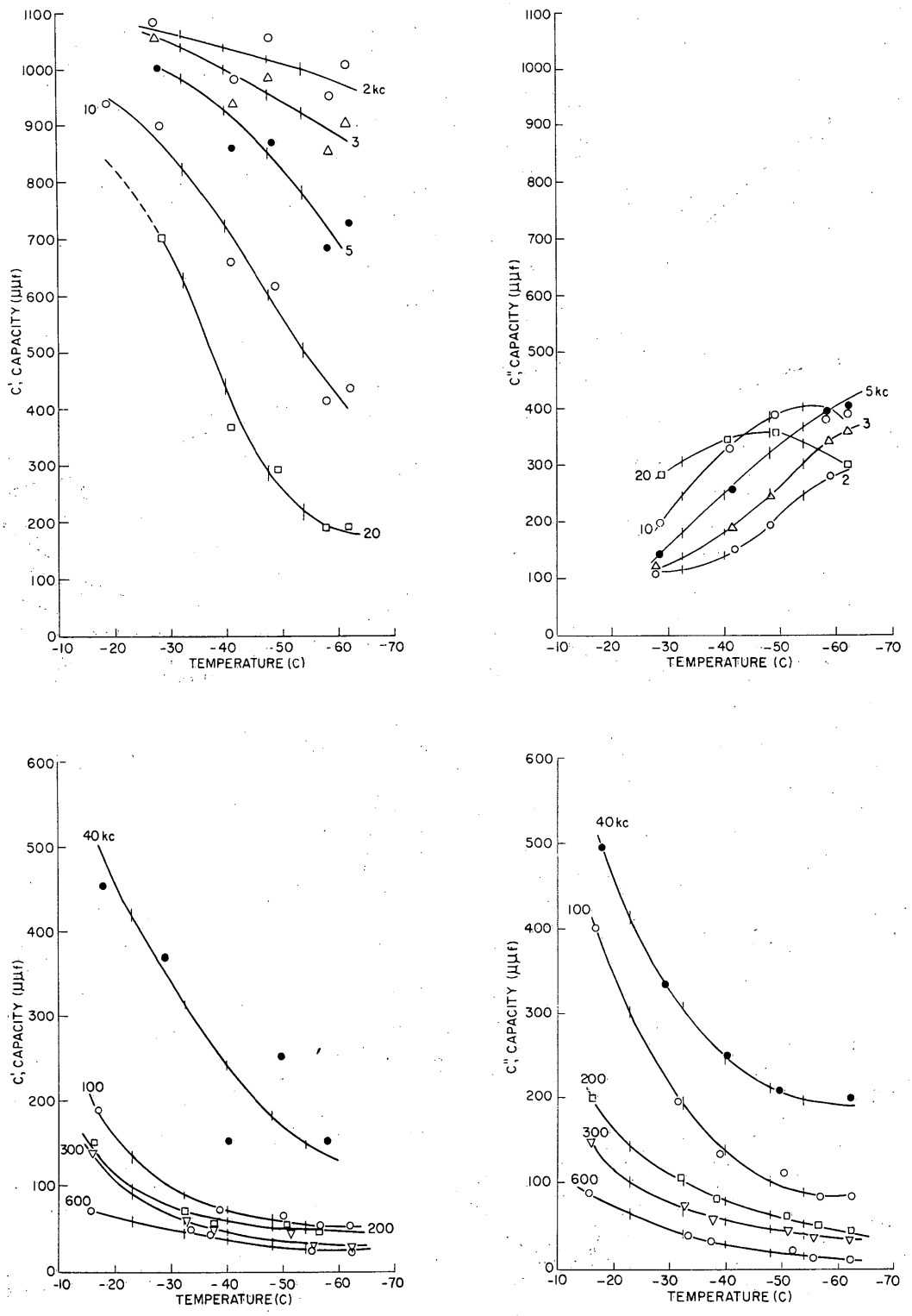

Figure 31. Capacity vs. temperature for different frequencies. 0.15% NH_4F.

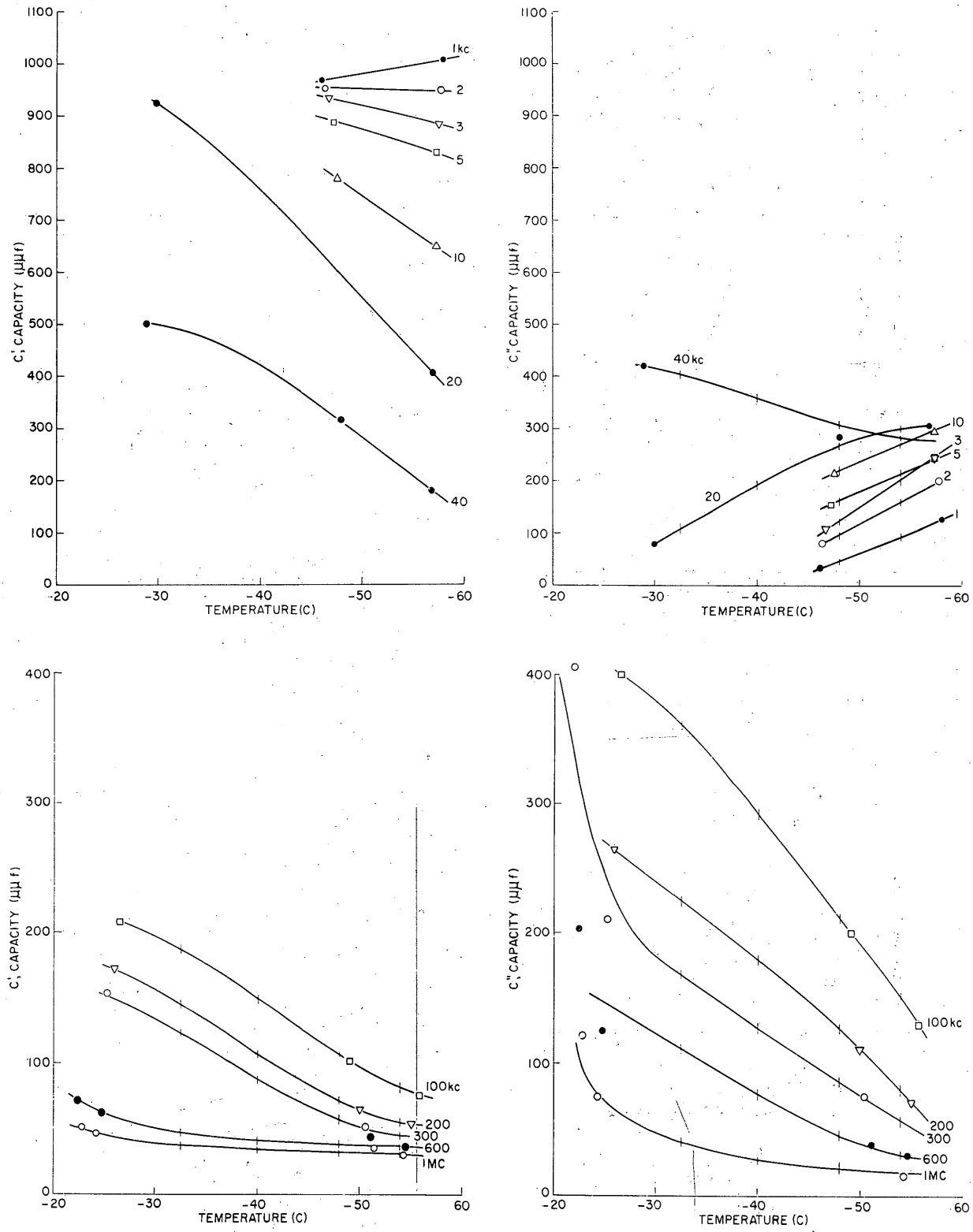

Figure 32. Capacity vs. temperature for different frequencies. 0.4% NH_4F.

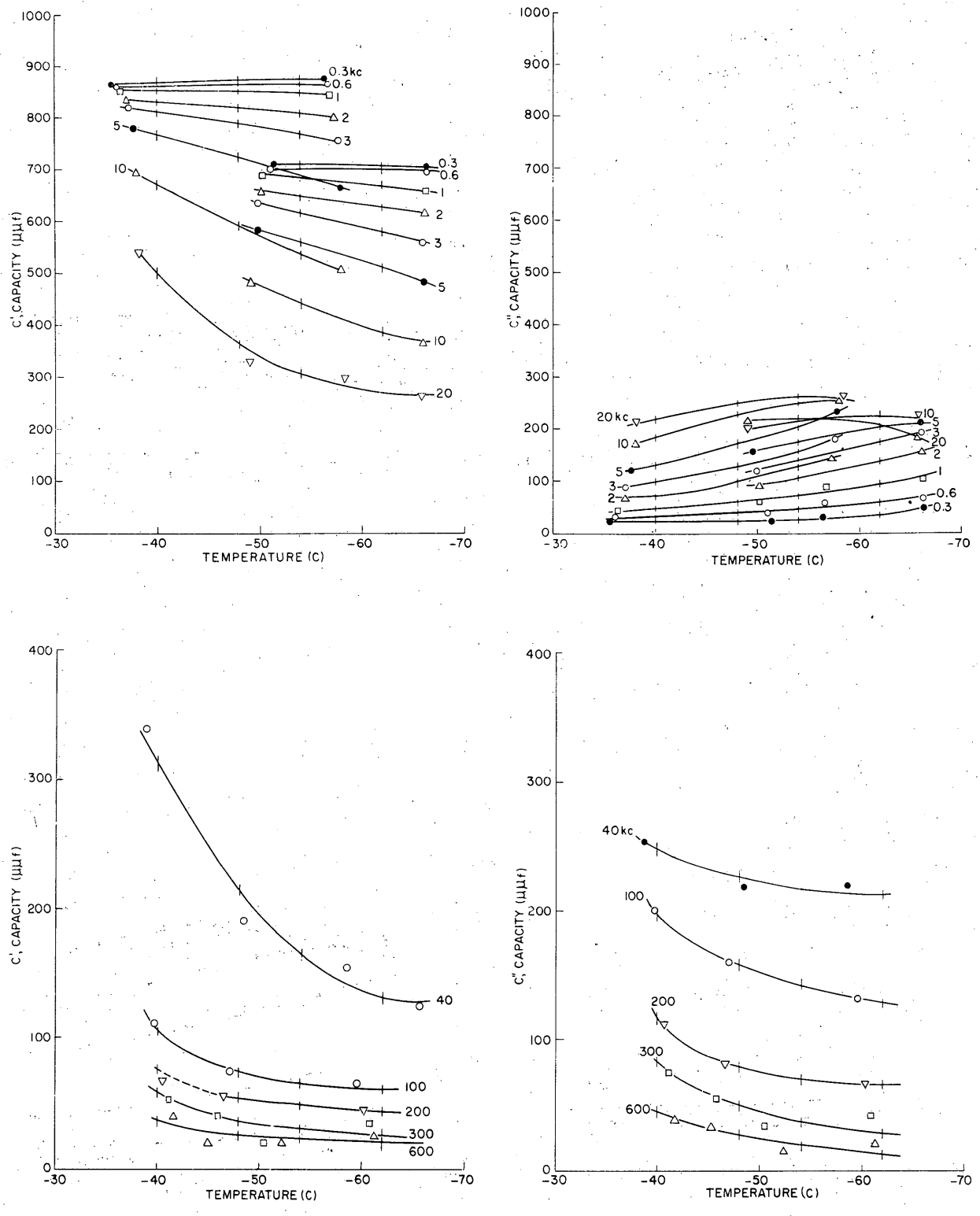

Figure 33. Capacity vs. temperature for different frequencies. 1% NH_4F.

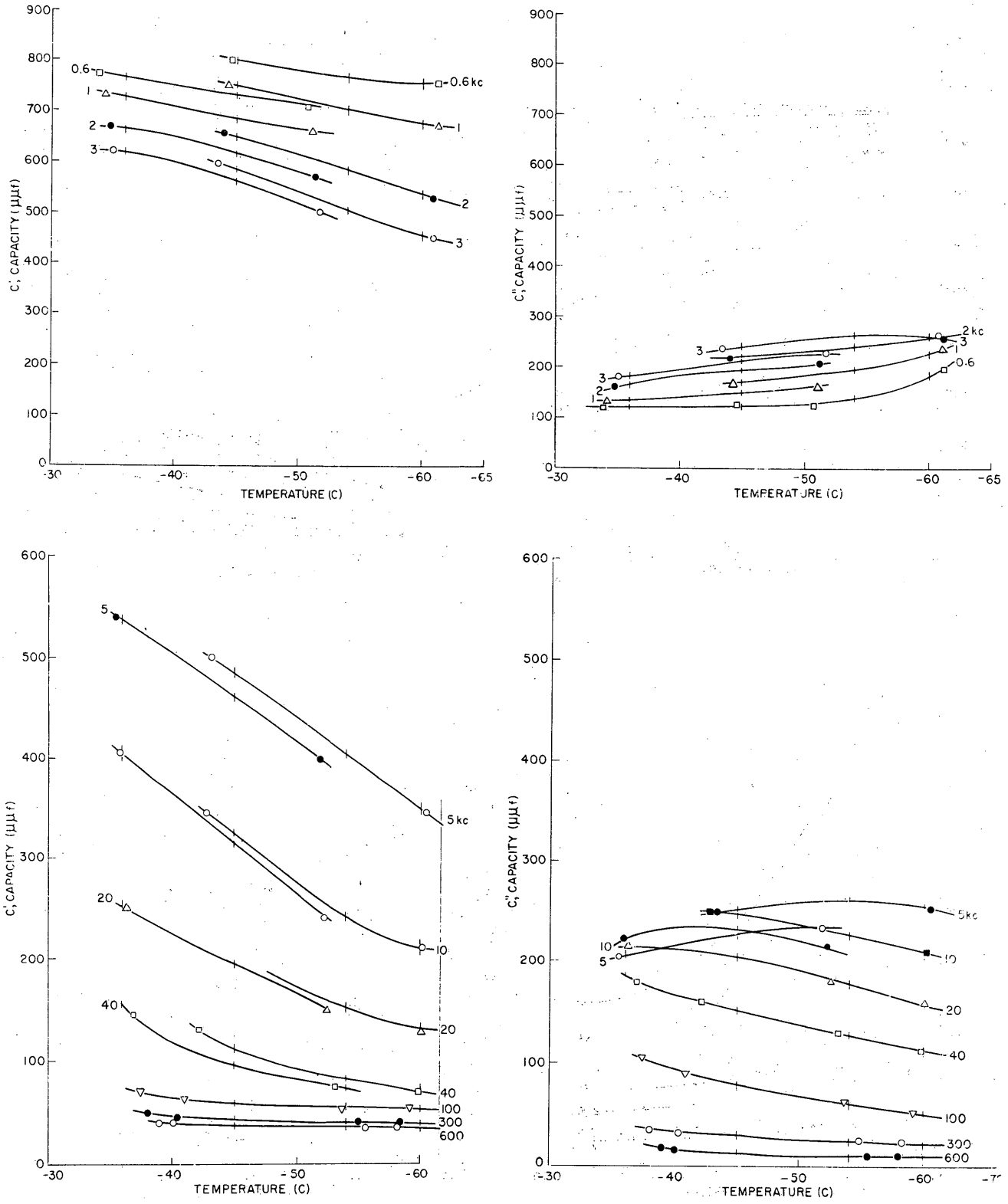

Figure 34. Capacity vs. temperature for different frequencies. 10% NH_4F.

GPO 826455-5

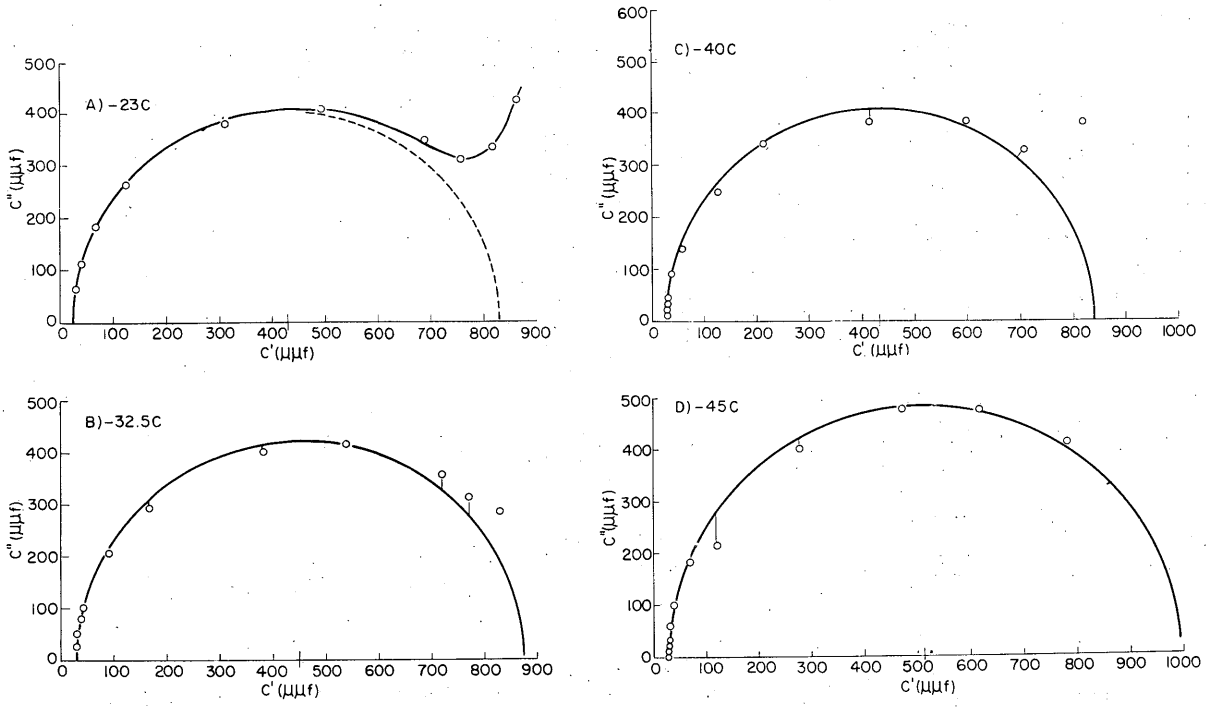

Figure 35. Cole plots for pure ice.

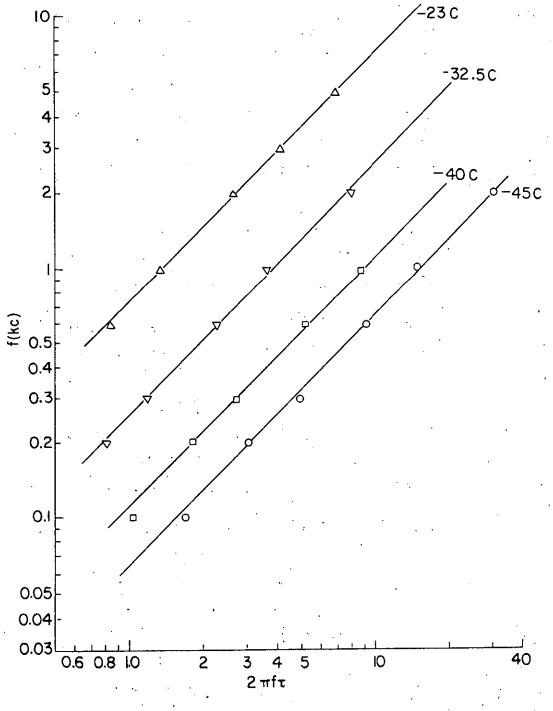

Figure 36. Determination of τ for pure ice.

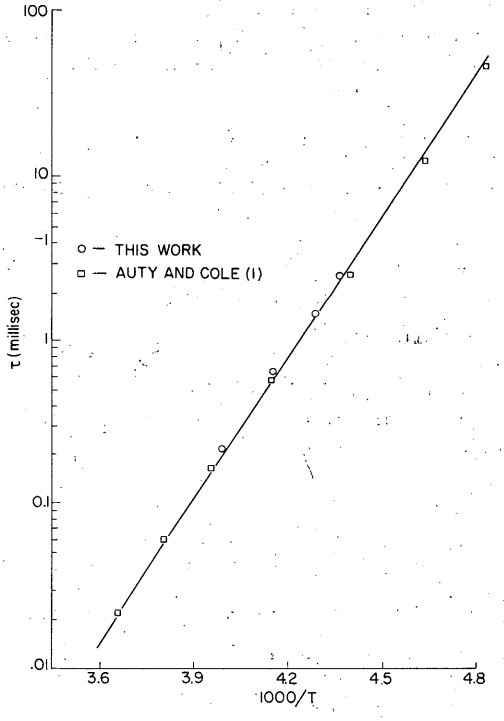

Figure 37. Dielectric relaxation time of pure ice.

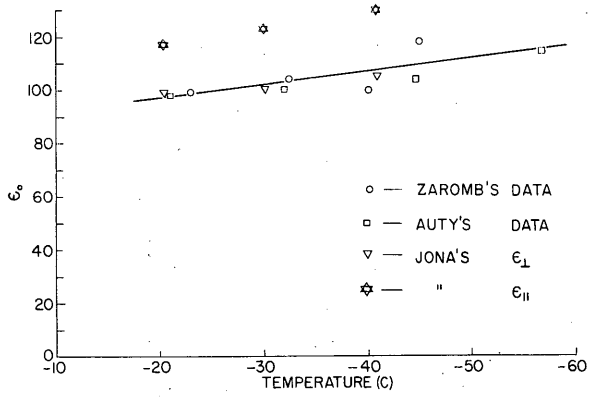

Figure 38. Static dielectric constant of pure ice.

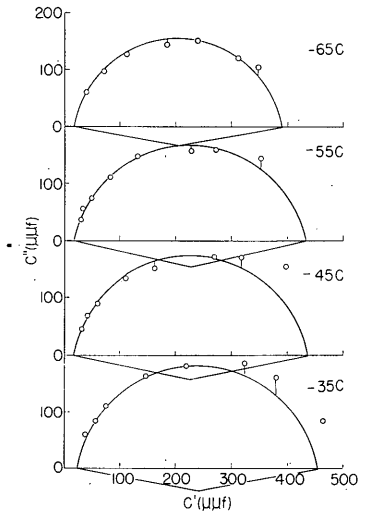

Figure 39. Cole plots for ice-NH_4F mixed crystals. 0.002% NH_4F.

On the other hand, Figure 37 shows that the variation of τ with temperature is much larger than that of ϵ_o. Furthermore, the values of τ_o obtained from Figures 39-46 (Fig. 47) show variations with concentration by two or more orders of magnitude. Hence, the maximum discrepancy of circa 10% shown in Figure 37 could certainly not prevent us from drawing quantitative conclusions as to the effect of NH_4F on τ. The question which now arises is whether the maximum error of 10% in τ found in our measurements on pure ice could also represent the maximum error in other measurements. To answer this it is necessary to analyze more carefully the main sources of error in all measurements.

In pure ice, the range of frequencies most useful for determining τ was between 0.1 and 10 kc. This range was also useful for most of the measurements on ice-NH_4F. However, for concentrations of 0.15-1% NH_4F, the dispersion region was shifted over to frequencies so high that measurements at 10-600 kc became of greatest importance. The calibration of the bridge showed that the performance of the measuring circuit was much better at frequencies up to 10 kc than at higher frequencies. Hence, the limit of error could be larger for samples of ice containing 0.15 to 1% NH_4F.

The reliability of the graphical evaluation of τ_o depends on the accuracy of the individual measurements of ϵ' and ϵ''. When these individual measurements are good, the points plotted in Figures 39-46 lie close to the correct circle and there is no uncertainty as to the best circle to draw. In other cases, however, the graphical evaluation is somewhat equivocal. Extreme examples are shown in Figures 43 and 44, where values of τ_o differing by 6 - 20% are obtained depending on the way the circular arcs are drawn. These two samples fall into the above-mentioned concentration range.

In the samples themselves, polarization due to d-c conductivity and inhomogeneities in sample composition may be the biggest sources of error. Polarization was most important in measurements at low frequencies. For very low concentrations of NH_4F, the dispersion region was not shifted far relative to that for pure ice, whereas d-c conductivity, and therefore polarization, was greater than in pure ice. That is why data obtained with the cylindrical condensers for concentrations of less than 0.006% NH_4F were completely useless, and even those for 0.006% NH_4F appear questionable. For concentrations higher than 0.006%, polarization became less troublesome but still had to be taken into account. The magnitude of error in τ_o due to polarization was estimated by drawing the circles in two different ways through the Cole plots in Figure 41

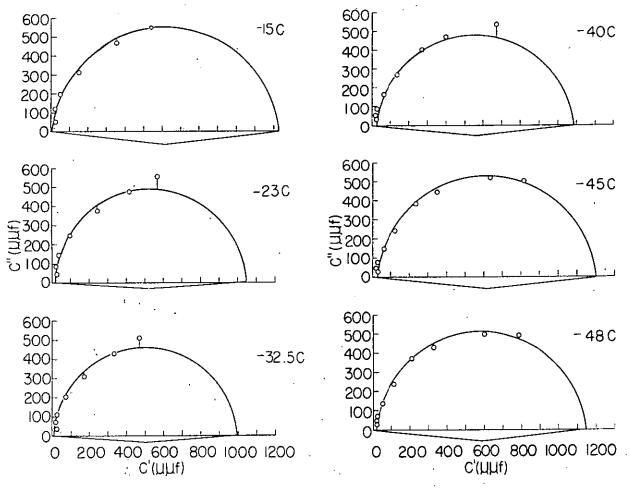

Figure 40. 0.006% NH_4F.

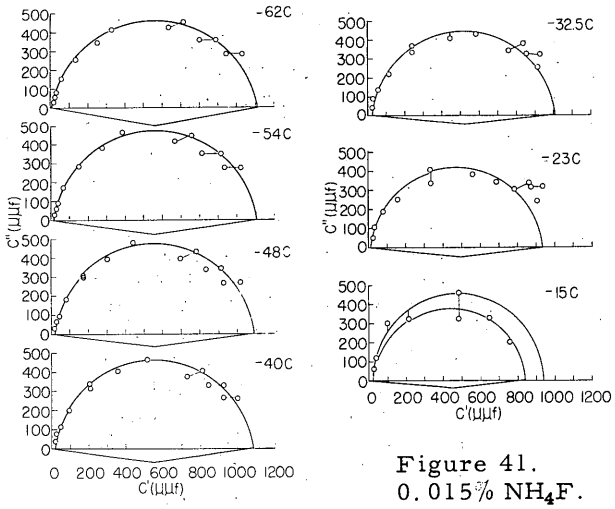

Figure 41. 0.015% NH_4F.

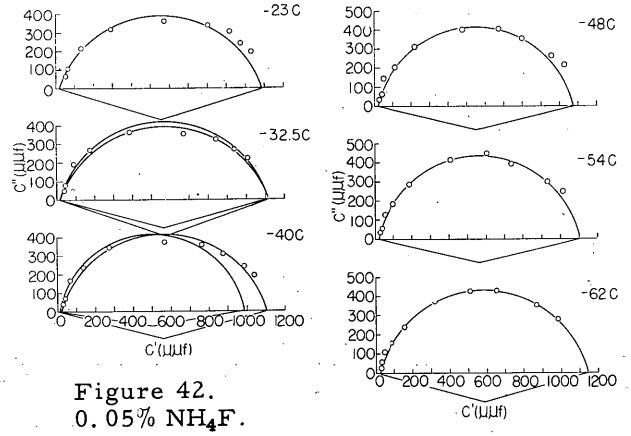

Figure 42. 0.05% NH_4F.

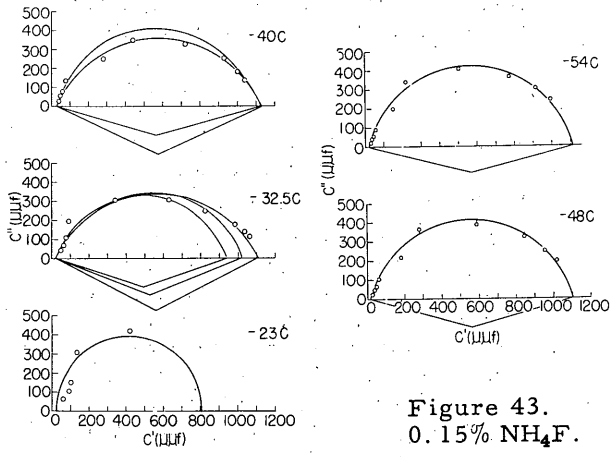

Figure 43. 0.15% NH_4F.

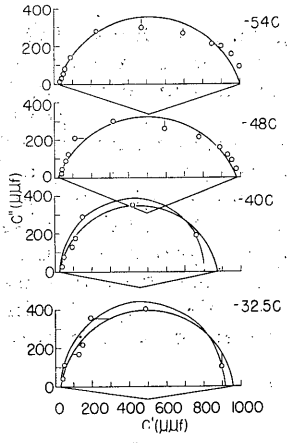

Figure 44. 0.4% NH_4F.

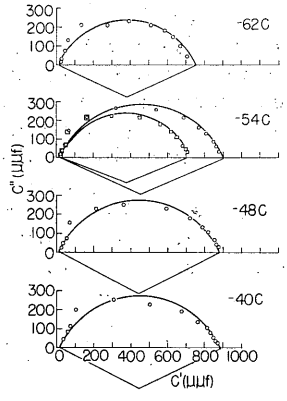

Figure 45. 1% NH_4F.

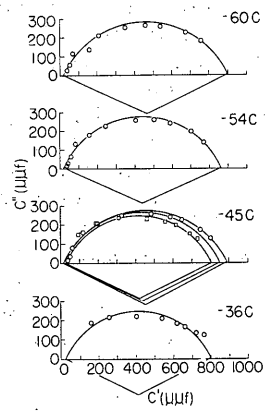

Figure 46. 10% NH_4F.

Figures 40-46. Cole plots for ice-NH_4F mixed crystals.

for -15C and in Figure 42 for -40C, completely ignoring the low-frequency measurements in one case and considering them as much as other measurements in the other. The difference in the values of τ_o obtained in the two ways is 15 - 20%.

For the highest concentrations, on the other hand, inhomogeneities in composition were probably most responsible for any discrepancies. The magnitude of error in τ_o due to this last source was estimated by drawing separate Cole plots for each of two supposedly identical condensers in Figure 45 for -54C and in Figure 46 for -45C. The discrepancies in the resulting values of τ_o are circa 15%. It must be mentioned here that the solutions of 1.0 and 10% NH_4F were not frozen in the manner described before, but were instead, rather improperly, frozen somewhat more rapidly (circa $\frac{1}{4}$ - $\frac{1}{2}$ hr) in a dry ice storage box. These measurements, therefore, were discarded and are not shown in Figure 47.

It appears then that the errors in τ_o quoted above occurred only in extreme cases. Moreover, each of the different sources of error became significant under different circumstances. Hence, except for the concentration of 0.006% NH_4F, the maximum error in τ_o should not be greater than 20%.

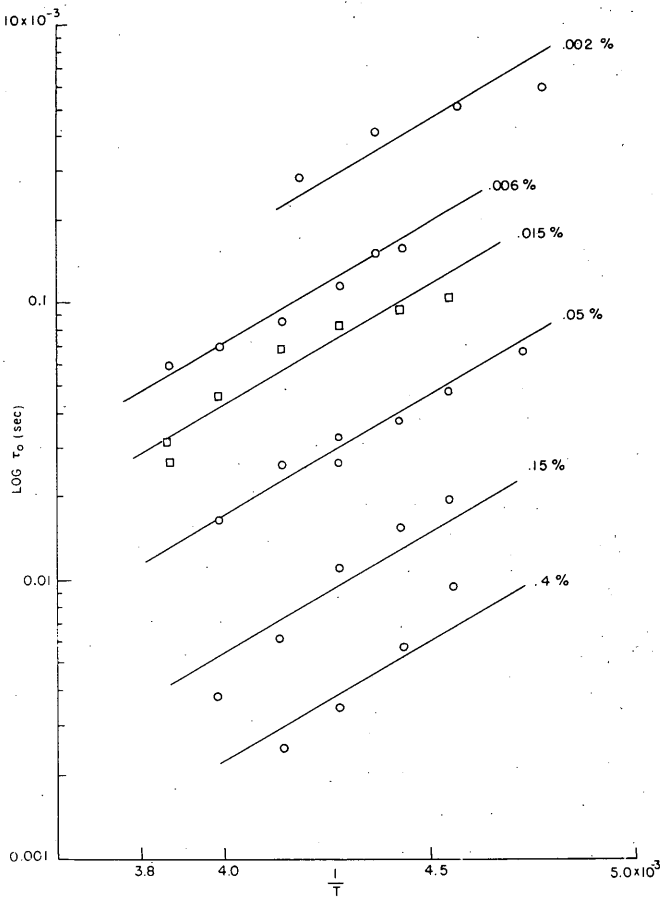

Figure 47. Arrhenius plots for samples of different compositions.

However, the measured values of τ_o are probably valid only for solid solutions prepared and heat treated in the manner described. This is equivalent to saying that, although the value of τ_o is known with an accuracy of better than 20%, the effective concentration of NH_4F to which it corresponds is not quite as certain. The reason for this uncertainty is our ignorance of the diffusion coefficient of NH_4F in ice and of the concentration gradients in the ice-NH_4F during and after freezing. If the samples are cooled rather quickly, as was done in our case, the range of composition of all samples covers a region of concentrations up to the eutectic composition. Obviously a sample prepared from a solution of higher concentration can contain much more eutectic material than a sample obtained from a solution of low concentration of NH_4F. Hence the amount of eutectic material present in samples of very low concentration might be neglected, and even the amount of material with higher concentration cannot be very relevant. But in specimens prepared from solutions of higher concentration, the effective inhomogeneity might be appreciable.

The results obtained during the period covered by this report, therefore, are to be considered as preliminary only. *

Possible methods of evaluation: In Figures 39-46, most of the arcs in the Cole plots are less than 180°. This indicates, as mentioned above, that more than one relaxation time is generally involved. Equation (35):

$$1/\tau^* = Ae^{-E/RT},$$

shows that, for a single relaxation time, τ_i, a straight line would be obtained if log τ_i were plotted against $1/T$. However, when more than one τ_i is involved, one must write:

$$\frac{1}{\tau_o} = \Sigma_i \frac{w_i}{\tau_i} = \Sigma_i w_i A_i e^{-E_i/RT} \qquad (39)$$

where $1/\tau_o$ is the relaxation rate evaluated as described on page 34, w_i is a weighting factor for the contribution of the relaxation rate $1/\tau_i$ to the observed rate $1/\tau_o$, and A_i and E_i are constants similar to those in equation (35) but applying the i-th relaxation process. Generally, this could mean that equation (39) should not yield a straight line when log τ_o is plotted against $1/T$. However, if one of the terms in the summation is much bigger than the others or if the most significant terms have values of E_i closely approaching each other, then a plot of log τ_o versus $1/T$ would not differ appreciably from a straight line.

Since the measurements are preliminary, we drew straight lines through the observed points on a log τ_o vs. $1/T$-diagram (Fig. 47). Parallel lines can be drawn within our limit of error through the points observed at different concentrations. Exceptions, perhaps, are the points obtained for 0.15 and 0.4% NH_4F, which indicate a steeper slope.

From the Arrhenius equation:

$$1/\tau_o = Ae^{-E/RT}$$

it follows:

$$\ln \tau_o = \frac{E}{RT} - \ln A.$$

Consequently the slope of the straight lines in Figure 47 determines the activation energy E for dipole rotation in our mixed crystals. This activation energy was found to be 13 kcal/mol for pure water. The corresponding value for the mixed crystals is 4 kcal/mol, and, if the straight lines in Figure 47 are right, is constant for all concentrations of NH_4F up to 0.4%. The influence of NH_4F in ice within this range of concentrations consists, therefore, in a remarkable lowering of the activation energy of dipole rotation.

The rotation of dipoles in ice can be due either to a shift of hydrogen atoms (or of protons) or to the rotation of complete water molecules. According to Bjerrum (1951), the number of proton jumps per time unit is much too small to explain the dielectric properties of ice ("150 per sec per ice molecule, whereas 10^6 are required"). However the existence of fault sites in ice, characterized by two hydrogens or by none between the two oxygens, would give a quantitative explanation of the dielectric properties.

* More precise later measurements have shown that the preliminary results of this report are exact at very low concentrations only. At higher concentrations, serious deviations appear. However, the conclusions drawn in this report from preliminary results are in agreement with our more precise measurements.

Water molecules in the direct neighborhood of fault sites require an activation energy for rotation of about 2.5 kcal/mol and the creation of the fault site itself requires 10.5 kcal/mol, so that a total activation energy of 13 kcal is required for dipole rotation. This activation energy agrees with the one observed in dielectric measurements. Bjerrum also estimates the number of fault sites of this kind to be of the order of 10^{-6} per molecule. This number would explain the dielectric properties of ice if 4.8×10^{11} turns per sec occur at a fault site. This latter figure he obtains from the frequency of hindered rotation in ice, $\nu = 2.4 \times 10^{13}$, and the energy threshold between the two positions before and after rotation.

The fact that the activation energy of dipole rotation is dependent on the concentration of NH_4F between 0.002 and 0.4% could be explained on the basis of Bjerrum's theory, if we assume that fault sites are automatically formed at places where NH_4^+ or F^- ions are located. This would mean that the larger part of the total activation energy of dipole rotation, namely the 10.5 kcal/mol for the creation of a fault site, does not have to be spent if enough NH_4F is present in ice, and the activation energy for dipole rotation would drop to 2.5 kcal/mol. This value is not very different from the one found in our mixed crystals with NH_4F.

The lowest concentration in our samples was 0.002% NH_4F. This corresponds to 1×10^{-5} mols of NH_4F in 5.5 mols of H_2O, or to a concentration of fault sites of about 4×10^{-6} per H_2O molecule. This figure is of the same order of magnitude and a little higher than that required by Bjerrum's considerations. It, therefore, seems reasonable that, even at our lowest concentrations, the influence of the faults with an activation energy of about 4 kcals prevails so much that the presence of ordinary ice faults does not become evident.

The explanation given above is oversimplified. The dipoles in the immediate neighborhood, and thus in the strong electric field, of an ion should not be influenced by the much weaker outer fields applied at the measurements. In reality a distortion of the lattice might take place characterized by a misalignment of molecules in the field of the ions. This misalignment then might create weaker lattice distortions at regions far enough from the ions that the mobility of water molecules is increased*. More precise experiments are required to clarify the molecular mechanism on which the dielectric behavior of these mixed crystals is based.

IV. INVESTIGATIONS BY X-RAY AND NEUTRON DIFFRACTION

Introduction

According to present knowledge, described in section III, the ice lattice is formed by molecules H_2O, the oxygen atoms being arranged tetrahedrally and the H-atoms on or very close to the line connecting two oxygens. On each of these lines one hydrogen atom is located. But two equilibrium positions are present on each line, the hydrogen atom being attached to one or the other of the two neighboring oxygen atoms. Generally, each hydrogen will occupy one of these equilibrium positions in such a way that only two hydrogens are bound to each oxygen. If this is done most regularly, a single crystal of ice should have a polar $\underline{c}$-axis if the elementary cell is small and has the dimensions accepted at present:

$$\underline{a} = 4.53 \text{ Å}, \quad \underline{c} = 7.41 \text{ Å}.$$

In this case no center of symmetry should be present in the ice lattice.

However, because of the existence of two equilibrium positions between two oxygens in ice, it is very probable that ordinary single crystals are microtwinned in such a

* This hypothesis is supported by the observation that the number of sites with more mobile water molecules begins to decrease at a certain concentration with increasing concentration of NH_4F. This suggests an overlapping of domains with mobile water molecules at the outer border. The experimental results on which this more detailed picture is based were obtained at a time not covered by this report.

way that the polarity of the c-axis disappears. Hence, any investigation dealing with this problem requires a real single crystal.

In the absence of a center of symmetry, the intensity I_{hkl} of a reflection hkl at neutron- or x-ray-diffraction is given by the square of the absolute value of a complex number:

$$I_{hkl} = \left|F_{hkl}\right|^2 = \left|X_{hkl} + iY_{hkl}\right|^2. \qquad (40)$$

Therefore determination of the magnitudes of X and Y from the one intensity I_{hkl} is impossible. But the values of X and Y are required to determine the atomic positions. Since they depend also upon h, k and l there is no general method for obtaining the atomic parameters in a direct way.

However, in the case of ice, the oxygen positions alone have a center of symmetry. This means that their contributions to the diffracted intensity contain a real part only. Moreover, the positions of the oxygens in the lattice are well known so that the contribution of the oxygen atoms to the intensity can be calculated. Thus equation (40) can be solved in the following way:

Denoting the known contribution of the oxygen atoms by X_O we obtain from equation (40):

$$F_{hkl} = X_{O,hkl} + X_{H,hkl} + iY_{H,hkl} \qquad (41)$$

where X_H and Y_H are contributions of hydrogens. Equation (41) can be represented in the vector diagram to the right, with $Z_{H,hkl} = X_H + iY_H$.

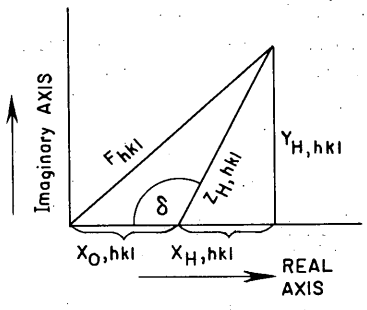

Suppose now we carry out intensity measurements of neutron diffraction with heavy water as well as with ordinary water. We obtain the same figure for heavy water, $X_{O,hkl}$ being unchanged and X_H replaced by X_D. Now, since there is no appreciable difference between the O-H and the O-D distance, the phase angle δ should be the same for both substances. Consequently we obtain the following vector representation for both substances and a given combination hkl. The vector Z_D for the heavy water is drawn in the opposite direction to the vector Z_H, because at neutron scattering a phase shift of 180° takes place on H, but no phase shift occurs on D-atoms. We are able to measure F_H and F_D, which is the actual length of these vectors. We can calculate X_O if we know the effect of heat movement for the oxygen atoms and we know the ratio Z_H/Z_D from the ratio of the scattering powers of H and D. Therefore, we are able to calculate the length of Z_H and Z_D as well as the phase angle δ. This means then, that we also know Y_H and Y_D, so that the actual positions of the hydrogen atoms can be determined.

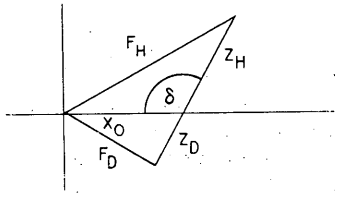

Hence, it is possible to decide by means of neutron-diffraction whether or not ice has a polar axis, provided (1) that absolute measurements of the reflected intensities are made (and not only relative ones as usual) and (2) that a real single crystal is available which is not microtwinned. It also is necessary to know the influence of temperature on the contribution of the oxygen atoms to the scattered intensity.

For obtaining the latter data, we measured x-ray intensities of reflections 00ℓ with ℓ = 2, 6, and 8.* The scattering power of oxygen for x-rays is so much larger than that for hydrogen that the hydrogen contributions to these reflections can be neglected.

*Looped ℓ is used where confusion with numeral 1 might be possible.

GPO 804860-5

We thought that very old ice crystals from Alaska, after aging at temperatures close to 0C, might consist chiefly of real single crystals. Such crystals were furnished by SIPRE, and investigation by means of neutrons showed that the crystals might be good enough for our purposes. Unfortunately, however, the interaction between neutrons and these crystals was strong enough to disturb the almost ideal structure very quickly during the measurement. These experiments were carried out by Drs. Corliss and Hastings at the National Laboratory in Brookhaven. Excellent recorded diagrams were obtained from the ice samples. But, when the same measurements were repeated with the same crystals, it was always found that the intensities of the strong lower orders increase with the exposure time of the crystal. This is due to an increase of mosaic-structure in the crystal caused by the irradiation of neutrons. An ideal crystal shows extinction which diminishes the reflected intensities. The more this ideal structure is destroyed, the more the extinction decreases and, thus, the more the intensity of reflection increases. Continuing the irradiation finally leads to the formation of visible bubbles in the crystal and the intensity diminishes again. These bubbles form in spite of the fact that the crystal is kept at a temperature of -35C. We do not know whether these bubbles contain a gas (air) formerly dissolved in the ice and segregated by the irradiation or whether water is decomposed at certain centers. Because of these difficulties we gave up the experiments that were planned.

Temperature movement in ice

Since intensity measurements on ice were already begun to determine the temperature factor for the oxygen atoms, this part of the work was continued. During this work, we also found the hitherto not observed reflection 004 of ice. Our instrument was sensitive enough to measure the intensity of this reflection accurately. Since this intensity is caused by hydrogen atoms exclusively, we tried to determine separately the temperature factor of the hydrogen atoms.

The equipment. An ionization chamber was used for measuring the diffracted x-ray intensities. The ionization current was amplified by a direct-current amplifier containing two FP-54 electrometer tubes and the intensity of this current was measured by a galvanometer. The deflection of the galvanometer mirror was recorded on a photographic paper in a special camera. A block diagram of the experimental arrangement is shown in Figure 48. Crystal monochromatized Cu K_α-radiation was used for the measurements.

The ice crystal was placed in a special housing (G in Figure 49) on the spectrometer table (A) and rotated about an axis perpendicular to the table so that the reflecting planes of the crystal can gradually be moved through the positions of reflection. The speed of rotation was synchronized with the speed of the number of the galvanometer readings. The spectrometer table was provided with angular scales and verniers to determine the angular position of the crystal as well as that of the chamber. The ionization chamber (B, Fig. 49) could be rotated independently about the same axis as the crystal.

The crystal was fastened to a vertical plate fixed at the back-wall of the housing (Fig. 50). This plate could be slightly tilted and moved back and forth by means of two spring-loaded screws (Fig. 51). These were the only movements necessary to adjust the crystal for basal reflections. The side of the housing exposed to the x-rays consisted of two walls of very thin polystyrene sheets. The inner space between the two sheets was completely sealed off from the inside and outside of the housing and served as heat insulation. At the top of the housing was an inlet (visible in Fig. 50) for the cooling medium. The outlet and an opening for a thermocouple were on the back wall of the housing. A similar housing was constructed for x-ray diffraction on ice in transmission.

To obtain the desired temperature at the ice crystal, the flow rate of the cooling medium, cold nitrogen gas from a tank containing liquid nitrogen, could be adjusted by an electric heater (small spiral of Nichrome wire) inside the liquid nitrogen. The temperature of the crystal was measured by a copper-constantan thermocouple.

GPO 826455-4

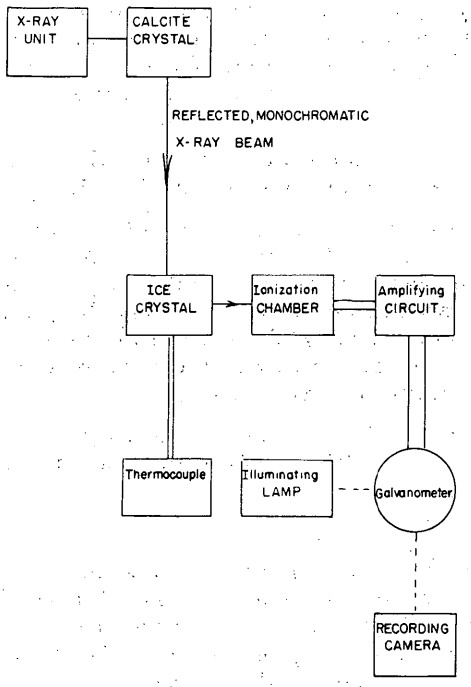

Figure 48. Block diagram of experimental arrangement, x-ray intensity measurements on ice.

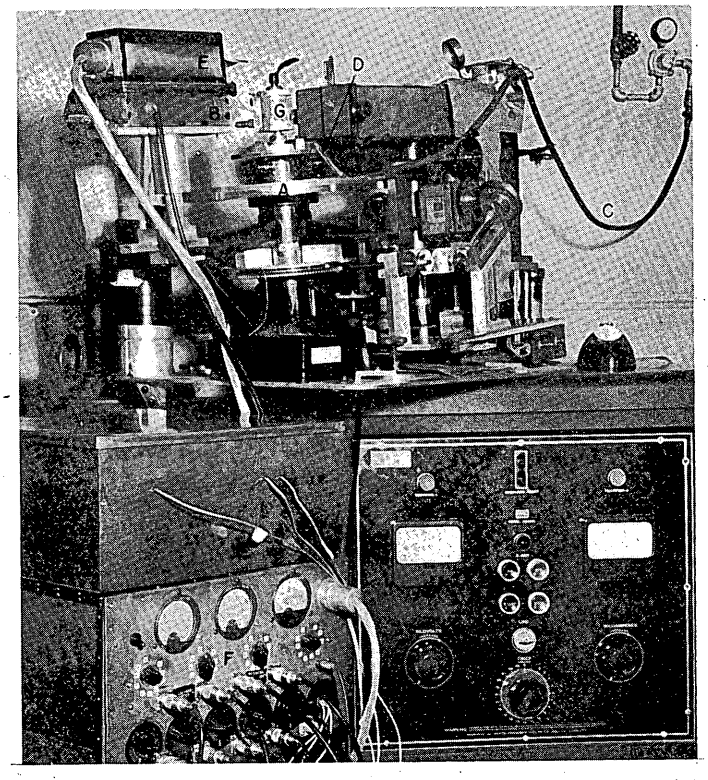

Figure 49. Experimental set-up, x-ray intensity measurements on ice.

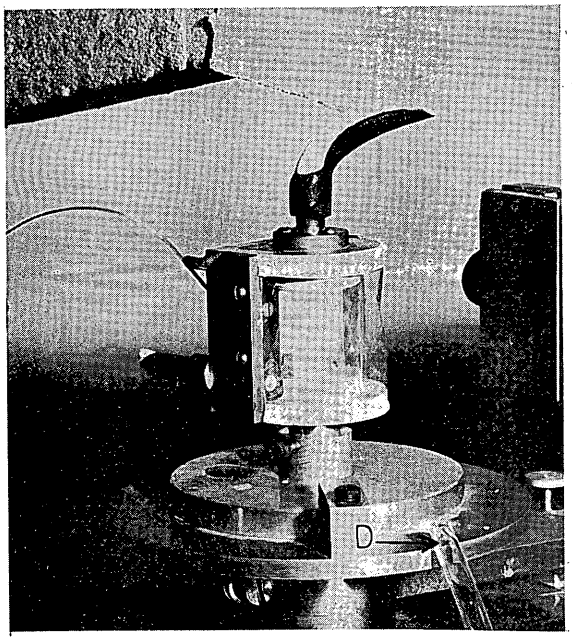

Figure 50. Special housing for ice crystal.

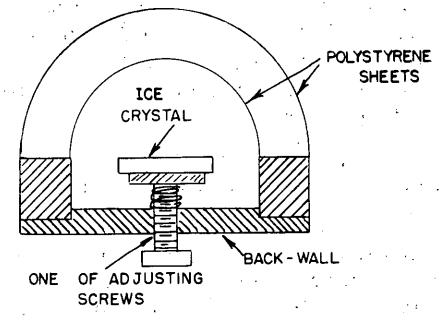

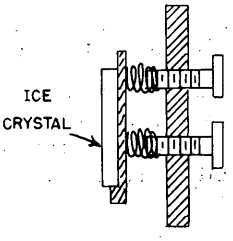

Figure 51. Details of housing for ice crystal.

When measurements were made below -20C, the outside polystyrene wall of the housing of the crystal became covered with mist. This was blown off by compressed air. The rubber tubing (C) leading from the compressed air valve can be seen in Figure 49. It ends with a glass tubing (D) which leans against a disk on which the housing is placed (Fig. 50).

The ionization chamber was constructed and operated in the usual way (Brill et al., 1939) and all the precautions mentioned in this paper were taken (see Figs. 52, 53).

It might be mentioned that the ionization chamber together with the type of detecting circuit used here gives a very sensitive device for detecting diffracted x-rays. As evidence we cite the possibility of measuring with ease and accuracy the intensity of the 004 order from both the H_2O and D_2O crystals. The absolute intensity of this order, as determined by us, is about 2.40×10^{-5}. This figure can be compared with the absolute intensity of the 600 order from NaCl which is 650×10^{-5}. In other words the intensity of the 004 reflection of ice is less than 1/200 of that of a medium strong reflection.

An intensity curve of the 006 order from H_2O-ice (Fig. 54) serves as an example of the resolution of the instrument. The two peaks correspond to the $K\alpha_1$ and $K\alpha_2$ of the copper radiation used. Their separation is 7.22'.

Determination of the temperature factor.

Preparation of the ice crystals: The H_2O crystals used in this work were either grown in this laboratory or were crystals from glaciers in Alaska. The latter ones were found to be excellent for our work. The crystals grown in our laboratory were obtained by slowly freezing a large quantity (about 2000 cm^3) of water in an ordinary tin box. The water was distilled in vacuum to remove the dissolved air. Immediately after transferring it from the distilling apparatus to the box, the surface of the water was covered with a layer of dodecane to prevent air being dissolved in the water. These precautions resulted in an almost bubble-free ice. Investigation of the ice samples between polaroids showed that the middle section of the frozen water near the surface contained large single crystals with the c-axis oriented perpendicular to the surface.

The D_2O crystals were prepared in a similar manner except that smaller quantities of D_2O were used and no distillation was necessary, because this water, obtained in sealed glass bottles, was found to be free from air. However, once the heavy water was frozen and remelted, then it was necessary to boil it in vacuum to free it from air.

To reduce the amount of vibration during freezing, the simple arrangement shown in Figure 55 was used and found very efficient. The polyethylene tank is very convenient since its walls allow the expansion of water on freezing.

A piece of single crystal was selected and cut to a size of $1 \times 1 \times 1/4$ in. with the c-axis perpendicular to the large surface. The large surfaces were made exactly parallel by melting down between plane parallel metal plates. This simple procedure could be applied because we were interested only in x-ray reflections from planes perpendicular to the c-axis. A copper-constantan junction was inserted from the side by melting a hole in the crystal with a warm wire, inserting the junction, and letting it freeze. The crystal was then carefully painted with Polyweld cement to prevent it from evaporating when placed in its housing and surrounded by streaming nitrogen.

The crystal was placed in the housing and adjusted so that the reflected beam would pass into the ionization chamber if the ice crystal was in the reflecting position. This position was found by rotation of the housing. The position of maximum reflected intensity was obtained by tilting the crystal using two screws on the movable plate (Fig. 51).

Measurement of reflected intensities: The intensities of reflections were measured in the usual way. The ionization chamber was set at twice the Bragg angle, the entrance slit wide open. With the chamber fixed at this position, the crystal was rotated through the Bragg angle. It was important to make the angular range of rotation large enough that the recorded curve contained a large part of the linear background on

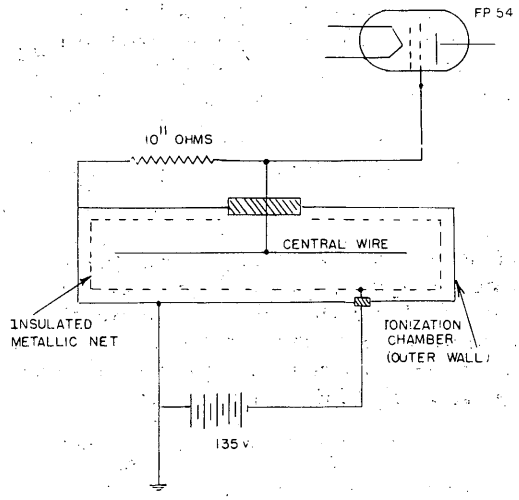

Figure 52. Method of applying potential to the ionization chamber.

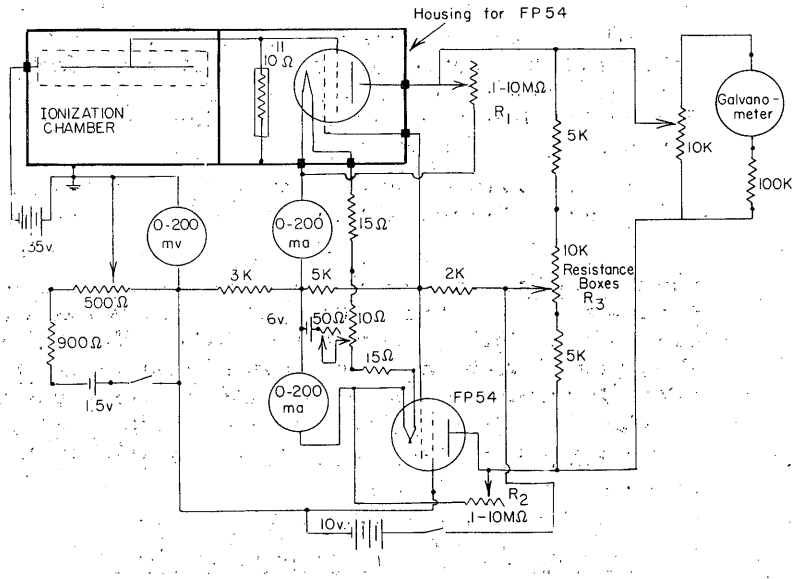

Figure 53. Detecting circuit.

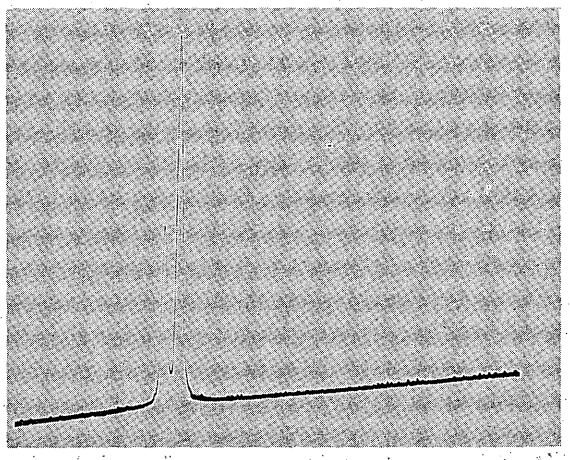

Figure 54. Intensity curve of the 006 order from H_2O-ice.

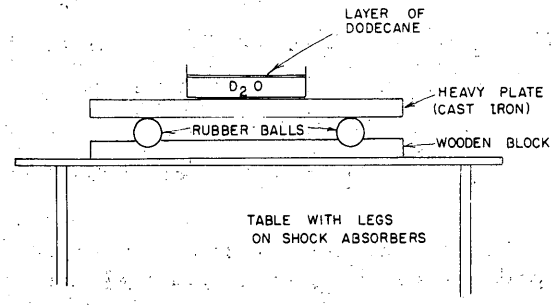

Figure 55. Arrangement for freezing D_2O.

both sides of the Bragg angle, as shown in Figure 54. The background intensity was subtracted graphically from the intensity of the reflection, given by the area of the reflection. This area was measured with a planimeter.

Evaluation of measurements: This determined intensity I is defined by $I = E\omega$, where E is the energy falling into the camera and ω the angular velocity of the crystal. The ratio

$$E\omega/I_o,$$

with I_o being the intensity falling onto the crystal, is connected with the scattering power of the crystal in the following way:

$$\frac{E\omega}{I_o} = \left(\frac{e^2}{mc^2}\right)^2 \times \frac{\lambda^3}{v^2} \times \left|F_{hkl}\right|^2 \times W \times V = Q \times V \tag{42}$$

$$W = \frac{1+\cos^2 2\vartheta_1 \cos^2 2\vartheta_2}{\sin 2\vartheta_1 \,(1+\cos^2 2\vartheta_2)} \tag{42a}$$

where e^2/mc^2 = the amplitude scattered by a single electron (e = charge of the electron, m its mass and c = velocity of light), λ = wavelength of x-rays, v = the volume of the elementary cell, F the structure factor, ϑ_1 = the Bragg angle of the ice crystal, ϑ_2 the Bragg angle of the monochromator crystal, and V = the volume of the crystal contributing to the reflection. In our case of surface reflection, the volume V has to be replaced by $1/(2\mu)$ (for any order of reflection) because of the influence of absorption (coefficient of absorption μ) in the crystal. Hence:

$$\frac{E\omega}{I_o} = \frac{I}{I_o} = \frac{Q}{2\mu}. \tag{43}$$

This formula is valid if the crystal is so thick that practically no radiation penetrates it, if irradiated under the Bragg angle. If this is not the case, equation (43) has to be replaced by:

$$\frac{E\omega}{I_o} = \frac{Q}{2\mu}\left[1-\exp(-2\mu t/\sin\vartheta)\right]. \tag{44}$$

where t is the thickness of the crystal.

The structure factor is defined by:

$$F_{hkl} = \Sigma_n f_n \exp[-2\pi i(x_n h+y_n k+z_n \ell)] \cdot \exp[-B_n(\sin\vartheta/\lambda)^2]. \tag{45}$$

The summation has to be taken over the n-atoms in the elementary cell with atomic coordinates x_n, y_n, z_n, measured in units of the length of the edges of the elementary cell. The f_n are the atomic scattering factors for the n-atoms. In B_n the influence of thermal motion on F, and hence also on I, is contained. It is:

$$B_n = \frac{6h^2 T}{m_n k \theta_n^2}\left[\phi(x)+x/4\right] \tag{46}$$

$$\phi(x) = \frac{1}{x}\int_0^x \frac{y\,dy}{e^y-1} \tag{47}$$

where h = Planck's constant, k = Boltzmann's constant, m_n = the mass of the nth atom and θ_n its characteristic temperature, $x = \theta/T$, T = the absolute temperature.

The influence of the temperature on the reflected intensities is determined by measuring the magnitude B in equation (45). To do this it may be assumed that, in first approximation, the temperature motion of all the different kinds of atoms in a crystal can be described by an average $\bar{B}$. Then equation (45) can be written in the form:

$$F_{hkl} = \exp[-\overline{B}(\sin\vartheta/\lambda)^2 \sum f_n \exp[-2\pi i(x_n h + y_n k + z_n \ell)] \quad (48)$$

$$= \exp[-\overline{B}(\sin\vartheta/\lambda)^2 F^\circ_{hkl}$$

where F°_{hkl} is the structure factor at 0K.

Thus we obtain from (42):

$$\frac{Q_{hkl}}{2\mu} = \frac{I_{hkl}}{I_\circ} = \left(\frac{e^2}{mc^2}\right)^2 \cdot \frac{\lambda^3}{v^2} \left|F^\circ_{hkl}\right|^2 \cdot W\exp[-2\overline{B}(\sin\vartheta/\lambda)^2] \quad (49)$$

or

$$\exp[-2\overline{B}(\sin\vartheta/\lambda)^2] = \frac{2\mu}{Q_{hk\ell}} \left(\frac{e^2}{mc^2}\right)^2 \frac{\lambda^3}{v^2} \left|F^\circ_{hkl}\right|^2 W. \quad (50)$$

If the values $\underline{F}^\circ_{hkl}$ are known and if $\underline{Q}$ is measured, $\overline{\underline{B}}$ can be calculated directly from equation (50). For ice $\underline{F}^\circ_{hkl}$ is not known exactly, as the coordinates of the hydrogen atoms are not known precisely. Hence, $\overline{\underline{B}}$ can only be determined by measuring $\underline{Q}_{hkl}$ at different temperatures. In this case it is also not necessary to know the absolute value of $\underline{Q}$ since any proportionality constant drops out if ratios of $\underline{Q}$-values are formed. Thus, from (50), for a given reflection measured at $\underline{T}_1$ and $\underline{T}_2$:

$$\mathrm{Exp}[2(B_{T_1} - B_{T_2})(\sin\vartheta/\lambda)^2] = \frac{Q_{T_2}}{Q_{T_1}}. \quad (51)$$

The parameters $x_n y_n z_n$ for the oxygen atoms in ice are well known and the parameters of the hydrogens can be estimated with a fair degree of accuracy from the neutron diffraction results of Wollan, Shull and Davidson (1945). Using their data and assuming the hydrogen atoms on the line connecting two oxygens and 1 Å from the oxygen to which a hydrogen is bonded, F_{hkl} values can be calculated which cannot be too far away from the correct values. Especially the distance H-O influences the F-values only slightly. The calculation gives the following figures for the contributions of oxygen and hydrogen atoms to the total scattered intensity:

Indexes	Contribution of oxygens	Contribution of hydrogens	F°_{hkl}
002	-19.37	-3.04	22.41
004	0	1.81	1.81
006	8.34	-0.70	9.04
008	8.60	0.12	8.72

The table contains the data for four orders of the basis reflections. Higher orders cannot be obtained with our equipment and with Cu K-radiation. The figures indicate that our approximation of a mean $\overline{B}$-value is quite satisfactory because the intensity for the 2nd, 6th, and 8th order chiefly stems from scattering at oxygen atoms and hydrogens contribute exclusively to the 4th order.

Now, the function $\phi(x) + x/4$ in equation (46) deviates from 1 only slightly.

For values of x between 0 and 1 the deviation is not more than 2%; at $x = 2.5$ the deviation is 16%. In second approximation $\phi(x)+{}^{x}/4$ can be represented by:

$$\phi(x)+\frac{x}{4} = 1+ax. \tag{52}$$

The accuracy obtained this way is rather high if x does not change more than a unity; i. e., if the temperatures T_1 and T_2 do not differ too much, equation (52) can be considered to be correct with an appropriate value of a.

From (51) it follows:

$$B_{T_1}-B_{T_2} = \frac{1}{2}\left(\frac{\lambda}{\sin\vartheta}\right)^2 \ln\frac{Q_{T_2}}{Q_{T_1}}. \tag{53}$$

On the other hand, from (46) and (52):

$$B = \frac{6h^2T}{mk\theta^2}(1+ax) = \frac{6h^2}{mk\theta x}(1+ax) = \frac{6h^2}{mk\theta x}+\frac{6h^2}{mk\theta}a$$

and hence:

$$B_{T_1}-B_{T_2} = \frac{6h^2}{mk\theta^2}(T_1-T_2). \tag{54}$$

Thus the member containing a drops out. From (54) and (53) it follows finally:

$$m\theta^2 = \frac{12h^2}{k}\left(\frac{n}{2d}\right)^2\frac{T_1-T_2}{\ln(Q_{T_2}/Q_{T_1})}. \tag{55}$$

Here $\left(\frac{\sin^2\vartheta}{\lambda}\right)$ is replaced by $\left(\frac{n}{2d}\right)^2$ according to Bragg's law.

For our final evaluation we used equation (55) in the form:

$$\theta\sqrt{m} = \frac{nh}{d}\sqrt{\frac{3}{k}}\cdot\sqrt{\frac{T_1-T_2}{\ln(Q_{T_2}/Q_{T_1})}}.$$

The values obtained are as follows:

Temperature Range*	$\sqrt{m}\theta \times 10^9$		
	004	006	008
High	.61 ± .01 mean of 11 exp.	(1.01 ± .01) mean of 9 exp.	1.03 ± .04 mean of 11 exp.
Intermediate	.81 ± .04 mean of 8 exp.	1.20 mean of 3 exp.	1.30 † mean of 3 exp.
Low	1.15 single exp. (-40C, -80C)	1.20 single exp. (-60C, -88C)	1.16 single exp. (-63C, -87C)
	1.14 single exp. (-72C, -108C)		
	1.17 single exp. (-62C, -91C)		

* The limits of the temperature ranges are different for different measurements. The high temperature range goes from a few degrees below 0C to about -45C; the intermediate from about -35C to about -65C. The limits of the low range are indicated in the table.

† The three values in this case are: 1.495, 1.281, 1.123. It seems that the first one is erroneous. If it is rejected, the mean of the remaining two figures fits the general pattern of all the results much better.

Discussion of the results. The above values, which represent the condensation of all our experiments, show that in the lowest region of temperatures, between -60C and -90C, the values of $\sqrt{m}\theta$ are practically constant for all orders. In the range between -35C and -65C, the $\sqrt{m}\theta$ values are unchanged for the 6th and 8th order, but decrease for the 4th order. At the highest temperature range, between -5C and -45C, there seems to be a slight drop of $\sqrt{m}\theta$ for the 6th and 8th order, and again a definite drop for the 4th order.

Now, a priori, it is not accurate to describe the heat movement of a molecule like H_2O by only one characteristic temperature. Several θ values are required for describing translational motions of the whole molecule, rotations and vibrations of the molecule, and internal vibrations of the atoms composing the molecule. Our results indicate that, in the lowest range, between -60 and -90C, translational motion of the whole molecule is chiefly responsible for the change of intensities. This also follows from the fact that $\sqrt{m}\theta$ for the 4th order, which is caused by H-atoms alone, is the same as that for the 6th and 8th order, where O-atoms contribute chiefly to the intensities. This means that m at the 4th order is equal to the m at the 6th and 8th order and this m, obviously, has to be the mass of the whole molecule.

Inserting this value in

$$\sqrt{m}\theta = 1.2K$$

one obtains

$$\theta = 219K.$$

In the medium range of temperature, the values $\sqrt{m}\theta$ for the 6th and 8th order are not changed. This means that the contributions of the hydrogens to the intensities of these orders are still too small to give any effect. At the 4th order, however, the change in $\sqrt{m}\theta$ indicates that, in the medium range, the oscillations of the hydrogens already exert a remarkable influence. In the highest range of temperatures, this shows up at all orders. A further evaluation, which was not completed in the time covered by this report, should give more details about the thermal movement of the hydrogens.

To check whether or not the above value of the characteristic temperature is reasonable, different methods were used:

By definition:

$$\theta = \frac{h\nu_m}{k}$$

with ν_m = maximum-frequency of elastic waves in the lattice according to Debye's theory, $\underline{h}$ and $\underline{k}$ = Planck's and Boltzmann's constant.

Considering the water molecules as harmonic oscillators at the low temperature range, Debye's theory would be applicable. Hence, from measured $\underline{c}_p$-values, the corresponding $\underline{c}_v$-values can be calculated:

$$c_p - c_v = \frac{TV\beta^2}{k}$$

$\underline{c}_p$ = specific heat at constant pressure; $\underline{c}_v$ = specific heat at constant volume; β = coefficient of thermal expansion; $\underline{k}$ coefficient of compressibility; $\underline{V}$ = molar volume. Since values of compressibility are available only close to 0C, the Nernst-Lindemann approximation had to be used:

$$c_p - c_v = Ac_p^2T$$

$$A = \frac{V\beta^2}{kc_p^2} .$$

The magnitude $\underline{A}$ is constant and independent of the temperature, so that $\underline{c}_p - \underline{c}_v$ can be calculated if $\underline{A}$ is known for any temperature and $\underline{c}_p$-values are available at very low temperatures, which is the case. The trial shows that it is difficult to fit the observed values into a Debye curve. This exemplifies that, even at low temperatures, ice behaves as a simple substance only approximately. This could be expected. However a rough mean value of 270K can be calculated.

The same objections as regards the Debye curve can be made, of course, if other methods are used. Considering the ice molecules as harmonic oscillators, the above-defined maximum frequency ν_m can be calculated according to

$$\nu_m = 2.91 \times 10^{11} \sqrt{\frac{c_v}{\beta M V^{2/3}}} .$$

With $\underline{V}$ = 18 cm^3 and $\underline{c}_p$ = 6.54, $\beta = 1.19 \times 10^{-4}$/degree (both for -75C, i.e., the mean temperature of our lowest range) one obtains:

GPO 826455-3

$$\nu_m = 6.15 \times 10^{12}$$

and

$$\theta = 295\text{K}.$$

This value agrees with the one calculated from Debye's theory within the rather large limit of error of these calculations, which are based on very rough approximations and assumptions which are not fulfilled by a substance like ice.

Since the Lindemann formula in many cases gives results which agree with those obtained by other methods, it was also applied. But, this formula, of course, is the least exact one. The characteristic temperature is calculated from the melting point, T_m, the molecular weight, M, and the molar volume according to:

$$Q = 134\sqrt{\frac{T_m}{MV^{2/3}}} = 134\sqrt{\frac{273}{18 \times 18^{2/3}}} = 200\text{K}.$$

In any event all these theoretical values are not in contradiction to our experimental value $\theta = 220$K. Hence, it is concluded that this value is correct and characterizes the translational vibrations of the whole molecule.

Further evaluation of these measurements in connection with similar measurements on heavy ice and on extension of the measurements to higher orders should elucidate the role of the hydrogen atoms at thermal vibrations in ice and might, eventually, shed some light on the hydrogen bond in ice. The temperature-dependency of $\sqrt{m}\theta$ for the 4th order (which is due to hydrogens exclusively) already indicates a large inharmonicity of the O-H vibration.

REFERENCES

Auty, Robert P., and Cole, Robert H. (1952) Dielectric properties of ice and solid D_2O, Journal of Chemical Physics, vol. 20, p. 1309-1314.

Bacon, G. E., and Pease, R. S. (1953) A neutron diffraction study of potassium dihydrogen phosphate by Fourier synthesis, Proceedings of the Royal Society (London), A 220, p. 397.

Becker, R. (1925) Elastische Nachwirkung und Plastizität (Elastic after-effect and plasticity), Zeitschrift für Physik, Bd. 33, p. 185 (text in German).

Bjerrum, Niels (1951) Structure and properties of ice. Kgl. Danske Videnskab. Selskab. Mat. fys. Medd. 27, No. 1, p. 1-56.

Böttcher, C. J. F. (1952) Theory of electric polarization. Amsterdam: Elsevier.

Briegleb, G. (1949) Zwischenmolekulare Kräfte (Intermolecular forces). Karlsruhe: G. Bauer, p. 1ff (text in German).

Brill, R.; Grimm, H.; Hermann, C.; and Peters, Cl. (1939) Anwendung der röntgenographischen Fourieranalyse auf Fragen der chemischen Bindung (Application of Fourier-analysis to problems of chemical bond), Annalen der Physik, 5. Folge, Bd. 34, Heft 5, p. 393 (text in German).

Cole, Kenneth S., and Cole, Robert H. (1941) Dispersion and absorption in dielectrics. I. Alternating current characteristics, Journal of Chemical Physics, vol. 9, p. 341-351.

Cottrell, A. H. (1953) Dislocations and plastic flow in crystals. Oxford: Clarendon Press.

Debye, P. (1929) Polare Molekeln (Polar molecules). Leipzig: Akad. Verlagsgesellschaft (text in German).

Dorsey, N. E. (1940) Properties of ordinary water substance. New York: Reinhold Publishing Corp., p. 445.

Eucken, A. (1950) Lehrbuch der chemischen Physik II. Leipzig: Akad. Verlagsgesellschaft, p. 84 (text in German).

Eyring, H. (1936) Viscosity, plasticity, and diffusion as examples of absolute reaction rates, Journal of Chemical Physics, vol. 4, no. 4, p. 283.

Frank, F. C. (1936) The chemical kinetics of dielectric relaxation. Transaction of the Faraday Society, vol. 32, p. 1634-1647.

General Radio Co., Cambridge, Mass., Operating instructions for Bridge Type 650-A.

Giguere, P. A., and Maass, O. (1940) Solid solutions of hydrogen peroxide and water, Canadian Journal of Research, vol. 18B, p. 66-73.

Griggs, D. T., and Coles, N. E. (1954) Creep of single crystals of ice. Snow Ice and Permafrost Research Establishment, Corps of Engineers, U. S. Army, Report 11, 24 pages.

Haggis, G. H.; Hasted, J. B.; and Buchanan, T. J. (1952) The dielectric properties of water in solutions, Journal of Chemical Physics, vol. 20, p. 1452-1465.

Hess, H. (1902) Elasticität und innere Reibung des Eises (Elasticity and internal friction of ice), Annalen der Physik, Vierte Folge, Bd. 8, Heft 1, p. 405 (text in German).

Humbel, F.; Jona F.; and Scherrer, P. (1953) Anisotropie der Dielektrizitätskonstante des Eises (Anisotropy of the dielectric constant of ice). Helvetica Physica Acta, vol. 26, p. 17-32 (text in German with English summary).

Iatlov, V. S., and Poliakova, E. M. (1945) Equilibrium in the systems NH_4F-H_2O and NH_4HF_2-H_2O, Journal of General Chemistry USSR, vol. 15, p. 724-8.

Kolthoff, I. M., and Sandell, E. B. (1949) Textbook of quantitative inorganic analysis. New York: MacMillan Co.

König, A. (1886) Über eine neue Methode zur Bestimmung des Elastizitätsmodulus (A new method for the determination of the elastic modulus), Annalen der Physik und Chemie, Neue Folge, Bd. XXVIII, Heft 1, p. 108 (text in German).

Kubachewski, O., and Weber, H. (1950) Erstarrungsdiagramm, Mischungswärmen und Dichten des Systems Wasser-Wasserstoffsuperoxyd (Phase diagram, heat of mixing and density of the system water-hydrogen peroxide), Zeitschrift für Elektrochemie und angewandte physikalische Chemie, Bd. 54, nr. 3, p. 200 (text in German).

Lamb, John, and Turney, A. (1949) The dielectric properties of ice at 1.25 cm wavelength, Proceedings of the Royal Society (London), vol. 62B: p. 272-273 (Letters to the editor).

Lequear, H. A., and Lubahn, J. D. (1952) Symposium on strength and ductility of metals at elevated temperatures, with particular reference to effects of notches and metallurgical changes, American Society for Testing Materials, Special Technical Publication 128.

Leschen, J. S.; Carreker, R. P.; and Hollomon, J. H. (1948) Metals technology, vol. 15, A. I. M. E. Technical Publication No. 2436.

Lonsdale, Kathleen, (1948) Statistical structure of ice and ammonium-fluoride. Nature, vol. 158, p. 582 (Letters to the Editors).

Mair, B. J.; Glasgow, A.F.; and Rossini, F. D. (1941) Determination of freezing points and amounts of impurity in hydrocarbons from freezing and melting curves, Journal of Research of the National Bureau of Standards, vol. 26, p. 601.

Mironov, K. E., and Bergman, A. G. (1951) State diagram of the binary system water-hydrogen peroxide, Akad. Nauk USSR, vol. 81, p. 1081.

Murphy, E. J. (1934) The temperature dependence of the relaxation time of polarizations in ice. Transactions of the Electrochemical Society, vol. 65, p. 133-142.

Nukasawa, K.; Tanaka, J.; and Nagakura, S. (1953) A note on the hydrogen bond, Journal of Phys. Soc., Japan, vol. 8, p. 792.

Pauling, L. (1948) Nature of the chemical bond. Cornell University Press, p. 302.

Powles, J. G. (1952) A calculation of the static dielectric constant of ice, Journal of Chemical Physics, vol. 20, p. 1302-1309.

Rundle, R. E. (1953) The structure and residual entropy of ice, Journal Chem. Phys., vol. 21, p. 1311 (Letter to Editor).

———— (1954) Polar versus nonpolar ice, Journal Chem. Phys,, vol. 22, p. 344.

Schellman, J. A., Jr. (1950) The theory of the dielectric properties of ice. Princeton University (Ph. D. Thesis), 80 pages.

Seltz, H. (1934) Thermodynamics of solid solutions I. Perfect solutions, Journal of the American Chemical Society, vol. 56, p. 307.

Shockley (1949) Symposium on cold working of metals. American Society for Metals.

Smyth, C. P., and Hitchcock, C. S. (1932) Dipole rotation in crystalline solids. Journal of the American Chemical Society, vol. 54, p. 4631-4647.

Wollan, E. O.; Davidson, W. L.; and Shull, C. G. (1949) Neutron diffraction study of the structure of ice, Physical Review, vol. 75, p. 1348-1352.

Workman, E. J. (1951) Some electrical properties of the ice of dilute aqueous solutions, New Mexico School of Mines. 6 pages (Appendix H of Final report on Thunderstorm Electricity).

GPO 826455—2